DOCTOR OF PHILOSOPHY

Real-world solutions for improving estimates of land-atmosphere exchanges in heterogeneous landscapes

He, Yufeng

Award date:
2016

Awarding institution:
Bangor University

Real-world solutions for improving estimates of land-atmosphere exchanges in heterogeneous landscapes

A thesis submitted for the degree of Doctor of Philosophy

To

PRIFYSGOL
BANGOR
UNIVERSITY

By

Yufeng He

MSc. ECNU

BSc. ECNU

School of Environment, Natural Resources and Geography

Bangor University

September 2016

Declaration and Consent

Details of the Work

I hereby agree to deposit the following item in the digital repository maintained by Bangor University and/or in any other repository authorized for use by Bangor University.

Author Name: Yufeng He

Title: Real-world solutions for improving estimates of land-atmosphere exchanges in heterogeneous landscapes

Supervisor/Department: Dr M. Rayment / SENRGy, Dr J. Gibbons / SENRGy

Funding body (if any): Bangor University – China Scholarship Council (CSC)

Qualification/Degree obtained: PhD in Environmental Science

This item is a product of my own research endeavours and is covered by the agreement below in which the item is referred to as "the Work". It is identical in content to that deposited in the Library, subject to point 4 below.

Non-exclusive Rights

Rights granted to the digital repository through this agreement are entirely non-exclusive. I am free to publish the Work in its present version or future versions elsewhere.

I agree that Bangor University may electronically store, copy or translate the Work to any approved medium or format for the purpose of future preservation and accessibility. Bangor University is not under any obligation to reproduce or display the Work in the same formats or resolutions in which it was originally deposited.

Bangor University Digital Repository

I understand that work deposited in the digital repository will be accessible to a wide variety of people and institutions, including automated agents and search engines via the World Wide Web.

I understand that once the Work is deposited, the item and its metadata may be incorporated into public access catalogues or services, national databases of electronic theses and dissertations such as the British Library's EThOS or any service provided by the National Library of Wales.

I understand that the Work may be made available via the National Library of Wales Online Electronic Theses Service under the declared terms and conditions of use (http://www.llgc.org.uk/index.php?id=4676). I agree that as part of this service the National Library of Wales may electronically store, copy or convert the Work to any approved medium or format for the purpose of future preservation and accessibility. The National Library of Wales is not under any obligation to reproduce or display the Work in the same formats or resolutions in which it was originally deposited.

Statement 1:

This work has not previously been accepted in substance for any degree and is not being concurrently submitted in candidature for any degree unless as agreed by the University for approved dual awards.

Signed ..... (candidate)

Date .....

Statement 2:

This thesis is the result of my own investigations, except where otherwise stated. Where correction services have been used, the extent and nature of the correction is clearly marked in a footnote(s).

All other sources are acknowledged by footnotes and/or a bibliography.

Signed ..... (candidate)

Date .....

Statement 3:

I hereby give consent for my thesis, if accepted, to be available for photocopying, for inter-library loan and for electronic storage (subject to any constraints as defined in statement 4), and for the title and summary to be made available to outside organisations.

Signed ..... (candidate)

Date .....

NB: Candidates on whose behalf a bar on access has been approved by the Academic Registry should use the following version of Statement 3:

Statement 3 (bar):

I hereby give consent for my thesis, if accepted, to be available for photocopying, for inter-library loans and for electronic storage (subject to any constraints as defined in statement 4), after expiry of a bar on access.

Signed ..... (candidate)

Date .....

Statement 4:

Choose **one** of the following options

a) I agree to deposit an electronic copy of my thesis (the Work) in the Bangor University (BU) Institutional Digital Repository, the British Library ETHOS system, and/or in any other repository authorized for use by Bangor University and where necessary have gained the required permissions for the use of third party material.	
b) I agree to deposit an electronic copy of my thesis (the Work) in the Bangor University (BU) Institutional Digital Repository, the British Library ETHOS system, and/or in any other repository authorized for use by Bangor University when the approved bar on access has been lifted.	
c) I agree to submit my thesis (the Work) electronically via Bangor University's e-submission system, however I opt-out of the electronic deposit to the Bangor University (BU) Institutional Digital Repository, the British Library ETHOS system, and/or in any other repository authorized for use by Bangor University, due to lack of permissions for use of third party material.	

Options B should only be used if a bar on access has been approved by the University.

In addition to the above I also agree to the following:

1. That I am the author or have the authority of the author(s) to make this agreement and do hereby give Bangor University the right to make available the Work in the way described above.
2. That the electronic copy of the Work deposited in the digital repository and covered by this agreement, is identical in content to the paper copy of the Work deposited in the Bangor University Library, subject to point 4 below.
3. That I have exercised reasonable care to ensure that the Work is original and, to the best of my knowledge, does not breach any laws – including those relating to defamation, libel and copyright.
4. That I have, in instances where the intellectual property of other authors or copyright holders is included in the Work, and where appropriate, gained explicit permission for the inclusion of that material in the Work, and in the electronic form of the Work as accessed through the open access digital repository, or that I have identified and removed that material for which adequate and appropriate permission has not been obtained and which will be inaccessible via the digital repository.
5. That Bangor University does not hold any obligation to take legal action on behalf of the Depositor, or other rights holders, in the event of a breach of intellectual property rights, or any other right, in the material deposited.
6. That I will indemnify and keep indemnified Bangor University and the National Library of Wales from and against any loss, liability, claim or damage, including without limitation any related legal fees and court costs (on a full indemnity bases), related to any breach by myself of any term of this agreement.

Signature: ..... Date: .....

To the memory of my father.

To my mother and to my wife Yingying,
for their consistent support and understanding.

Acknowledgements

It is a genuine pleasure to express my deep gratitude to my primary supervisor, Dr Mark Rayment, for his persistent support and trust. His incredible insights and creativities in science have always been inspirational. His open-mind and great personality have deeply influenced my personal philosophy of life.

I own sincere thanks to my co-supervisor, Dr James Gibbons, for his constructive advice and statistical supports whenever it was required.

This PhD was made possible by the joint programme between Bangor University and China Scholarship Council (CSC). I would also like to acknowledge HPC wales, for providing bursary and access to high performance computation.

Many thanks to the committee members at SENRGy, Dr Andy Smith and Prof John Healey, who helped me progress my PhD by offering timely and effective suggestions.

Thanks are also due to Dr Sophie Williams and Prof Julia Jones, for their kindness and encouragements at the early stage of my study; My colleague Pippa Jones, for an efficient and interesting collaboration on the windbreak/sheep study; And Dr Luke Ridley, for his support of the field work at Cors E and the collaboration on writing a paper.

Thanks to all friends and great people from six continents, who made my time at Bangor enjoyable and memorable.

Abstract

Accurately quantifying land-atmosphere exchanges is essential at every spatial scale, from aiding a better understanding of climate change globally to informing land management decisions at the smallest scale (e.g. agricultural land management). This quantification may be dealt with relatively easily for homogeneous land surfaces, but in the real world, landscapes are spatially heterogeneous and simple approaches are often inadequate. This thesis uses mathematically advanced methods and/or models to find robust solutions to land-atmosphere exchange problems that accommodate spatial heterogeneity.

A two-stage sampling strategy (2SS) was developed to reduce the uncertainties in the estimation of chamber-based GHG fluxes when sample size is inadequate to fully capture spatial heterogeneity. A Monte Carlo simulation showed that 2SS improves the estimation of soil GHG fluxes in all but the most homogeneous situations, with the improvement being directly related to the amount of spatial heterogeneity present.

EC-based measurements of GHG fluxes invariably contain data gaps that require filling to generate long-term cumulative fluxes, i.e. integrating over a temporally heterogeneous time-series. Gap-filling methods introduce uncertainty. A robust method based on image inpainting is introduced to fill gaps via a two-dimensional representation of a one-dimensional data, i.e. the flux fingerprint. Results show that this unsupervised method, using a more compact and simple form, compares favourably with a widely-used traditional method and can outperform it when applied to de-noised data.

The most robust measurements of surface carbon fluxes will be generated when using two independent measurement methods simultaneously. To investigate CO_2 and CH_4 fluxes from a heterogeneous fen, EC- and chamber-based measurements of surface carbon fluxes were implemented from 2013 to 2015. To implement a direct comparison between these measurements made at differing scales, the chamber-measured data were up-scaled, both temporally by model-based interpolations and spatially by flux footprint modelling. Results show a good linear correlation in CO_2 flux and a near zero correlation in CH_4 flux between methods. Further analysis on CH_4 flux, however, show that the two differed only by a Gaussian distribution, implying the existence of white noise in the signal. The cumulative CO_2 flux for the whole season measured by chambers was -376.5 g/m^2, 33% higher than the estimated measured by EC (-281.8 g/m^2). Similarly, the final cumulative CH_4 flux was 4.01 g/m^2 by chamber-based estimates, 43% more than EC (2.81 g/m^2).

The final part of this study investigates the surface flux of momentum in a structured heterogeneous land surface. A logarithmic normal distribution was developed to model the wind speed reduction around a tree-based windbreak. The model showed an excellent fit to field observations made at a real-world windbreak on farm land. A graphical method that describes a 3-d space of wind-chill temperature vs. ambient temperature and wind speed was created to quantify the potential thermal benefits gained by introducing windbreaks and reducing wind speed. The wind-chill thermal tolerance (WTT) of sheep was estimated and compared for a lowland and an upland site. Distinct differences to reduced wind speed were found between the sites, with greater thermal benefits at the upland site.

The methods and models generated and developed in this study contribute to an improved quantification of land-atmosphere exchanges, and have potential to be applied to surface fluxes generally, either of mass (GHGs) or energy (heat, momentum), and to landscapes other than those dominated by vegetation. For example, the statistical idea of the two-stage sampling approach provides a generic solution to sample size deficiency in heterogeneous land surfaces; The inpainting-based gap-filling method, as an image processing technique, may be applicable to any signals that can be represented as an image, i.e. a two-dimensional space in which individual locations (pixels) have numerical attributes that can be used as RGB values; The WTT plot/analysis, used here in the context of sheep in upland sites, provides an intuitive and powerful scheme for analysing the thermal tolerance of any animal in any energetically heterogeneous landscape.

Table of Contents

Ch 1. General introduction

1.1 Why land-atmosphere exchanges matter

For more than 200 years it has been understood that the land surface exchanges energy, water and carbon with the atmosphere (Sellers, 1997). These exchanges constitute the highly complex climate system and interactions between these two components determine the climate at various spatial and temporal scales. At large scales, for example, there is a major effort to understand the mechanism(s) behind increasing atmospheric carbon dioxide concentration during the last century (Jones et al., 1999) and, critically, how the earth system will respond to this change, both biologically and physically, in the short and medium term (Bonan, 2008; Falkowski et al., 2000). Researchers are particularly interested in the climatic sensitivity of water, carbon and energy exchange to extreme events and anomalies (e.g. Ciais *et al.*, 2005; Zhao & Running, 2010) and how and why land–atmosphere exchanges vary as ecosystems recover from past disturbance (Goulden et al., 2006) .

At smaller scales, there are questions about the impact of urbanization on climate change (Kalnay and Cai, 2003), and questions about agricultural (e.g. vegetation and fertility) and horticultural sensitivity to climate change (Howden et al., 2007) and air pollution (Unsworth and Ormrod, 2013), and questions about the social, economic and political aspects of climate change (Adger et al., 2009; Stern, 2007). All of these questions require that we can measure and understand land-atmosphere exchanges, as a fundamental component of a quantitative understanding of all aspects of climate change, and this has focussed attention on the interaction between the disciplines of atmospheric science, agriculture, ecology, biology and social science.

In physics, exchanges are termed by fluxes; a vectorised quantity that has both magnitude and direction, in contrast to a scalar, such as concentration, that has only magnitude. In particular, land-atmosphere exchanges often refer to the generally vertical fluxes of energy, water and carbon. By convention, a positive flux means an exchange from land to atmosphere (i.e. the land is the source) and conversely for a negative flux (i.e. the land is a sink). In the context of this thesis, the two terms, exchanges and fluxes may appear concurrently and are interchangeable.

1.2 Micrometeorology and land surface heterogeneity

Micrometeorology, or microscale meteorology, deals with atmospheric phenomena and observations at the smallest scales of time and space, normally shorter than a day and smaller than 1 km^2 (AMS Glossary, 2016). Micrometeorology naturally inherits most of its theoretical basis from hydrodynamic and meteorological studies, such as theories of turbulence, gas transportation and thermal dynamics. However, because near-ground microscale events often interact with the underlying land surface (such as plant-dominated ecosystems and water bodies), micrometeorology is a highly interdisciplinary topic involving physics, biology, ecology, hydrology, and geography.

At the early stage of micrometeorological measurements in the 1950s, field experiments were conducted in quasi-homogeneous sites using, for example, the profile approach used in the ground-breaking O'Neill experiment in 1953 (Lettau and Davidson, 1957). The eddy covariance (EC) method, as a direct measure of turbulent fluxes, emerged almost at the same time, along with the development of sonic anemometers (Leclerc et al., 2014). Between 1960s and 1980s, both the EC method and sonic anemometers had gone through a series of improvements in their theoretical basis and practical designs (Kaimal and Businger, 1963; Moncrieff, 2004), but it was not until the late 1980s that micrometeorological experiments became feasible for larger and more complex surfaces. In 1987s the first ISLSCP (International Satellite Land Surface Climatology Project) field experiment (FIFE) was conducted on the Konza Prairie in Kansas, looking at several homogeneous field-scale areas that together made up a heterogeneous landscape study area of 15*15 km (Sellers et al., 1988), and soon afterwards, in 1990, a similar experiment was developed and conducted in southwest France over a non-homogeneous forest system (André et al., 1990). Since the late 80s, as a result of the significant progress made in computer technology, studies looking at numerical solutions for the equations of fluid dynamics have become increasingly active (Cai and Leclerc, 2007; Gash, 1986; Schmidt and Schumann, 1989). More recently, further developments in informatics (data science) and parallel computing have enabled us to retrieve unprecedented levels of information from big data sets using, for instance, artificial neural network and image processing (Dengel et al., 2013; He and Rayment, 2016; Papale et al., 2006). The modern era of micrometeorology integrated with advanced computer techniques and data science has begun.

Nonetheless, making measurements and developing process understanding of interactions in heterogeneous land surfaces are still challenging and large uncertainties remain (Hollinger and Richardson, 2005; Moncrieff et al., 1996; Wohlfahrt et al., 2008). Land surfaces are heterogeneous in many ways affecting local climate and land-atmosphere exchanges through a variety of mechanisms, but it is always the surface properties (e.g. surface roughness, canopy height and other obstacles) that determine the near-surface atmospheric processes (e.g. greenhouse gas exchange). The impact of some types of heterogeneity can be illustrated relatively simply using the change in the vertical profile of wind speed (momentum) as shown in Fig. (1.1). Over a perfectly homogeneous field (Fig. 1.1a), the wind profile at each patch will be identical (at least when averaged over a timescale longer than the dominant characteristic turbulent frequency). In contrast, wind profiles over an irregularly heterogeneous field (Fig. 1.1b) will be diverse, reflecting the different surface properties for each patch, and therefore the overall wind profile, considered as an integration of all patches, differs significantly from the patch profiles at each patch of a heterogeneous field. Surface heterogeneity may be quasi-random and natural (i.e. patches of different vegetation reflecting natural succession dynamics) but may also be artificially introduced and structured. Fig. (1.1c) shows a homogeneous land surface with a line of trees as a windbreak, where the wind profile varies systematically around the windbreak. We may call this a quasi-heterogeneous land surface, somewhere between (a) and (b). Estimate land-atmosphere exchanges in a heterogeneous landscape requires an understanding of the spatial variation of fluxes, significantly increasing both the theoretical and experimental difficulties.

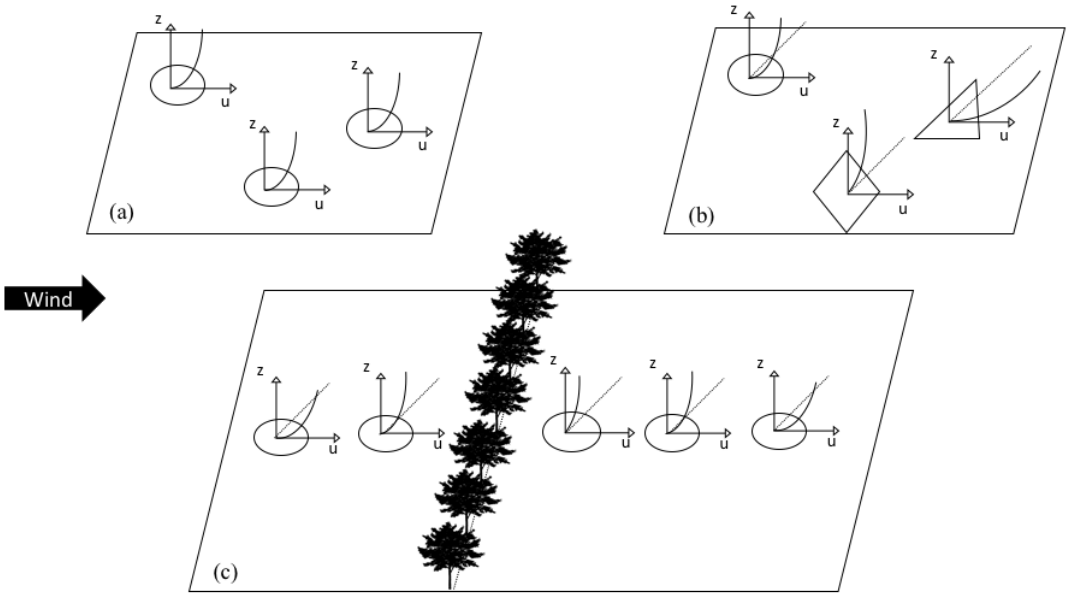

Figure 1.1. Wind profiles for different types of land surface. (a) Wind profile is constant across a homogeneous land surface. (b) Wind profile varies with different patches across a heterogeneous land surface. (c) Wind profile shows systematic variations across a quasi-heterogeneous land surface (i.e. a homogeneous surface with a windbreak). Image produced by Y. He on 21 Sep. 2016.

1.3 Eddy covariance- and chamber-based measurements

For the sake of compactness, here I review the two most commonly used methods of environmental gas flux measurement, eddy covariance (EC) and chamber-based methods. Both methods require measurements of other environmental driving variables (e.g. solar irradiance, air and soil temperature, wind speed and direction, water content, heat etc.) to form a complete observation system of land-atmosphere exchanges, but because such ancillary measurements are usually observations made using direct sensors, they are thus more reliable and less controversial than gas flux measurement which is, in fact, a derived product of multiple direct measurements. This derivation requires certain assumptions and thus inevitably introduces more uncertainties. This will become clearer in the details of flux measurements following below.

EC and chambers have been used to measure gas exchange between the atmosphere and land surface for decades (Baldocchi, 2003; Davidson et al., 2002). Each of these two independent measurement techniques, built on distinct theoretical bases, has advantages, as well as limitations, making each more or less suited to specific situations. Here we shall start with a brief retrospective of the chamber-based technique, a traditional tool (at least from the

perspective of the EC community) which can be traced back to early-stage soil science in 1920s (Lundegårdh, 1927).

The idea of chamber-based measurements, or enclosure-based measurements (Livingston and Hutchinson, 1995), is very straightforward. A cube or cylinder box is placed directly onto the target area, trapping a small amount of vegetation and air in the box, forming a closed space. A gas analyser is then connected to the box, sucking in air and measuring the changing concentration of gas (e.g. CO_2 and CH_4) over time. An example of a cubic chamber system is shown in Fig. (1.2). Chambers are easy to deploy and operate, reasonably adaptable to ecosystem type, and costs are relatively low compared with a EC-based system. Because chambers are predominately manually operated *in situ*, they have good controllability in real-time, bettered only by lab conditions. Moreover, the small area sampled makes chamber-based observations relatively homogeneous (i.e. there is negligible spatial variation within a chamber).

A number of drawbacks and limitations of this method are noteworthy. First, it can be very difficult to access certain field sites, such as wetlands and plateaus. Second, chambers have poor continuity in both spatial and temporal sampling. The spatial variation of fluxes at a field scale can only be interpolated based on a limited number of scattered, discrete observations. Similar issues occur in capturing temporal variation and model-based estimation is necessary for obtaining full temporal coverage and calculating long-term budgets. Thirdly, operating such system requires considerable and intensive labour efforts, further disturbing the ambient environment and introducing artificial uncertainties (Davidson et al., 2002; Rayment, 2000).

Figure 1.2. An example of chamber-based measurements using a cube at Cors Erddreiniog national nature reserve, Anglesey. Photo by Yufeng He on 17 Dec 2013.

EC-based measurement of gas exchanges is a micro-meteorology technique, and is fundamentally different from chamber-based technique. Here the term "eddy" refers to the smallest structure of turbulence and "covariance" means, loosely speaking, the statistical covariance between vertical wind speed and gas concentration[1]. A detailed definition of eddy covariance has been frequently reviewed elsewhere (Baldocchi, 2003; Baldocchi et al., 1988; Massman and Lee, 2002). Here I shall only have a quick description and deduction on the theoretical basis of eddy covariance. For given air mass density (ρ) and vertical wind speed (w), we may write the vertical transport rate (V) as,

$$V = \frac{\partial \rho w}{\partial z} \qquad (1.1)$$

where z is height above land surface.

[1] Using vertical wind speed is simply because we concerned primarily with the vertical flux. A similar process can be applied to estimating fluxes for any directions.

Using the Reynolds decomposition, for a certain period (e.g. 30 minutes) Eq. (1.1) can then be written as,

$$V = \frac{\partial(\overline{\rho}+\rho')(\overline{w}+w')}{\partial z} \qquad (1.2)$$

where $\bar{\rho}$ and $\overline{w}$ are the average density and wind speed during the given period. ρ' and w' are the instantaneous fluctuations of density and wind speed against the averages respectively. Eq. (1.2) can be simplified by assuming negligible mean density and speed (i.e. $\bar{\rho} = 0, \overline{w} = 0$),

$$V = \frac{\partial\overline{\rho' w'}}{\partial z} \qquad (1.3)$$

The $\overline{\ }$ simply indicates that we take the average value over the entire period. The vertical flux (F) can then be calculated by the integral of V from the land surface to the measurement height (h),

$$F = \int_{z=0}^{h} \frac{\partial\overline{\rho' w'}}{\partial z}\,\mathrm{dz} = \overline{\rho' w'(h)} - \overline{\rho' w'(0)} \qquad (1.4)$$

Since the transportation at surface layer is negligible in comparison to the flux at the measurement height, Eq. (1.4) becomes,

$$F = \overline{\rho' w'} \qquad (1.5)$$

Eq. (1.5) can also be interpreted as the covariance between mass density and vertical wind speed, which are measured by a gas analyser and an anemometer respectively in an EC-based observation system.

A typical EC-based system (Fig. 1.3) consists of an open path CO_2/H_2O analyser (LI-COR LI-7500), an open path CH_4 analyser (LI-COR LI-7700), a 3-D anemometer for measuring wind flow (Campbell CSAT3), a radiation sensor (LI-COR LI-190R), a data logger (Campbell CR3000) and power supplies. The height of the tower may vary with vegetation types and the area of land surface, where sufficient turbulence mixing and fetch of flux footprint need to be ensured. An orientation of the anemometer towards the dominant wind direction at the given geographical region is preferable so that the turbulence distortion effect is minimized.

After an initial set up of software and hardware, this system can be almost autonomous, requiring little maintenance and minimizing interference with ambient conditions. Most systems will take samples continuously at a high sampling frequency (e.g. 20 Hz) for a long

term (e.g. years), this being a major advantage over chamber-based techniques. Such systems thus provide a powerful tool towards a comprehensive understanding of the temporal variation of land-atmosphere exchanges (Baldocchi et al., 2001). A second major advantage compared to chambers is that EC is a relatively direct measure of fluxes at a field scale, obviating the need for the spatial interpolation and integration required by chamber methods.

Figure 1.3. A typical system of EC-based measurements at Cors Erddreiniog. Photo by Yingying Xuan on 9 Feb 2016, edited by Yufeng He.

Although an EC-based system has significant advantages, drawbacks and limitations are still noteworthy. Importantly, for EC to work, several micrometeorological conditions must be met (Burba and Anderson, 2010), namely:

- Incoming air flow is sufficiently turbulent
- Measurements are taken within the boundary layer
- Effective fetch (i.e. flux footprint) is adequate – fluxes are measured only at area of interest

- Terrain is horizontal and uniform[2]

Interestingly, none of these assumptions apply to a chamber-based system. Therefore, it is fair to say that neither EC nor chambers are inherently better than the other, and the use of two independent and complementary methods observing the same phenomenon can increase the confidence in our estimations of gas fluxes and oftentimes both methods are implemented concurrently in practice, Indeed, such an approach represents the most rigorous application of the scientific method.

1.4 Difficulties in quantifying exchanges at heterogeneous land surfaces

A heterogeneous land surface creates a flux source field with a significant degree of spatial variation, and capturing this is one of the main challenges for both chamber- and EC-based measurements. Emission factors for GHG fluxes generated from the quantification of total or mean GHG emissions from specific land use categories are typically based on chamber measurements that are relatively sparse in time and space, and any errors or uncertainty in the quantified emissions are directly and linearly propagated into national accounts (IPCC, 2000). What confidence do we have in the accuracy of our estimates? Very little, especially for CH_4 and N_2O where uncertainty spans orders of magnitude (Maljanen et al., 2010; Rayment and Jarvis, 2000; Rochette and Eriksen-Hamel, 2008; Venterea et al., 2009), and limited sample size inhibits a robust estimation of flux by chamber-based measurements (He et al., 2016). In some systems, particularly agricultural ones, intensive soil management has the effect of reducing spatial heterogeneity to manageable levels, thereby reducing the number of measurements required to capture population variance accurately, however this is not generally true. In most systems, spatial heterogeneity combined with limited sample size presents considerable opportunity for biases to enter into our measurements such that even when attempts are made to stratify sampling according to known sources of variance, uncertainty estimates remain large (Raupach et al., 2005).

While EC-based measurements at the whole ecosystem or canopy-scale have the advantage (compared to chambers) of integrating over the entire area (Baldocchi, 2003)**,** this integration makes observations less spatially explicit in terms of describing fluxes at any given point on the heterogeneous land surface. An EC-measurement signal consists of superposition of partial signals from a large area, the analysis of which is not problematic given a

[2] Uniformity, in fact, is only a requirement for idealised situations. With the flux footprint models, we can stretch this idea to include patchiness and address non-uniform problems.

homogeneous source field[3]. In a heterogeneous land surface, however, where the flux source exhibits large spatial variation, the integrated signal becomes more difficult to interpret. Specifically, this requires advanced inverse modelling techniques to decompose a point signal (from the met tower) back into its component sources, commonly known as the flux footprint. This process is particularly necessary for (a)- estimating accurately the total flux budget from the whole region and (b) comparing flux estimates between EC- and chamber measurements. The former (a) is simply because the EC-measured signal samples the area directly upwind and therefore tends to focus on the area determined by the prevailing wind direction therefore to derive an explicit map of the entire flux source are we need to separate out and estimate emissions for areas that are not covered by the prevailing wind. The latter (b) is the result of the mismatch in the spatial extent of EC- and chamber-based measurements. A direct comparison of methods is only feasible when this spatial representation gap is bridged. Flux footprint models are the main tools used to address both these problems.

1.5 Flux footprint models

The initial development of flux footprint models actually had little to do with GHG fluxes, but was motivated by a practical interest in the dispersion of atmospheric pollutants and the exchange of momentum, heat and water vapour in the atmospheric boundary layer (Pasquill, 1972). In Pasquill's paper, the concept of effective fetch was introduced for the first time to address the problem of surface inhomogeneity. Since then there have been a number of developments in modifying footprint models to describe transfer processes over heterogeneous land-surfaces (Schmid, 2002; Schuepp and Leclerc, 1990), where the spatial representativeness of flux measurement (i.e. both horizontal and vertical variations) needs to be considered and estimated. The source area is the fraction of the surface (predominantly upwind) that contains effective sources and sinks contributing to measurements at any given point (Kljun et al., 2002). The term "footprint" can then be defined as the relative contribution of each element of the source area to the measured vertical flux or concentration (Kljun et al., 2002). In application, footprints is typically described as a 2-D probability distribution function of the contribution from each element, called the footprint function or the source weight function (Schmid, 1994). More specifically, the footprint function f is implicitly given by the integral equation over the entire source area (Schmid, 2002):

[3] The problem of sample size deficiency for chamber-based measurements is also trivial in a homogeneous source field.

$$\eta(\vec{r}) = \int_{\Re} Q_\eta(\vec{r}+\vec{r}')\, f(\vec{r},\vec{r}')d\vec{r}' \qquad (1.1)$$

where η is the measured concentration or flux at the sensor location $\vec{r}$. Q_η is the emission rate [4] at the position $\vec{r}+\vec{r}'$. f is the flux footprint function satisfying the relation, $\int_{\Re} f(\vec{r},\vec{r}')d\vec{r}' = 1$.

Again, f (dimensionless) represents the probability distribution over the source area and can be seen as the weights attached to the emission rate Q_η. An estimation of the footprint function f is not straightforward and several theoretical approaches have been developed over the past decades. There are four types of footprint models in general (Vesala et al., 2008): (i) analytical models, (ii) Lagrangian stochastic particle dispersion models, (iii) large-eddy simulations (LES) and (iv) ensemble-averaged closure models. Readers are referred to a wide range of literature (Foken and Leclerc, 2004; Kljun et al., 2004b; Schmid, 2002; Vesala et al., 2008) for details on the description and validation of these models.

For the practical purposes of understanding EC measurements at the field-scale, stochastic particle dispersion models provide the most tractable and computationally-efficient approach, and in chapter 4, a parameterised two-dimensional flux footprint model (Kljun et al., 2015, 2004a) is used for footprint simulations over a heterogeneous fen/peatland in the UK.

1.6 Modelling methodology

1.6.1 Modelling and gap filling CO_2 & CH_4 flux

Inferential modelling is a general term that covers both prediction (i.e. extrapolation, saying something about the future) and data gap filling (i.e. interpolation, saying something about the past) These two purposes are exactly the two main motives that have stimulated developments of GHG flux models and gap filling strategies. In particular, an inference is normally conducted on the temporal variation in flux values, i.e. interpolation and/or extrapolation of a time series. Samples of chamber-based measurement, for instance, are often sparse in time (e.g. monthly) and regression models against some environmental driving variables are used to generate a flux series with a better temporal resolution (e.g. half-hourly). EC-based measurements, on the other hand, though having finer temporal resolution, often

[4] Conventionally, positive value of Q_η means an exchange from land to atmosphere (source) and negative value means the opposite direction (sink).

have a significant amount of data gaps to fill as the result of technical failure or meteorological conditions that do not meet underlying theoretical requirements.

Traditional modelling and gap filling approaches typically take a linear perspective on data, either using data derived statistically from a moving window, or using a simple function based on a best-guess understanding of the processes driving exchange (Table 1-1). The former approach is limited in its ability to capture non-linear trends, and the latter is limited in situations where the flux response to driving variables is poorly understood or unknown (e.g. the response of gas exchange to, for example, water table depth in wetlands). The drawbacks of these methods are especially notable for complex processes, the mechanism of which is less understood, such as CH_4 and N_2O flux. Estimating CH_4 emission events, for example, is much more complex than CO_2. CH_4 flux has a higher emission variability than CO_2 flux, often involving multiple events (Dengel et al., 2013). For example, precipitation and water table can have a lagged effect on CH_4 fluxes (Bubier et al., 1995), making its estimation unreliable if these effects were not considered.

Table 1-1 Modelling and gap filling methods for CO_2 & CH_4 flux from the literatures

GHG Type	CO_2 (NEE)	CH_4
Methods	1. NEE partition: ***Daytime***: $F = -(\frac{\alpha \times PPFD \times \beta}{\alpha \times PPFD + \beta} - x)$ (Michaelis-Menten Equation) ***Night-time***: $R = R_{10} e^{E_0(\frac{1}{283.15} - \frac{1}{T - T_0})}$ (Lloyd and Taylor, 1994; Veenendaal et al., 2007)	1. $F_{CH4} = a * F_{CO2} + b \; or \; F_{CH4} = e^{48.5 - \frac{12000}{T+273}}$ (Hargreaves et al., 2001)
		2. $F = a * e^{b * T_{soil}}$ (Rinne et al., 2007; Yu et al., 2013)
		3. $F = \alpha * \beta^{(T-10)/10}$ (Long et al., 2010)
	2. Look-up tables (Falge et al., 2001)	4. $F_{CH4} = a * b^{\frac{T - T_{ref}}{10}} * c^{(u_* - u_{*ref})}$ (Wille et al., 2008)
	3. Marginal distribution sampling (MDS) (Reichstein et al., 2005)	5. $F_{CH4} = a * T^2 + b * T + c$, T is air temp (Baker-Blocker et al., 2011)
	4. Mean diurnal variation (MDV) (Falge et al., 2001)	6. $log(F_{CH4+5}) = a + b * Z_{WT}^2 + c * Z_{WT}^3 + d * T_s + e * Z_{WT} * T_s$ $log(F_{CH4+5}) = a + b * Z_{WT} + c * Z_{WT}^2 + d * Z_{WT}^3 + e * T_s$ (Olefeldt et al., 2013)
	5. Artificial neural network (Braswell et al., 2005; Papale and Valentini, 2003)	7. Neural networks (Dengel et al., 2013)

In chapter 3, we introduce a state of the art technique known as image inpainting to fill gaps in a two dimensional representation of the one-dimensional data, i.e. the flux fingerprint[5]. This has the advantage that any temporal structure (i.e. day to day covariance) is better incorporated into gaps in the flux signal without implying any particular functional response to driving environmental variables. In this way, data gaps are filled solely using information contained in robust, primary data.

[5] Note that flux fingerprint and flux footprint are in no way related

1.6.2 Regression methods

Traditional regression methods, whether linear or non-linear, are typically based on ordinary least square (OLS). These methods make some assumptions about the underlying structure of variance which may not be appropriate in all cases. In chapter 4 we introduce two advanced regression methods that have distinct advantages over the traditional methods, and as these methods have received little attention in environmental science, it is worth taking a brief look at the basis.

Regression methods (or regression analyses) are widely used in scientific research for establishing relationships between a dependent variable (y) and independent variables (x_i). In terms of data analysis, regression is used in two common ways: 1) to measure the linear relationship between exactly two datasets (e.g. two sets of observations, two sets of modelling results, or one set of observations and one set of modelling results) by fitting the linear equation ($\overrightarrow{y_1} = \alpha \cdot \overrightarrow{y_2} + \beta$); or 2) to identify the relationship between a dependent variable and multiple independent variables, commonly known as multivariate regression. The orthogonal and Lasso regression methods shown below are related to 1) and 2) respectively.

1.6.2.1 The orthogonal regression

When two series of observations or estimations both contain random errors, traditional regression analysis based on the ordinary least square (OLS) is not strictly suitable for determining the nature of the correlation between these because errors in only one single direction (e.g. vertical = errors in the "dependent" variable) are considered, although errors also exist in other (orthogonal) direction (e.g. horizontal = errors in the "independent" variable). In chapter 4, The orthogonal regression (Leng et al., 2007) which is based on total least square (TLS) and minimises errors in both the vertical and horizontal directions is used to implement regression analyses of two independent estimations of NEE and of CH_4 flux (Eq. 1.2). The regression coefficients can be easily calculated by using the principle components (Eq. 1.3):

$$y = \beta_1 x + \beta_0 \qquad (1.2)$$

$$\beta_1 = \frac{v_y}{v_x}\ ,\ \beta_0 = \bar{y} - \beta_1 \bar{x} \qquad (1.3)$$

where (v_x, v_y) is the first eigenvector of the 2*2 covariance matrix constructed from (x, y), a two column matrix made up of the time series of NEE and CH_4 flux. $\bar{x}$ and $\bar{y}$ are the mean values of x and y respectively. Since the traditional way of calculating the coefficient of determination (r^2) is not appropriate for TLS, the squared Pearson's correlation coefficient is used to show the strength of the linear correlation between x and y.

1.6.2.2 The Lasso regression

Traditional regression methods (e.g. linear regression and stepwise regression) are based on least-square minimization, that is the regression coefficients are determined by minimizing the summation of squared residuals. Despite its simplicity, the estimation is prone to extreme values and more importantly, for the purpose of this study, to overfitting (e.g. stepwise regression) (Hastie et al., 2009). Moreover, in the process of multivariate analysis such as the stepwise regression, non-zero coefficients are not helpful to choose the trivial terms that we expect to remove. Previous studies have shown that the traditional regression methods based on the simple least square are unreliable to fulfil both needs (e.g. Tibshirani, 1996). The Lasso regression is thus developed to mitigate the drawbacks by regularizing the minimization of the least-square as follows (Hastie et al., 2009),

$$\min_{\beta_0,\beta}\left(\frac{1}{2N}\sum_{i=1}^{N}(y_i-\beta_0-{x_i}^T\beta)^2+\lambda\sum_{j=1}^{p}|\beta_j|\right) \qquad (1.4)$$

where N is the number of samples. y_i is the CH_4 flux. x_i is a combination of the normalized driven variables, a vector of p values at observation i. λ is a nonnegative regulation parameter. The parameters β_0 and β are regression coefficients to be determined by the minimization process. 5-fold cross validation[6] was used to evaluate the model with different values of λ. The Lasso tends to find a sparse solution by setting some coefficients to 0, which automatically "select" an optimized model based on its performance on the cross validation datasets. It is also more robust in terms of preventing overfitting because of the existence of the regulation term (i.e. bounded coefficients).

[6] In k-fold cross-validation, the original sample is randomly divided into k subsamples. Of the k subsamples, 1 subsample is used as the validation set, and the remaining k-1 subsamples are used as training set. The cross-validation process is repeated k times (the folds), with each of the k subsamples used exactly once as the validation set. The k results from the folds can then be averaged to produce a single estimation.

1.7 Thesis aims and structure

Overall, this thesis aims to use advance mathematical techniques to improve the measurement of vectors (i.e. fluxes of scalar quantities) in the types of heterogeneous landscapes found in the real world.

1. To develop generic methods for improving the estimates of gaseous carbon exchange at heterogeneous land surfaces.

This thesis aims to reduce the estimation errors of gaseous carbon flux introduced by the two most commonly used methods, chamber and EC. In chapter 2, a two-stage sampling strategy is developed to improve the sampling accuracy of chamber-based measurements. In chapter 3, a robust method based on image inpainting is developed to gap-filling eddy covariance (EC) measurements and the uncertainty introduced by any gap-filling method is thoroughly investigated.

2. To improve overall confidence in flux measurements by reconciling two independent methods of flux measurement

Because the "true" surface flux is impossible to evaluate in practice, verification of fluxes is possible only through reconciling estimates based on multiple independent field-based estimates. In chapter 4, such a comparison is conducted for long-term measurements of CO_2 and CH_4 fluxes at a heterogeneous UK fen.

3. To characterise the transfer of momentum around structural landscape features

The heterogeneity of fluxes across a landscape can have positive effects, for example where structural heterogeneity impacts wind-speed to the benefit of animal or plant micro-climate. In chapter 5, a simple model is developed and parameterised to characterise the wind-speed reduction around a windbreak, and how this impacts crop and sheep productivity through reduced wind-chill effects.

This thesis is structured around a series of papers (chapters 2-5), each as submitted to the scientific press (but without journal-specific formatting), i.e. conclusions are necessarily concise. The methods developed among chapters are summarised as:

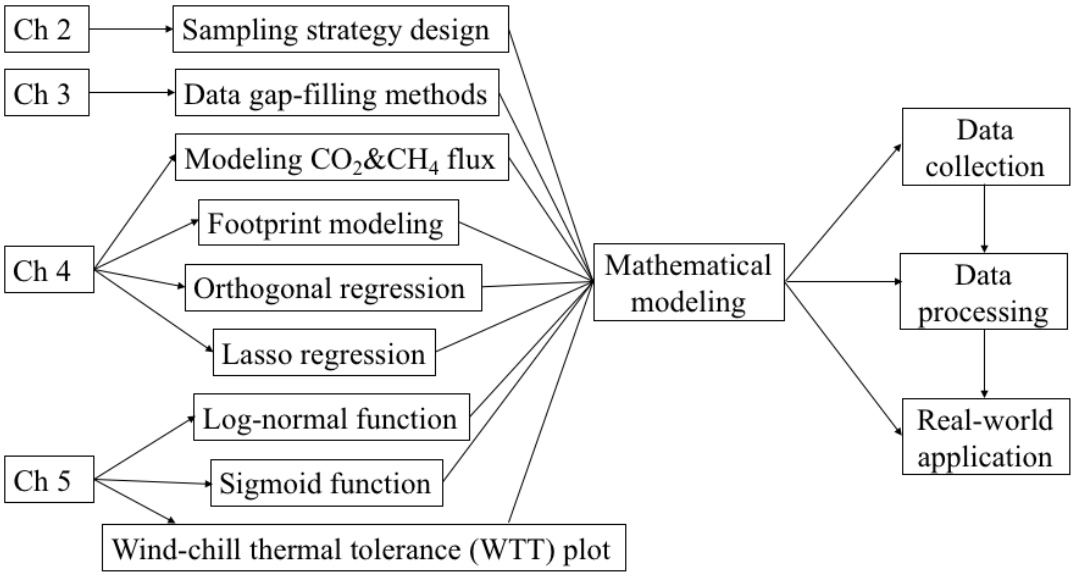

Figure 1.4 Thesis structure and methods generated/developed in the four main chapters.

Although the whole thesis deals with land-atmosphere exchange, the study object is not directly equivalent between chapter 2-4 and chapter 5: the former studies surface carbon exchange, in the form of either CO_2 flux or CH_4 flux; the latter studies momentum exchange, in the form of wind speed affected by windbreaks. Carbon exchange is a special type of mass exchange, which is mainly driven by the energy exchange such as momentum. In fact, this relationship can be seen more clearly in the fundamentals of the eddy-covariance technique (Eq. 1.5), where the mass exchange is not a direct observation, but an estimated result from the momentum exchange. Therefore, surface heterogeneity would modify the local microclimate and energy exchange, which would ultimately determine the transport of any substances between the atmosphere and land surface.

Publication status of each main chapter:

- He, Y., Gibbons, J., Rayment, M., (2016) A two-stage sampling strategy improves chamber-based estimates of greenhouse gas fluxes, Agricultural and Forest Meteorology, doi: 10.1016/j.agrformet. 2016.06.015
- He, Y. and Rayment, M. (2016) A robust gap-filling method for Net Ecosystem Exchange based on Cahn-Hilliard inpainting, Geosci. Model Dev. Discuss., doi:10.5194/gmd-2016-108, (In review)

- He, Y., Ridley, L., Brown, E., Callaghan, N., Rayment, M., (2016) Greenhouse gas exchange from a heterogeneous UK fen: Understanding the difference between eddy covariance and chamber measurements, JGR: Biogeoscience (In review)
- He, Y., Jones, P., Rayment, M., (2016) A simple parameterisation of windbreak effects on wind speed, thermal microclimate, crop productivity and livestock welfare, Agriculture and forest meteorology (In review)

1.8 The Defra project SP1210

Aims 1 and 2 were completed within the framework of the Defra project SP1210: Lowland peatland systems in England and Wales – evaluating greenhouse gas fluxes and carbon balances. Lowland peatlands account for 15% (Joint Nature Conservation Committee, 2011) of the total peat area and 50% of the total GHG emissions from peat in the UK (Worrall et al., 2005). The project aimed to address existing data and knowledge gaps through a comprehensive and integrated programme of measurements at a large number of representative sites across multiple lowland peat regions of England and Wales, ranging from conservation-managed fens and raised bogs under semi-natural vegetation, through sites under extensive and intensive agricultural grassland management, to highly drained and modified arable and peat extraction sites (Evans et al., 2016). The study shown in chapter 4 focused on a heterogeneous high-nutrient fen at Cors Erddreiniog in Anglesey, Wales. This site comprises 85% of bogs, marshes, water fringed vegetation and fens, 13% of grassland and woodland and 2% of inland water bodies. Both chamber- and EC-based measurements were implemented from 2013 to 2015. Refer to Chapter 4 for a detailed description of the field site and flux measurements.

1.9 Project: MULTI-LAND

Aim 3 was completed within the framework of the MULTI-LAND project: Enhancing agricultural productivity and ecosystem service resilience in multifunctional landscapes. Intensively managed agricultural systems, such as on many livestock farms in Wales, can become less resilient to extreme events, such as drought or floods, as a result of the erosion of ecosystem functioning. In contrast, the presence of hedgerows and trees in pasture can increase livestock productivity through the provision of shelter, whilst creating a multifunctional landscape where synergies in agricultural or ecological niches may be exploited to sustainably intensify farming practices. With a partnership among Bangor

University, Aberystwyth University, CEH, Woodland Trust, National Trust, Natural Resources Wales, Coed Cymru and Snowdonia NPA, this project aims at promoting sustainable agricultural practices, exploiting potential synergies in tree-livestock-soil interactions in the landscape, developing understanding of ruminant behaviour and nutrition, and improving ecosystem service resilience. In this study, field experiments are implemented at the Henfaes Research Platform of Bangor University. Please refer to Chapter 5 for details on the site description.

1.10 References

Adger, W.N., Dessai, S., Goulden, M., Hulme, M., Lorenzoni, I., Nelson, D.R., Naess, L.O., Wolf, J., Wreford, A., 2009. Are there social limits to adaptation to climate change? Clim. Change. doi:10.1007/s10584-008-9520-z

AMS Glossary, 2016. Micrometeorology (web page) [WWW Document]. Am. Meteorol. Soc. URL http://glossary.ametsoc.org/wiki/Micrometeorology (accessed 8.28.16).

André, J.C., Bougeault, P., Goutorbe, J.P., 1990. Regional estimates of heat and evaporation fluxes over non-homogeneous terrain. Examples from the HAPEX-MOBILHY programme. Boundary-Layer Meteorol. 50, 77–108. doi:10.1007/BF00120519

Baker-Blocker, A., Donahue, T.M., Mancy, K.H., 2011. Methane flux from wetlands areas. Tellus A 245–250. doi:10.3402/tellusa.v29i3.11353

Baldocchi, D., Falge, E., Gu, L., Olson, R., 2001. FLUXNET: A new tool to study the temporal and spatial variability of ecosystem-scale carbon dioxide, water vapor, and energy flux densities. Bull. Am. Meteorol. Soc. 82, 2415. doi:10.1175/1520-0477(2001)082<2415:FANTTS>2.3.CO;2

Baldocchi, D.D., 2003. Assessing the eddy covariance technique for evaluating carbon dioxide exchange rates of ecosystems: Past, present and future. Glob. Chang. Biol. 9, 479–492. doi:10.1046/j.1365-2486.2003.00629.x

Baldocchi, D.D., Hicks, B.B., Meyers, T.P., 1988. Measuring biosphere-atmosphere exchanges of biologically related gases with micrometeorological methods. Ecology. doi:10.2307/1941631

Bonan, G.B., 2008. Forests and climate change: forcings, feedbacks, and the climate benefits of forests. Science (80-.). 320, 1444–1449. doi:10.1126/science.1155121

Braswell, B.H., Sacks, W.J., Linder, E., Schimel, D.S., 2005. Estimating diurnal to annual ecosystem parameters by synthesis of a carbon flux model with eddy covariance net ecosystem exchange observations. Glob. Chang. Biol. 11, 335–355. doi:10.1111/j.1365-2486.2005.00897.x

Bubier, J.L., Moore, T.R., Juggins, S., 1995. Predicting Methane Emission from Bryophyte Distribution in Northern Canadian Peatlands. Ecology 76, 677–693. doi:10.2307/1939336

Burba, G., Anderson, D., 2010. A brief practical guide to eddy covariance flux measurements:

principles and workflow examples for scientific and industrial applications. Li-Cor Biosciences.

Cai, X., Leclerc, M.Y., 2007. Forward-in-time and backward-in-time dispersion in the convective boundary layer: The concentration footprint. Boundary-Layer Meteorol. 123, 201–218. doi:10.1007/s10546-006-9141-x

Ciais, P., Reichstein, M., Viovy, N., Granier, a, Ogée, J., Allard, V., Aubinet, M., Buchmann, N., Bernhofer, C., Carrara, a, Chevallier, F., De Noblet, N., Friend, a D., Friedlingstein, P., Grünwald, T., Heinesch, B., Keronen, P., Knohl, a, Krinner, G., Loustau, D., Manca, G., Matteucci, G., Miglietta, F., Ourcival, J.M., Papale, D., Pilegaard, K., Rambal, S., Seufert, G., Soussana, J.F., Sanz, M.J., Schulze, E.D., Vesala, T., Valentini, R., 2005. Europe-wide reduction in primary productivity caused by the heat and drought in 2003. Nature 437, 529–533. doi:10.1038/nature03972

Davidson, E.A., Savage, K., Verchot, L. V, Navarro, R., 2002. Minimizing artifacts and biases in chamber-based measurements of soil respiration. Agric. For. Meteorol. 113, 21–37. doi:10.1016/S0168-1923(02)00100-4

Dengel, S., Zona, D., Sachs, T., Aurela, M., Jammet, M., Parmentier, F.J.W., Oechel, W., Vesala, T., 2013. Testing the applicability of neural networks as a gap-filling method using CH4 flux data from high latitude wetlands. Biogeosciences 10, 8185–8200. doi:10.5194/bg-10-8185-2013

Evans, C., Morrison, R., Burden, A., Williamson, J., Baird, A., Brown, E., Callaghan, N., Chapman, P., Cumming, A., Dean, H., Dixon, S., Dooling, G., Evans, J., Gauci, V., Grayson, R., Haddaway, N., He, Y., Heppell, K., Holden, J., Hughes, S., Kaduk, J., Jones, D., Matthews, R., Menichino, N., Misselbrook, T., Page, S., Pan, G., Peacock, M., Rayment, M., Ridley, L., Robinson, I., Scowen, M., Stanley, K., Worrall, F., 2016. Lowland peatland systems in England and Wales – evaluating greenhouse gas fluxes and carbon balances. Final report to Defra on Project SP1210, Centre for Ecology and Hydrology, Bangor.

Falge, E., Baldocchi, D., Olson, R., Anthoni, P., Aubinet, M., Bernhofer, C., Burba, G., Ceulemans, R., Clement, R., Dolman, H., Granier, A., Gross, P., Grünwald, T., Hollinger, D., Jensen, N.O., Katul, G., Keronen, P., Kowalski, A., Lai, C.T., Law, B.E., Meyers, T., Moncrieff, J., Moors, E., Munger, J.W., Pilegaard, K., Rannik, Ü., Rebmann, C., Suyker, A., Tenhunen, J., Tu, K., Verma, S., Vesala, T., Wilson, K., Wofsy, S., 2001. Gap filling strategies for defensible annual sums of net ecosystem exchange. Agric. For. Meteorol. 107, 43–69. doi:10.1016/S0168-1923(00)00225-2

Falkowski, P., Scholes, R.J., Boyle, E.E.A., Canadell, J., Canfield, D., Elser, J., Gruber, N., Hibbard, K., Högberg, P., Linder, S., 2000. The global carbon cycle: a test of our knowledge of earth as a system. Science (80-.). 290, 291–296.

Foken, T., Leclerc, M.Y., 2004. Methods and limitations in validation of footprint models, in: Agricultural and Forest Meteorology. pp. 223–234. doi:10.1016/j.agrformet.2004.07.015

Gash, J.H.C., 1986. A note on estimating the effect of a limited fetch on micrometeorological evaporation measurements. Boundary-Layer Meteorol. 35, 409–413.

Goulden, M.L., Winston, G.C., Mcmillan, A.M.S., Litvak, M.E., Read, E.L., Rocha, A. V., Rob Elliot, J., 2006. An eddy covariance mesonet to measure the effect of forest age on land-atmosphere exchange. Glob. Chang. Biol. 12, 2146–2162. doi:10.1111/j.1365-

2486.2006.01251.x

Hargreaves, K.J., Fowler, D., Pitcairn, C.E.R., Aurela, M., 2001. Annual methane emission from Finnish mires estimated from eddy covariance campaign measurements. Theor. Appl. Climatol. 70, 203–213. doi:10.1007/s007040170015

Hastie, T., Tibshirani, R., Friedman, J., 2009. The Elements of Statistical Learning. Data Mining, Inference, and Prediction, Springer Series in Statistics. doi:10.1007/b94608

He, Y., Gibbons, J., Rayment, M., 2016. A two-stage sampling strategy improves chamber-based estimates of greenhouse gas fluxes. Agric. For. Meteorol. 228, 52–59. doi:10.1016/j.agrformet.2016.06.015

He, Y., Rayment, M., 2016. A robust gap-filling method for Net Ecosystem Exchange based on Cahn–Hilliard inpainting. Geosci. Model Dev. Discuss. doi:10.5194/gmd-2016-108

Hollinger, D.Y., Richardson, A.D., 2005. Uncertainty in eddy covariance measurements and its application to physiological models. Tree Physiol. 25, 873–885. doi:10.1093/treephys/25.7.873

Howden, S.M., Soussana, J.-F., Tubiello, F.N., Chhetri, N., Dunlop, M., Meinke, H., 2007. Adapting agriculture to climate change. Proc. Natl. Acad. Sci. 104, 19691–19696.

IPCC, 2000. Land Use, Land-Use Change, and Forestry, Forestry. doi:DOI: 10.2277/0521800838

Joint Nature Conservation Committee, 2011. Towards an assessment of the state of UK Peatlands, JNCC report.

Jones, P.D., New, M., Parker, D.E., Martin, S., Rigor, I.G., 1999. Surface air temperature and its changes over the past 150 years. Rev. Geophys. 37, 173–199. doi:10.1029/1999RG900002

Kaimal, J.C., Businger, J. a., 1963. A Continuous Wave Sonic Anemometer-Thermometer. J. Appl. Meteorol. doi:10.1175/1520-0450(1963)002<0156:ACWSAT>2.0.CO;2

Kalnay, E., Cai, M., 2003. Impact of urbanization and land-use change on climate. Nature 423, 528–531. doi:10.1038/nature01649.1.

Kljun, N., Calanca, P., Rotach, M.W., Schmid, H.P., 2015. A simple two-dimensional parameterisation for Flux Footprint Prediction (FFP). Geosci. Model Dev. 8, 3695–3713. doi:10.5194/gmd-8-3695-2015

Kljun, N., Calanca, P., Rotach, M.W., Schmid, H.P., 2004a. A simple parameterisation for flux footprint predictions. Boundary-Layer Meteorol. 112, 503–523. doi:10.1023/B:BOUN.0000030653.71031.96

Kljun, N., Kastner-Klein, P., Fedorovich, E., Rotach, M.W., 2004b. Evaluation of Lagrangian footprint model using data from wind tunnel convective boundary layer, in: Agricultural and Forest Meteorology. pp. 189–201. doi:10.1016/j.agrformet.2004.07.013

Leclerc, M.Y., Foken, T., Savage, M.J., Göckede, M., 2014. Footprints in micrometeorology and ecology, Footprints in Micrometeorology and Ecology. doi:10.1007/978-3-642-54545-0

Leng, L., Zhang, T., Kleinman, L., Zhu, W., 2007. Ordinary least square regression, orthogonal regression, geometric mean regression and their applications in aerosol

science. J. Phys. Conf. Ser. 78, 12084. doi:10.1088/1742-6596/78/1/012084

Lettau, H., Davidson, B., 1957. Exploring the atmosphere's first mile. Symposium Publications Division, Pergamon Press.

Livingston, G.P., Hutchinson, G.L., 1995. Enclosure-based measurement of trace gas exchange: applications and sources of error, Biogenic Trace Gases: Measuring Emissions from Soil and Water.

Lloyd, J., Taylor, J., 1994. On the temperature dependence of soil respiration. Funct. Ecol. 8, 315–323. doi:10.2307/2389824

Long, K.D., Flanagan, L.B., Cai, T., 2010. Diurnal and seasonal variation in methane emissions in a northern Canadian peatland measured by eddy covariance. Glob. Chang. Biol. 16, 2420–2435. doi:10.1111/j.1365-2486.2009.02083.x

Lundegårdh, H., 1927. Carbon dioxide evolution of soil and crop growth. Soil Sci. 23, 417–453.

Maljanen, M., Sigurdsson, B.D., Gu\dhmundsson, J., Óskarsson, H., Huttunen, J.T., Martikainen, P.J., 2010. Greenhouse gas balances of managed peatlands in the Nordic countries - present knowledge and gaps. Biogeosciences 7, 2711–2738. doi:10.5194/bg-7-2711-2010

Massman, W.J., Lee, X., 2002. Eddy covariance flux corrections and uncertainties in long-term studies of carbon and energy exchanges. Agric. For. Meteorol. 113, 121–144.

Moncrieff, J., 2004. Surface turbulent fluxes, in: Vegetation, Water, Humans and the Climate. Springer, pp. 173–182.

Moncrieff, J., Malhi, Y., Leuning, R., 1996. The propagation of errors in long-term measurements of land-atmosphere fluxes of carbon and water. Glob. Chang. Biol. 231–240.

Olefeldt, D., Turetsky, M.R., Crill, P.M., Mcguire, A.D., 2013. Environmental and physical controls on northern terrestrial methane emissions across permafrost zones. Glob. Chang. Biol. 19, 589–603. doi:10.1111/gcb.12071

Papale, D., Reichstein, M., Aubinet, M., Canfora, E., Bernhofer, C., Kutsch, W., Longdoz, B., Rambal, S., Valentini, R., Vesala, T., Yakir, D., 2006. Towards a standardized processing of Net Ecosystem Exchange measured with eddy covariance technique: algorithms and uncertainty estimation. Biogeosciences 3, 571–583. doi:10.5194/bg-3-571-2006

Papale, D., Valentini, R., 2003. A new assessment of European forests carbon exchanges by eddy fluxes and artificial neural network spatialization. Glob. Chang. Biol. 9, 525–535. doi:10.1046/j.1365-2486.2003.00609.x

Pasquill, F., 1972. Some aspects of boundary layer description. Q. J. R. Meteorol. Soc. 98, 469–494. doi:10.1002/qj.49709841702

Raupach, M.R., Rayner, P.J., Barrett, D.J., DeFries, R.S., Heimann, M., Ojima, D.S., Quegan, S., Schmullius, C.C., 2005. Model-data synthesis in terrestrial carbon observation: methods, data requirements and data uncertainty specifications. Glob. Chang. Biol. 11, 378–397. doi:10.1111/j.1365-2486.2005.00917.x

Rayment, M.B., 2000. Closed chamber systems underestimate soil CO_2 efflux. Eur. J. Soil Sci. 51, 107–110.

Rayment, M.B., Jarvis, P.G., 2000. Temporal and spatial variation of soil CO2 efflux in a Canadian boreal forest. Soil Biol. Biochem. 32, 35–45. doi:10.1016/S0038-0717(99)00110-8

Reichstein, M., Falge, E., Baldocchi, D., Papale, D., Aubinet, M., Berbigier, P., Bernhofer, C., Buchmann, N., Gilmanov, T., Granier, A., Grünwald, T., Havránková, K., Ilvesniemi, H., Janous, D., Knohl, A., Laurila, T., Lohila, A., Loustau, D., Matteucci, G., Meyers, T., Miglietta, F., Ourcival, J.M., Pumpanen, J., Rambal, S., Rotenberg, E., Sanz, M., Tenhunen, J., Seufert, G., Vaccari, F., Vesala, T., Yakir, D., Valentini, R., 2005. On the separation of net ecosystem exchange into assimilation and ecosystem respiration: Review and improved algorithm. Glob. Chang. Biol. 11, 1424–1439. doi:10.1111/j.1365-2486.2005.001002.x

Rinne, J., Riutta, T., Pihlatie, M., Aurela, M., Haapanala, S., Tuovinen, J.P., Tuittila, E.S., Vesala, T., 2007. Annual cycle of methane emission from a boreal fen measured by the eddy covariance technique, in: Tellus, Series B: Chemical and Physical Meteorology. pp. 449–457. doi:10.1111/j.1600-0889.2007.00261.x

Rochette, P., Eriksen-Hamel, N.S., 2008. Chamber Measurements of Soil Nitrous Oxide Flux: Are Absolute Values Reliable? Soil Sci. Soc. Am. J. 72, 331. doi:10.2136/sssaj2007.0215

Schmid, H.P., 2002. Footprint modeling for vegetation atmosphere exchange studies: a review and perspective. Agric. For. Meteorol. 113, 159–183. doi:10.1016/S0168-1923(02)00107-7

Schmid, H.P., 1994. Source areas for scalars and scalar fluxes. Boundary-Layer Meteorol. 67, 293–318. doi:10.1007/BF00713146

Schmidt, H., Schumann, U., 1989. Coherent structure of the convective boundary layer derived from large-eddy simulations. J. Fluid Mech. 200, 511–562.

Schuepp, P., Leclerc, M., 1990. Footprint prediction of scalar fluxes from analytical solutions of the diffusion equation. Boundary-Layer … 355–373.

Sellers, P.J., 1997. Modeling the Exchanges of Energy, Water, and Carbon Between Continents and the Atmosphere. Science (80-.). 275, 502–509. doi:10.1126/science.275.5299.502

Sellers, P.J., Hall, F.G., Asrar, G., Strebel, D.E., Murphy, R.E., 1988. The first ISLSCP field experiment (FIFE). Bull. Am. Meteorol. Soc. 69, 22–27.

Stern, N.H., 2007. The economics of climate change: the Stern review. cambridge University press, New York.

Tibshirani, R., 1996. Regression Selection and Shrinkage via the Lasso. J. R. Stat. Soc. B. doi:10.2307/2346178

Unsworth, M.H., Ormrod, D.P., 2013. Effects of gaseous air pollution in agriculture and horticulture. Butterworth-Heinemann.

Veenendaal, E.M., Kolle, O., Leffelaar, P.A., Schrier-Uijl, A.P., Van Huissteden, J., Van Walsem, J., Möller, F., Berendse, F., 2007. CO_2 exchange and Carbon balance in two

grassland sites on eutrophic drained peat soils. Biogeosciences Discuss. doi:10.5194/bgd-4-1633-2007

Venterea, R.T., Spokas, K.A., Baker, J.M., 2009. Accuracy and precision analysis of chamber-based nitrous oxide gas flux estimates. Soil Sci. Soc. Am. J. 73, 1087–1093. doi:10.2136/sssaj2008.0307

Vesala, T., Kljun, N., Rannik, U., Rinne, J., Sogachev, a, Markkanen, T., Sabelfeld, K., Foken, T., Leclerc, M.Y., 2008. Flux and concentration footprint modelling: state of the art. Environ. Pollut. 152, 653–66. doi:10.1016/j.envpol.2007.06.070

Wille, C., Kutzbach, L., Sachs, T., Wagner, D., Pfeiffer, E.-M.M., 2008. Methane emission from Siberian arctic polygonal tundra: eddy covariance measurements and modeling. Glob. Chang. Biol. 14, 1395–1408. doi:10.1111/j.1365-2486.2008.01586.x

Wohlfahrt, G., Fenstermaker, L.F., Arnone Iii, J.A., 2008. Large annual net ecosystem CO2 uptake of a Mojave Desert ecosystem. Glob. Chang. Biol. 14, 1475–1487. doi:10.1111/j.1365-2486.2008.01593.x

Worrall, F., Burt, T., Adamson, J., 2005. Fluxes of dissolved carbon dioxide and inorganic carbon from an upland peat catchment: Implications for soil respiration. Biogeochemistry 73, 515–539. doi:10.1007/s10533-004-1717-2

Yu, L., Wang, H., Wang, G., Song, W., Huang, Y., Li, S.G., Liang, N., Tang, Y., He, J.S., 2013. A comparison of methane emission measurements using eddy covariance and manual and automated chamber-based techniques in Tibetan Plateau alpine wetland. Environ. Pollut. 181, 81–90. doi:10.1016/j.envpol.2013.06.018

Zhao, M., Running, S.W., 2010. Drought-Induced Reduction in Global Terrestrial Net Primary Production from 2000 Through 2009. Science (80-.). 329, 940–943. doi:10.1126/science.1192666

Ch 2. A two-stage sampling strategy improves chamber-based estimates of greenhouse gas fluxes[1]

2.1 Abstract

Fluxes of greenhouse gases (GHG) are typically characterized by high spatial and temporal variability and large sample sizes (e.g. >30) are thus required to obtain a reliable estimate of the population mean and variance when using simple random sampling (SRS). Sample size, however, is often constrained by budget (time, labor) and therefore practical considerations induce significant (but unknown) measurement error and bias from sampling. In this paper we report a two-stage sampling strategy (2SS) by which the same level of sampling accuracy achievable by SRS can be achieved with significantly smaller sample sizes by optimizing sub-sample selection to retain the statistical characteristics of the sample population. Comparisons between 2SS and SRS were conducted using three datasets with low, medium and high coefficients of variance (*CV*). The size of the first (n') and second (n) stage samples had significant effects on overall sample accuracy. Across all datasets, 2SS reduced RMSE of mean and variance by an average of 30%. The absolute reduction in RMSE of mean and variance was found to be nearly proportional to the value of *CV*, such that the dataset with the largest *CV* showed the largest benefit from 2SS. Logarithmic relationships were found between the difference in the RMSEs and the ratio, n'/ n, serving as a guide to allocate sampling resources in practice. Employing 2SS will aid accurate quantification of soil GHG fluxes in all but the most homogeneous situations.

2.2 Introduction

Chamber-based measurements of the flux of greenhouse gases (GHG) emissions from soils at local scales (less than 1 km^2) are a pillar of Kyoto reporting, especially in agriculture and land use, land-use change and forestry (IPCC 2000). Emission factors generated from chamber-based measurements of total or mean GHG emissions from land use categories are typically based on relatively few measurements in time and space. Errors or uncertainty in the quantified emissions are directly and linearly propagated into the total national accounts.

[1] This chapter is based on: He, Y., Gibbons, J., & Rayment, M. (2016). A two-stage sampling strategy improves chamber-based estimates of greenhouse gas fluxes. *Agricultural and Forest Meteorology*, *228*, 52-59.

What confidence do we have in the accuracy of our estimates? Very little, especially for CH_4 and N_2O where uncertainty spans orders of magnitude (Maljanen et al. 2010; Rayment & Jarvis 2000; Rochette & Eriksen-Hamel 2008; Venterea et al. 2009).

Comparisons of chamber measurements, scaled to the field scale, with eddy covariance (EC) measurements directly measuring at the field scale (i.e. two methods purporting to measure the same thing) often reveal large and unsystematic differences (Davidson *et al*., 2002; Goulden *et al*., 1996; Jones *et al*., 2011; Reth *et al*., 2005). However estimates of, for example, annual net fluxes are typically presented with uncertainty bounds so large as to suggest that the estimates are, in fact, in agreement. Without suggesting that either chamber-based measurements or EC-based estimates are inherently better than the other, it is arguable that the EC community have confronted measurement uncertainty squarely and openly (Baldocchi 2003; Hollinger & Richardson 2005; Oren et al. 2006), and have produced methodologies for assessing and reporting uncertainties, directed towards the ultimate aim of reducing them (Baldocchi et al. 2000; Gu et al. 2012; Foken et al. 2004). On the other hand, the chamber-based measurement community, though revealing error sources from decades of experience has been slower to explore measurement uncertainty caused by sampling (Davidson et al. 2002).

Amongst the literature there are many attempts to grapple with the surrounding chamber design and operation (Rochette & Eriksen-Hamel 2008; Fang et al. 1998; Pumpanen et al. 2004; Rayment & Jarvis 1997), and methodological inter-comparison studies have attempted to harmonize the outputs from disparate methods for collecting and analyzing gas emissions from the soil surface (Butnor et al. 2005; Pumpanen et al. 2003). Similarly, effort has been made at the theoretical level to describe the relationship between fluxes and environmental variables such as soil temperature, moisture and management, allow the interpolation and/or stratification of fluxes, and reducing the sample size needed for measurements accordingly (Rochette et al. 1991; Xu & Qi 2001; Lin et al. 2011). Whilst these difficulties are not yet fully resolved, a complimentary approach is to develop a more efficient sampling strategy.

In soil science generally there is a significant amount of statistical guidance on the design of field experiments and surveys (Cochran 2007; John 1998) and this has served us well in our analysis of the effects of manipulative interventions and soil inventories. In trying to quantify soil GHG emissions, however, we face the simple practical constraint of sample size. The limited number of chambers (or collars) that can be deployed, the amount of time required for a single measurement (especially for CH_4 or N_2O fluxes), the limited number of gas samples

that can be collected and analyzed (in off-line closed systems) or the limited number of chambers that can be multiplexed together (in open systems) all act to limit the number of locations that can realistically be sampled within any given project situation.

In some soil systems, particularly agricultural ones, intensive management has the effect of reducing spatial heterogeneity to manageable levels, thereby reducing the number of measurements required to capture population variance accurately. This is not generally true and spatial heterogeneity combined with limited sample size presents considerable opportunity for bias to enter into our measurements such that even when attempts are made to stratify sampling according to known sources of variance, uncertainty estimates remain large (Raupach et al. 2005).

A large number of samples are required to maintain the accuracy of measurements because of the high spatial variability of the GHG fluxes (Ambus & Christensen 1994; Dai et al. 2012; Rayment & Jarvis 2000; Rodeghiero & Cescatti 2008). For a finite population, the number of samples needed for a given error in the population mean can be derived by:

$$n = \frac{n_0 N}{n_0 + N - 1}, \; n_0 = \frac{z^2 CV^2}{E^2} \qquad (2.1)$$

Where N is the population size, z =1.96 (for 95% confidence), E (%) is half-length of the confidence interval as a fraction of the population mean and *CV* is the coefficient of variation of the population. In practice, a pilot study or an investigation of historical data is necessary to estimate the *CV* (or at least establish an upper limit).

Constrained by several limitations such as labor effort, time and budget, the sample size required by simple randomized design is usually too large to apply in practice. Stratified sampling by vegetation or soil types (Fiener et al. 2012; Panosso et al. 2009; Schelde et al. 2012; Kreba et al. 2013), or topography (Imer et al. 2013; Fang et al. 1998) is widely used to reduce overall variance by applying simple random sampling to each strata. These stratifying methods may become invalid when the spatial variability of the GHG fluxes is controlled (even partially) by an unknown driver, or dominated by factors such as soil temperature and moisture that vary at the finest scale, even within strata (Rochette *et al*., 1991; Stoyan *et al*., 2000; Allaire *et al*., 2012). For these reasons, chambers have limited ability to measure accurately fluxes at such small scales and applying simple random sampling to each stratum may introduce large errors and biases in the estimate of population mean and variance.

With the aim of reducing measurement errors and biases associated with limited resources, here we present a staged approach to sampling that retains the essential characteristics of the population distribution within a small sample size. Related, but less effective approaches have been investigated previously (Folorunso & Rolston 1984; Rodeghiero & Cescatti 2008). Our method (see details below) expands the approach used in (Rodeghiero & Cescatti 2008), where a heterogeneous field was divided into sub-regions by a pre-sampling stage, which reduced the total variance of the whole region. There is an extent to which our method can be viewed as a mathematical stratification, leading to a completely general sampling method. Drawing on published datasets of soil GHG emissions across a range of spatial variability, we show that this sampling strategy reduces uncertainty in all cases compared with the simple random sampling, and particularly where sources of variance are large.

2.3 Methods and Data

Two sampling strategies were modeled using simulation: (1) simple random sampling (SRS); (2) a resampling or two-stage sampling (2SS). Staged sampling consisted of an initial survey where a relatively large number of samples were made. Two descriptive statistics (mean & variance) were calculated for this set of samples; the mean is of primary concern when quantifying total GHG flux and variance is the critical factor revealing spatial variability. A Monte Carlo method and a cost function were then used to select a sub-sample from the 1st-stage sample such that the descriptive statistics of the sub-sample were closest to those of the 1st-stage sample. Three datasets with low, medium and high variability or coefficient of variance (CV) were explored. Three analyses were made to compare 2SS with SRS and investigate the effects of sample size on the improvements: (1) the error distributions of the final-stage sample mean and variance; (2) the effects of the final sample size on the root-mean-square errors (RMSEs) of the sample mean and variance; (3) the relation between the RMSEs and the initial and final sample size.

2.3.1 Assumptions and sampling strategies

For calculation purposes, we assume that the GHG emissions for a given area are discretized to a finite population size of N. For simple random sampling (SRS), n final samples are directly drawn randomly from N. The two-stage sampling (2SS) developed here invokes an extra initial sample set of size n' between the population and the final samples (Fig. 2.1). The systematic/artificial errors between two independent measurements are assumed small

enough to be negligible compared to the errors caused by the sampling methods as shown by (Mathieu et al. 2006).

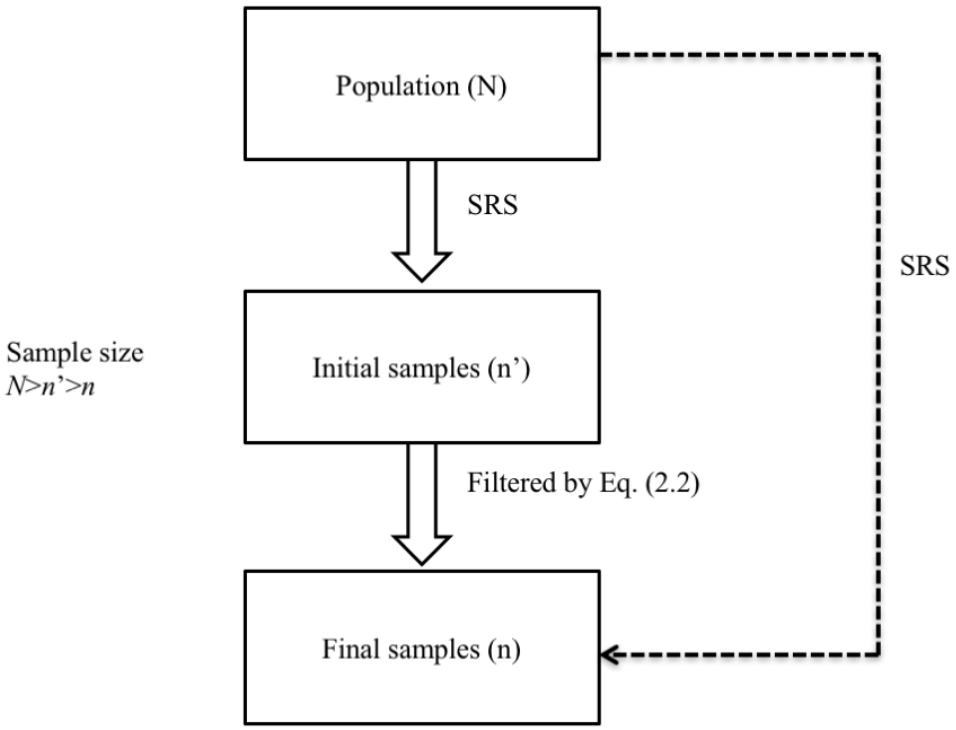

Figure 2.1 Workflow of the two-stage sampling (2SS), compared with the simple random sampling (SRS).

Note that n' > n; the filtering process from the initial sample to the final sample is performed by minimizing the cost or objective function:

$$\min \quad f = \frac{|\mu_i - \mu'|}{\mu'} + \frac{|\sigma_i - \sigma'|}{\sigma'} - \frac{|\mu_i - \mu'|}{\mu'} \cdot \frac{|\sigma_i - \sigma'|}{\sigma'}, \quad i = 1,2,3,\dots, C_{n'}^{n} \qquad (2.2)$$

Where μ' and σ' are the mean and standard deviation of initial samples, while μi and σi are the mean and standard deviation for each combination of n from n' ($C_{n'}^{n}$). The aim of this process is to minimize f by finding the set of final samples that is most representative of the initial sample in terms of the errors of both mean and standard deviation. The choice of this cost function is pragmatic and may depend slightly on the subjective view of these statistics and purpose for which the data are collected. The function provided here selects a sample with a representative estimate of both the mean and standard deviation, the two most important sample features for atmospheric and biological modeling of GHG flux. Without suggesting that one is more important than the other, we assumed an equal weighting as

implied in Eq. (2.2), however, in some cases a larger weight could be assigned to the sample mean if total flux is considered a higher priority. The first two terms in the function guarantee the choice of a sub-sample with a minimum sum of errors in mean and standard deviation and the third product term avoids choosing a sample with an extreme disparity between the first two terms, where one is overwhelmingly larger than the other. Weighting the mean and variance equally, this minimization process can be seen as a generalization of the method from a previous study (Rodeghiero & Cescatti 2008) where a simple approximation was achieved by stratifying the data by mean and variance and then selecting sub-samples at random from each strata.

In conventional two-stage sampling methods, the population is usually stratified into a sample of primary units from which a sample of secondary units is selected (Thompson 2012). While stratification is not explicit in 2SS, defining unequal strata and subsampling from these such that the sample represents the population would achieve similar results. The initial samples in 2SS can be considered as auxiliary information for improving the selection of the final samples, similar to the way in which double or two-phase sampling adopts auxiliary information to improve inference of the population (Thompson 2012).

2.3.2 Datasets and statistics

The 2SS approach is illustrated using a dataset extracted from Mathieu et al. (2006) where 36 points were sampled at 3 m spacing on a 20 m × 20 m plot of a cultivated Gleyic luvisol located at Citeaux in the Saone river plain, near Dijon (Eastern France) in April 2003. We used these 36 samples as an adequate approximation of the population. The CO2 flux dataset was used in this study and the flux unit was converted from g C ha^{-1} d^{-1} to g C m^{-2} d^{-1}.

In order to create datasets representing different degrees of variability without altering the mean, the original dataset A was expanded according to the following linear mapping,

$$y_i = (x_i - \mu) \cdot c + \mu, i = 1,2,3, \dots, 36 \qquad (2.3)$$

Where yi are the new data points and xi are the original ones. μ is the mean value of dataset A. The constant c ($\geqslant 0$) is an expanding factor. Two datasets with higher and lower CV were generated by setting c = 2 and c = 0.5 accordingly.

Note that the normality assumption for the distributions of the sample statistics is not appropriate for small sample size where the central limit theory becomes invalid. Therefore,

here we simply employed the sample mean and variance as the estimators for the population mean and variance based on the method of moments (Feller 1968).

RMSE was used as an evaluator for the goodness of the sampling strategies. For example, the RMSE of the mean is defined by

$$RMSE\ of\ Mean = \sqrt{\frac{\sum_{i=1}^{m}(\bar{x}_i-\mu)^2}{m}} \qquad (2.4)$$

Where μ is the mean of the population and $\bar{x}_i$ are means of samples. m is the sampling repetition and was set to 1000 in our simulations to get a sampling distribution. *RMSE* is the square root of the mean squared error (*MSE*), which is a risk function corresponding to the expected value of the squared (quadratic) error loss and measures the estimator's bias.

RMSE of variance was calculated similarly, replacing the terms of the mean in Eq. (2.4) with the terms of the population and sample variance. In the remainder of this paper, the *RMSE* of mean and variance are designated as *RMSEs* for clarity.

2.4 Results

2.4.1 Error distributions of the sample mean and variance

We started with a simple case that a fixed initial sample size at 18 (n'=18) and a fixed final sample size at 6 (n=6) that are typically used per date. Distributions of the errors in the sample mean and variance were given in Fig. (2.2). Compared with SRS, application of 2SS resulted in general improvements in the accuracy of sample mean and variance for all datasets. A normally distributed error suggests a good sampling method and it was clear from the fitted normal curves (smooth lines in Fig. 2.2) that SRS error distributions were not normally distributed. This was confirmed by the Anderson-Darling (AD) test which showed that none of the error distributions from SRS should be accepted as normal (p<0.01) at the 5% significance level, highlighting the shortcomings of SRS in capturing the population's features when the sample size was small (e.g. 6 in this case). In fact, assuming normality for the distributions of sample statistics in a Monte Carlo estimate is not appropriate when the sample size is small, and can lead to a biased or erroneous inference to the whole population. On the contrary, when using 2SS, the errors of the sample mean did not fall into the critical regions for any of the datasets (p = 0.9376, 0.5202 and 0.7426), implying more unbiased and accurate estimates of the population mean. Distributions of the errors in the sample variance

were non-normal for both methods, although clear improvements can be seen when 2SS was applied (Fig. 2.2d&e&f).

Bias and variance of a statistic estimator are used to quantify the amount of improvements in the sampling error and *RMSE* which incorporates both these aspects (i.e. *RMSE* can be written as the sum of the variance of the estimator and the bias of the estimator) is thus an appropriate evaluator. As shown in Table (2-1), the absolute reduction in *RMSEs* increased as the *CV* of the datasets increased, suggesting that the gain from 2SS may be proportional to the heterogeneity of the underlying population. In fact, the improvement in the *RMSE* of mean and variance were nearly proportional to the *CV* and CV^2 respectively (see below). Relative reductions in the two *RMSE*s were respectively around 55% and 58% for all datasets, demonstrating that the applying 2SS reduced the risk of getting unrepresentative samples by over 50% irrespective of the dataset's variability.

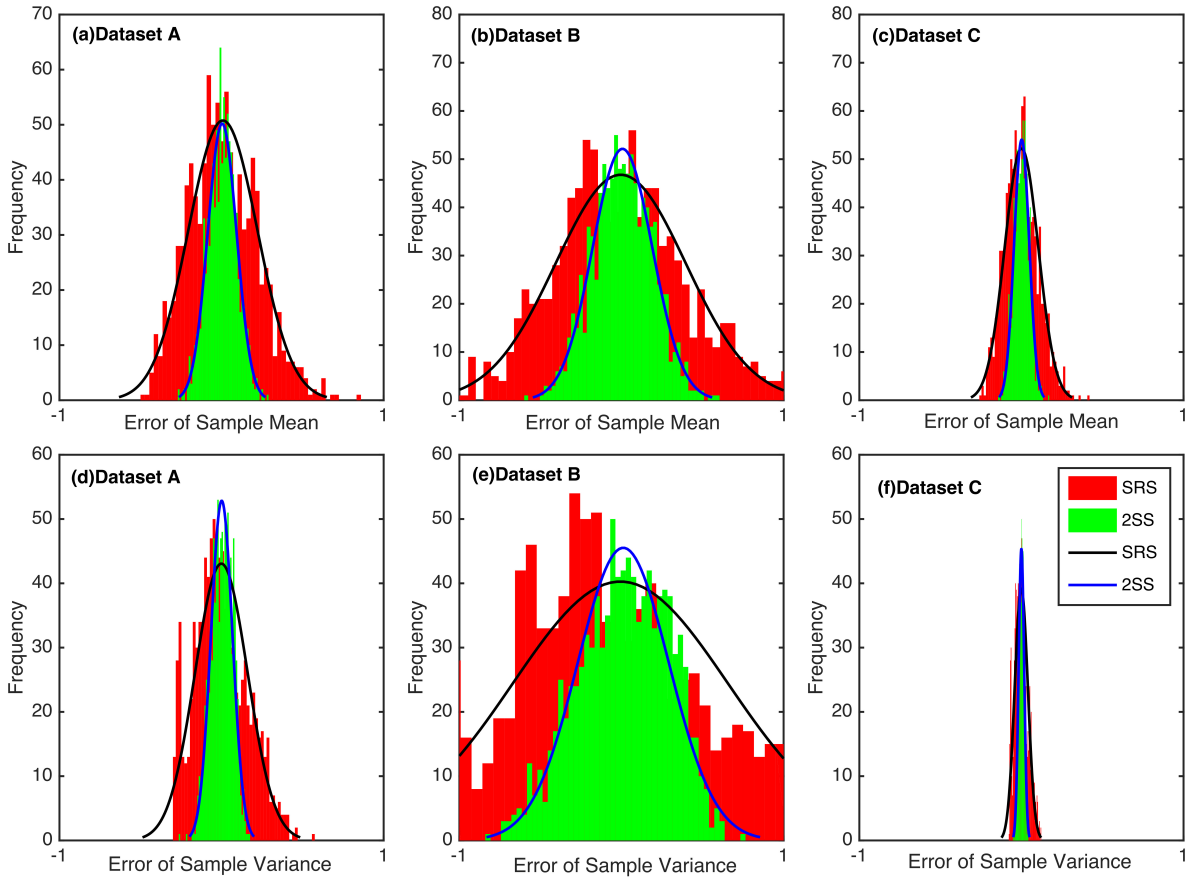

Figure 2.2 Error distributions of the sample mean and variance for the three datasets. The initial and final sample sizes were fixed at 18 and 6 respectively for 2SS. (a, b, c) Error distribution of the sample mean for dataset A, B and C. (d, e, f) Error distribution of the sample variance for dataset A, B and C.

Table 2-1. Improvements in RMSEs for the three datasets when using 2SS compared to SRS

Datasets	*CV*	*RMSE* (mean)		Absolute reduction	Relative reduction	*RMSE* (variance)		Absolute reduction	Relative reduction
		SRS	2SS			SRS	2SS		
A	0.603	0.202	0.090	0.112	55.6%	0.167	0.070	0.097	58.0%
B	1.205	0.420	0.199	0.221	52.5%	0.672	0.274	0.398	59.3%
C	0.301	0.102	0.046	0.056	54.6%	0.040	0.017	0.023	57.8%

2.4.2 Sample errors vs. the initial (n') and final (n) sample size

For a given initial sample size (*n'*), we can conduct a sensitivity analysis of the final sample size (*n*) to investigate how *RMSE*s vary with *n*. Without loss of generality, and to limit calculations to a manageable number in relation to the original dataset in Mathieu et al. (2006), *n'* was set to 18 while *n* ranged from 2 to 17. We calculated the *RMSE*s for the three datasets using the two sampling methods separately. As might be expected, datasets with higher *CV* produced larger *RMSE*s as shown in Fig. (2.3a&2.3b). *RMSE*s decreased gradually as *n* increased for SRS (dotted lines in Fig. 2.3a&2.3b) while for 2SS (solid lines with markers in Fig. 2.3a&2.3b), *RMSE*s remained almost constant for all final sample sizes greater than 2. This indicates that by using 2SS many fewer samples (e.g. 3) can achieve the same expected level of accuracy as a large sample number (i.e. 18 in this case) because of the efficacy from the combination of a larger initial sample size and the selection function Eq. (2.2). Additionally, in terms of the absolute difference between the two methods, dataset B (with the largest *CV*) showed the greatest decrease in *RMSE*s while dataset C showed the least, suggesting that the more heterogeneous sample area, the greater the absolute benefit of using 2SS. This result demonstrated that for 2SS, *RMSE*s were mainly determined by the initial samples and the cost function Eq. (2.2) performed well in selecting a set of samples with a reliable mean and variance.

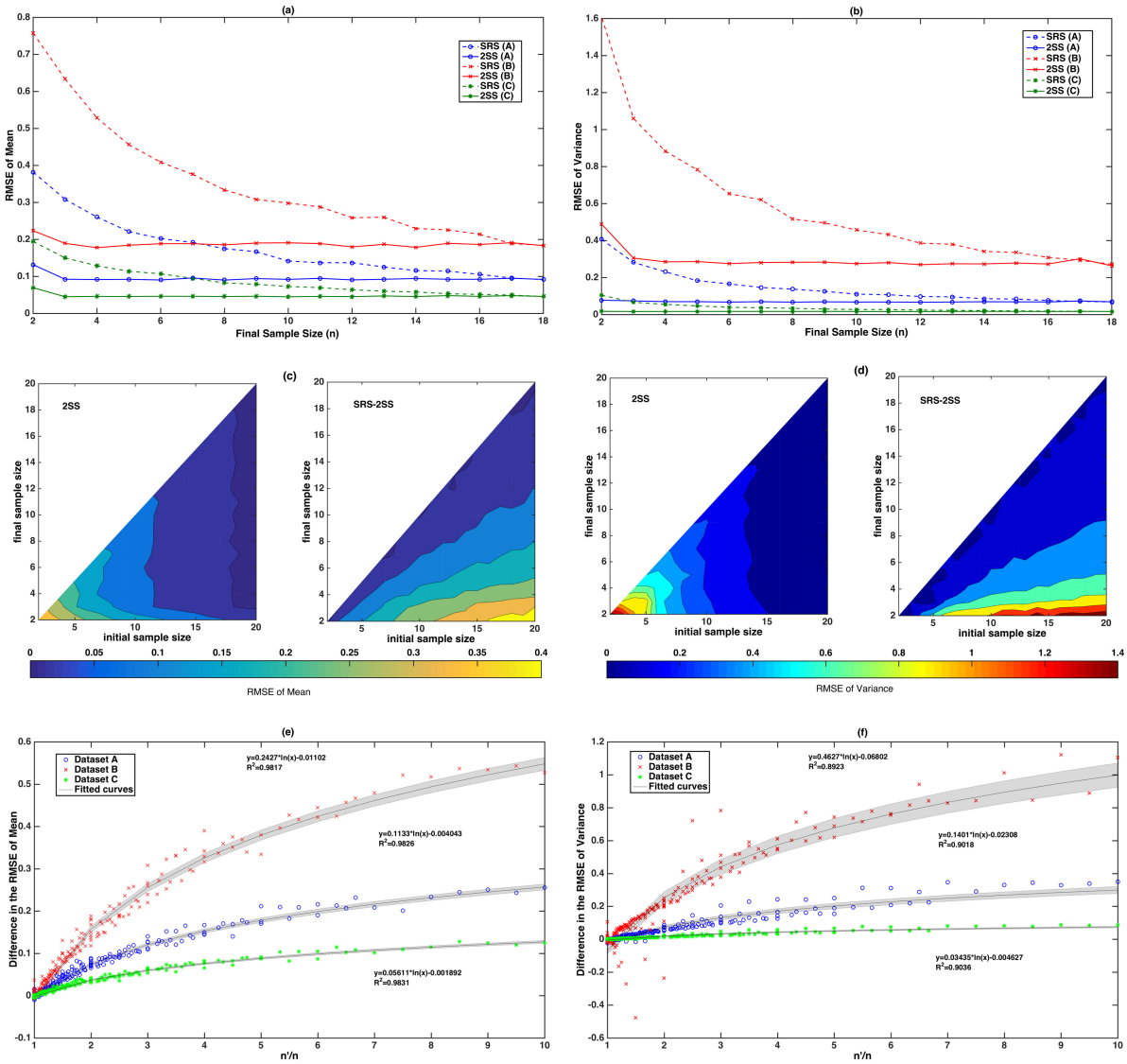

*Figure 2.3 Sample errors vs. the initial (n') and final (n) sample size. (a, b) RMSE of mean (a) and variance (b) for the three datasets when n' = 18 and 2 ⩽ n ⩽ 17. (c, d) The RMSE of mean (c) and variance (d) for all combinations of the initial and final sample sizes for dataset A. The difference in the RMSEs between SRS and 2SS (SRS-2SS) are shown on the right of each subplot. Only half of the graphic areas (triangle areas) are filled because n is necessarily ⩽ n'. (e, f) The difference in the RMSE of Mean (e) and Variance (f) against the ratio n'/n for the three datasets. Logarithmic curves, y = a * ln (x) + b, were fitted and the grey shaded area represents 95% confidence bounds for the parameters a and b.*

Recalculation of *RMSE*s was conducted for 2SS using every combination of n' and n satisfying $2 \leq n \leq n' \leq 20$ (resulting in 190 combinations in total) for each of the three datasets. Because the essential difference between the two methods is the filtering process represented by Eq. (2.2), SRS can thus be regarded as a quasi-two-stage sampling strategy without the filtering process, i.e. where the *RMSE*s will not vary with n'.

Unsurprisingly, except for the scale difference as indicated in Fig. (2.3a & 2.3b), the patterns of *RMSE*s were similar among the (related) datasets, therefore filled contours of *RMSE*s are only shown for dataset A in Fig. (2.3c & 2.3d). Compared to SRS, the *RMSE*s for 2SS were dominated by *n*' rather than *n* as the clear horizontal gradients show. Again, this suggests that the cost function, Eq. (2.2) worked well for selecting final samples that were representative of the initial ones. In other words, obtaining better accuracy in the estimate of mean and variance by applying a small *n* was achievable as long as *n*' and the cost function were chosen appropriately. 2SS worked to reduce *RMSE*s for nearly every combination of sample size as illustrated by the positive difference between SRS and 2SS (SRS-2SS) for all points on the plots. The average reduction in *RMSE*s was approximately 30% for all datasets.

The largest improvements were found at the lower right corner where the ratio, *n*'/*n* was large and appeared to decrease as the ratio *n*'/*n* decreased, suggesting a potential positive relation between them. A scatter plot of the difference in *RMSE* of the mean and *n*'/*n* showed a logarithmic relation ($y = a * \ln(x) + b$) for all datasets (Fig. 2.3e). The coefficient, *a* was found to be proportional to the dataset's *CV* while *b* was close to zero, suggesting the following,

Difference in the *RMSE* of the mean = $k_m * CV * \ln(n'/n)$ (2.5)

Where k_m is a constant number, e.g. 4.8 in this case. This provides us a good estimate of the gains obtainable by using 2SS and highlights that improvements increase proportionally with the variance of the population.

A similar relation was found between the difference in the *RMSE* of variance and the ratio n'/n (Fig. 2.3f). The coefficient *a,* however, was found to be proportional to the square of the dataset's *CV*, suggesting a similar function,

Difference in the *RMSE* of the variance = $k_v * CV^2 * \ln(n'/n)$ (2.6)

Here k_v is also a constant number, e.g. 3.2 in this case. Again, this result demonstrated that the improvement possible by employing 2SS rather than SRS can be quantified by basic functions, which can serve as guide to allocate limited measurement resources in practice.

2.5 Discussions and conclusions

Chamber-based measurement of GHG flux is straightforward and has many advantages compared to micrometeorological methods. In terms of capturing spatial variation, however,

it is easy to make unreliable inferences about the spatial average by accidentally using spatially unrepresentative samples, particularly when the sample size is small. In this study we have demonstrated the effectiveness of a new sampling strategy, 2SS, in reducing sampling error in both the sample mean and spatial variance. We have further demonstrated that the expected benefits of this approach increase with increasing spatial variability.

By constructing an appropriate cost function (e.g. Eq. 2.2), it was much easier to obtain a small set of final samples that was nonetheless representative of the initial samples, and provided an accurate estimate of the population mean and variance. Depending on the sample size chosen for the two stages, improvements in the sample mean and variance averaged 30% for all three datasets used in this study. Compact relations were found between the potential benefits and the sample size ratio (n'/n), providing an easy guideline to allocate sampling resources (Fig. 2.3). Considering that the GHG flux datasets tend to be highly spatially heterogeneous as a result of diverse vegetation types, land-surface types and/or soil conditions (Reichstein 2003; Valentini 2003), SRS cannot be recommended (often) without a manageably large sample size. 2SS is a rather simple statistical method, leading to a more advanced sampling strategy that could contribute to improving GHG flux estimates irrespective of site or gas measured. In fact, the technique could be employed to reduce sample error in any situations where spatial variance is higher than a manageable sample number can effectively capture. The three datasets used in this study differed in their *CV* values, however, one should be aware that the *CV* alone as an index is not sufficient to completely characterize the heterogeneity of a source field, even though it has been the most widely-used and intuitive statistics (Buczko et al. 2015).

In the agricultural example used here, a history of management interventions such as ploughing and fertilization may have tended towards homogenizing the soil properties and microbial communities which can eventually "rectify" any areas of particularly high or low carbon-cycling activity. As such, this case (represented by dataset C with the lowest CV value) possibly represents the minimum benefit that 2SS confers compared to SRS. In more natural and unmanaged ecosystems, heterogeneity is typically higher and furthermore increases with time. This is most clearly seen in forest/woodland systems where the development of soil properties is highly influenced by proximity to individual trees even at fine scales (e.g. 12.5 cm, Jackson & Caldwell 1993) and in grass/sedge systems which over time become increasingly dominated by tussocks, particularly when the water-table is seasonally close to the surface (Soussana et al. 2007; Reynolds et al. 1997). Such cases

represent a significant focus of GHG flux study and would particularly benefit from the use of 2SS. Similarly, even in highly managed systems, such as livestock grazing systems, where the soil is initially highly uniform, large heterogeneity is found in the fluxes of GHGs (primarily N_2O and CH_4) associated with inputs from animal excretion (Saggar et al. 2004). Accurate quantification of these would also benefit significantly from the use of 2SS.

With the simple random sampling approach, the ideal sample size is always "as many as possible", but the "optimal" sample size varies with many factors as mentioned previously, e.g. the financial and human labor capacity, the study site, etc. To our knowledge, the complexity of making such resource allocation decisions has not been discussed previously, and the method presented here provides a statistical view on a fundamental issue that is often glossed over. We provide as concrete and robust a methodology to address the problem of sample size deficiency as it is possible to provide without consideration of the specific project requirements that the audience may encounter. The same applies to all statistical methods.

In 2SS, the increased effort spent in conducting a larger initial sampling at the beginning of the project becomes worthwhile in a long-term measurement through a significant reduction both in the likely sample error, and in the long-term effort required (e.g. fewer samples needed for accurate quantification). Nevertheless, this does raise a question about whether the second-stage sample remains the optimum sub-sample if the population changes with time. Fully understanding this requires new datasets with greater spatial and temporal resolution and is beyond the discussion of this paper, nevertheless, despite the assumption suggested in (Rodeghiero & Cescatti 2008) that GHG fluxes are temporally invariable over a specified period or maintain a relatively similar rate of change with time (e.g. high flux areas remaining high flux areas and vice versa), we suggest that a seasonal repetition of the initial survey should be conducted to ensure that longer-term temporal variations are captured. For example, it is well known that the day-to-day variation in CO_2 flux is mainly driven by variations in light, temperature and water, but seasonal variation includes changes driven by, for instance, phenology. A few repetitions of the first stage sampling of 2SS at the critical stages of vegetation change (e.g. early and middle growing seasons) could update our choice of optimal sample location, thus increase the estimation confidence of flux.

Finally, here we have focused on two statistics, mean and variance, as these are the primary descriptors of a population. Nevertheless, these alone may not completely capture the true spatial pattern of GHG flux (i.e. two datasets with the same mean and variance may have different spatial patterns). This is particularly the case where the flux hotspots exist (Stoyan

et al. 2000; Parkin 1987), especially for CH_4 and N_2O fluxes. Long-term spatial hotspots can increase the spatial heterogeneity significantly through microbial processes at microscale (less than 1m), such as denitrification (Farquharson & Baldock 2008; Groffman et al. 2009) and/or methanogenesis (Wachinger et al. 2000). SRS is likely to under sample events with low probability and thus is not recommended for capturing hotspots. With a large sample size at the initial stage, 2SS is more likely to catch rare events. The current form of 2SS can be further improved by including skewness or kurtosis in the cost function, which would allow the final sample to express similar population characteristics as the overall population. If this inclusion is found to be important, the most comprehensive spatial treatment would be to derive the variogram (Isaaks & Srivastava 1989) for the sample area, and select a sub-sample that expressed similar variogram parameters, i.e. consider the spatial autocorrelation of the datasets (Wang et al. 2012). This, however, would require a significantly larger and more detailed initial samples to extract a reliable variogram function, and we leave this task to the next-stage research.

To conclude, SRS never outperforms 2SS, and 2SS always increases the sampling efficiency in the long term. Since it is a purely statistical model aimed at obtaining a better estimation of the population mean and variance, it can be easily applied to other datasets representing various types of land surfaces. Making the simplification that coefficient of variation (*CV*) is a reasonable measure of spatial heterogeneity, it is clear that the improvements gained through using 2SS are higher in more complex land surface types; the higher the *CV*, the higher the gain from using 2SS. Using a very simple form, the approach proposed here provides a statistical view on a very fundamental issue which should receive greater attention, and provides a concrete and robust methodology to address the problem of sample size deficiency.

2.6 References

Allaire, S.E. et al., 2012. Multiscale spatial variability of CO2 emissions and correlations with physico-chemical soil properties. *Geoderma*, 170, pp.251–260. doi: 10.1016/j.geoderma.2011.11.019.

Ambus, P. & Christensen, S., 1994. Measurement of N_2O emission from a fertilized grassland: An analysis of spatial variability. *Journal of Geophysical Research*, 99(D8), pp.16549–16555. doi: 10.1029/94JD00267.

Baldocchi, D.D., 2003. Assessing the eddy covariance technique for evaluating carbon dioxide exchange rates of ecosystems: Past, present and future. *Global Change Biology*, 9, pp.479–492. doi: 10.1046/j.1365-2486.2003.00629.x.

Baldocchi, D.D., Meyers, T.P. & Wilson, K.B., 2000. Correction of eddy-covariance measurements incorporating both advective effects and density fluxes. *Boundary-Layer Meteorology*, 97(3), pp.487–511. doi: 10.1023/A:1002786702909.

Buczko, U. et al., 2015. Spatial variability at different scales and sampling requirements for in situ soil CO_2 efflux measurements on an arable soil. *Catena*, 131, pp.46–55. doi: 10.1016/j.catena.2015.03.015.

Butnor, J.R., Johnsen, K.H. & Maier, C.A., 2005. Soil properties differently influence estimates of soil CO2 efflux from three chamber-based measurement systems. *Biogeochemistry*, 73(1), pp.283–301. doi: 10.1007/s10533-004-4022-1.

Cochran, W.G., 2007. *Sampling Techniques* Third Edit., New York.

Dai, Z. et al., 2012. Effect of assessment scale on spatial and temporal variations in CH_4, CO_2, and N_2O fluxes in a forested wetland. *Water, Air, & Soil Pollution*, 223(1), pp.253–265. doi: 10.1007/s11270-011-0855-0.

Davidson, E.A. et al., 2002. Minimizing artifacts and biases in chamber-based measurements of soil respiration. *Agricultural and Forest Meteorology*, 113(1), pp.21–37. doi: 10.1016/S0168-1923(02)00100-4.

Fang, C. et al., 1998. Soil CO_2 efflux and its spatial variation in a Florida slash pine plantation. *Plant and soil*, pp.135–146. doi: 10.1023/A:1004304309827.

Farquharson, R. & Baldock, J., 2008. Concepts in modelling N2O emissions from land use. *Plant and Soil*, 309(1-2), pp.147–167. doi: 10.1007/s11104-007-9485-0.

Feller, W., 1968. *An Introduction to Probability Theory and Its Applications*, doi: 10.2307/1266435.

Fiener, P. et al., 2012. Spatial variability of soil respiration in a small agricultural watershed — Are patterns of soil redistribution important? *Catena*, 94, pp.3–16. doi: 10.1016/j.catena.2011.05.014.

Foken, T. et al., 2004. Post-Field Data Quality Control. In *Handbook of Micrometeorology*. pp. 181–208. doi: 10.1007/1-4020-2265-4_9.

Folorunso, O.A. & Rolston, D.E., 1984. Spatial Variability of Field-Measured Denitrification Gas Fluxes. *Soil Science Society of America Journal*, 48, pp.1214–1219. doi: 10.2136/sssaj1984.03615995004800060002x.

Goulden, M.L. et al., 1996. Measurements of carbon sequestration by long-term eddy covariance: Methods and a critical evaluation of accuracy. *Global Change Biology*, 2(3), pp.169–182. doi: 10.1111/j.1365-2486.1996.tb00070.x.

Groffman, P.M. et al., 2009. Challenges to incorporating spatially and temporally explicit phenomena (hotspots and hot moments) in denitrification models. *Biogeochemistry*, 93(1-2), pp.49–77. doi: 10.1007/s10533-008-9277-5.

Gu, L. et al., 2012. The fundamental equation of eddy covariance and its application in flux measurements. *Agricultural and Forest Meteorology*, 152, pp.135–148. doi: 10.1016/j.agrformet.2011.09.014.

Hollinger, D.Y. & Richardson, A.D., 2005. Uncertainty in eddy covariance measurements and its application to physiological models. *Tree physiology*, 25(7), pp.873–885. doi: 10.1093/treephys/25.7.873.

Imer, D. et al., 2013. Temporal and spatial variations of soil CO_2, CH_4 and N_2O fluxes at three differently managed grasslands. *Biogeosciences*, 10(9), pp.5931–5945. doi: 10.5194/bg-10-5931-2013.

IPCC, 2000. *Land Use, Land-Use Change, and Forestry*, doi: 10.2277/0521800838.

Isaaks, E.H. & Srivastava, R.M., 1989. *An introduction to applied geostatistics*, New York: Oxford University Press.

Jackson, R.B. & Caldwell, M.M., 1993. Geostatistical Patterns of Soil Heterogeneity around Individual Perennial Plants. *Journal of Ecology*, 81(4), pp.683–692. doi: 10.2307/2261666.

John, P.W.M., 1998. *Statistical Design and Analysis of Experiments*, Philadelphia, PA: Society for Industrial and Applied Mathematics.

Jones, S.K. et al., 2011. Nitrous oxide emissions from managed grassland: a comparison of eddy covariance and static chamber measurements. *Atmospheric Measurement Techniques Discussions*, 4(1), pp.1079–1112. doi: 10.5194/amt-4-2179-2011.

Kreba, S. a. et al., 2013. Spatial and Temporal Patterns of Carbon Dioxide Flux in Crop and Grass Land-Use Systems. *Vadose Zone Journal*, 12(4). doi: 10.2136/vzj2013.01.0005.

Lin, X. et al., 2011. Response of ecosystem respiration to warming and grazing during the growing seasons in the alpine meadow on the Tibetan plateau. *Agricultural and Forest Meteorology*, 151(7), pp.792–802. doi: 10.1016/j.agrformet.2011.01.009.

Maljanen, M. et al., 2010. Greenhouse gas balances of managed peatlands in the Nordic countries - present knowledge and gaps. *Biogeosciences*, 7(9), pp.2711–2738. doi: 10.5194/bg-7-2711-2010.

Mathieu, O. et al., 2006. Emissions and spatial variability of N_2O, $N_2$and nitrous oxide mole fraction at the field scale, revealed with ^{15}N isotopic techniques. *Soil Biology and Biochemistry*, 38(5), pp.941–951. doi: doi:10.1016/j.soilbio.2005.08.010.

Oren, R.A.M. et al., 2006. Estimating the uncertainty in annual net ecosystem carbon exchange: Spatial variation in turbulent fluxes and sampling errors in eddy-covariance measurements. *Global Change Biology*, 12(5), pp.883–896. doi: 10.1111/j.1365-2486.2006.01131.x.

Panosso, a. R. et al., 2009. Spatial and temporal variability of soil CO2 emission in a sugarcane area under green and slash-and-burn managements. *Soil and Tillage Research*, 105(2), pp.275–282. doi: 10.1016/j.still.2009.09.008.

Parkin, T.B., 1987. Soil microsites as a source of denitrification variability. *Soil Science Society of America Journal*, 51, pp.1194–1199. doi: 10.2136/sssaj1987.03615995005100050019x.

Pumpanen, J. et al., 2004. Comparison of different chamber techniques for measuring soil CO_2 efflux. *Agricultural and Forest Meteorology*, 123(3), pp.159–176. doi:

10.1016/j.agrformet.2003.12.001.

Pumpanen, J. et al., 2003. Seasonal patterns of soil CO_2 efflux and soil air CO_2 concentration in a Scots pine forest: comparison of two chamber techniques. *Global Change Biology*, 9(3), pp.371–382. doi: 10.1046/j.1365-2486.2003.00588.x.

Raupach, M.R. et al., 2005. Model-data synthesis in terrestrial carbon observation: methods, data requirements and data uncertainty specifications. *Global Change Biology*, 11(3), pp.378–397. doi: 10.1111/j.1365-2486.2005.00917.x.

Rayment, M.B. & Jarvis, P.G., 1997. An improved open chamber system for measuring soil CO_2 effluxes in the field. *Journal of Geophysical Research: Atmospheres (1984–2012)*, 102(D24), pp.28779–28784. doi: 10.1029/97JD01103.

Rayment, M.B. & Jarvis, P.G., 2000. Temporal and spatial variation of soil CO2 efflux in a Canadian boreal forest. *Soil Biology and Biochemistry*, 32(1), pp.35–45. doi: 10.1016/S0038-0717(99)00110-8.

Reichstein, M., 2003. Modeling temporal and large-scale spatial variability of soil respiration from soil water availability, temperature and vegetation productivity indices. *Global Biogeochemical Cycles*, 17(4), p.1104. doi: 10.1029/2003GB002035.

Reth, S., Göckede, M. & Falge, E., 2005. CO_2 efflux from agricultural soils in Eastern Germany - comparison of a closed chamber system with eddy covariance measurements. *Theoretical and Applied Climatology*, 80(2-4), pp.105–120. doi: 10.1007/s00704-004-0094-z.

Reynolds, H.L. et al., 1997. Soil Heterogeneity and Plant Competition in Anannual Grassland. *Ecology*, 78(7), pp.2076–2090. doi: 10.1890/0012-9658(1997)078[2076:SHAPCI]2.0.CO;2.

Rochette, P., Desjardins, R. & Pattey, E., 1991. Spatial and temporal variability of soil respiration in agricultural fields. *Canadian Journal of Soil Science*, 196(90). doi: 10.4141/cjss91-018.

Rochette, P. & Eriksen-Hamel, N.S., 2008. Chamber measurements of soil nitrous oxide flux: are absolute values reliable? *Soil Science Society of America Journal*, 72(2), pp.331–342. doi: 10.2136/sssaj2007.0215.

Rodeghiero, M. & Cescatti, A., 2008. Spatial variability and optimal sampling strategy of soil respiration. *Forest Ecology and Management*, 255(1), pp.106–112. doi: 10.1016/j.foreco.2007.08.025.

Saggar, S. et al., 2004. A review of emissions of methane, ammonia, and nitrous oxide from animal excreta deposition and farm effluent application in grazed pastures. *New Zealand Journal of Agricultural Research*, 47(4), pp.513–544. doi: 10.1080/00288233.2004.9513618.

Schelde, K. et al., 2012. Spatial and temporal variability of nitrous oxide emissions in a mixed farming landscape of Denmark. *Biogeosciences*, 9(8), pp.2989–3002. doi: 10.5194/bg-9-2989-2012.

Soussana, J.F. et al., 2007. Full accounting of the greenhouse gas (CO2, N2O, CH4) budget

of nine European grassland sites. *Agriculture, Ecosystems and Environment*, 121(1-2), pp.121–134. doi: 10.1016/j.agee.2006.12.022.

Stoyan, H. et al., 2000. Spatial heterogeneity of soil respiration and related properties at the plant scale. *Plant and Soil*, 222(1-2), pp.203–214. doi: 10.1023/A:1004757405147.

Thompson, S.K., 2012. *Sampling*, Hoboken: John Wiley & Sons.

Valentini, R., 2003. *Fluxes of carbon, water and energy of European forests*, Heidelberg: Springer.

Venterea, R.T., Spokas, K.A. & Baker, J.M., 2009. Accuracy and precision analysis of chamber-based nitrous oxide gas flux estimates. *Soil Science Society of America Journal*, 73(4), pp.1087–1093. doi: 10.2136/sssaj2008.0307.

Wachinger, G., Fiedler, S. & Roth, K., 2000. Variability of soil methane production on the micro-scale: spatial. *Soil Biology & Biochemistry*, 32(8-9), p.1121. doi: doi:10.1016/S0038-0717(00)00024-9.

Wang, J.-F. et al., 2012. A review of spatial sampling. *Spatial Statistics*, 2, pp.1–14. doi: 10.1016/j.spasta.2012.08.001.

Xu, M. & Qi, Y., 2001. Soil-surface CO2 efflux and its spatial and temporal variations in a young ponderosa pine plantation in northern California. *Global Change Biology*, 7, pp.667–677. doi: 10.1046/j.1354-1013.2001.00435.x.

Ch 3. A robust gap-filling method for Net Ecosystem Exchange based on Cahn-Hilliard inpainting[1]

3.1 Abstract

Traditional gap-filling approaches adopt a temporally linear perspective on data; whether synthesizing data statistically within a moving window, or using complex functions based on a "best-guess" understanding of the processes driving exchange. The former approach is limited in its ability to capture non-linear trends, and the latter is limited in situations where the flux response to driving variables is poorly understood or unknown (e.g. the response of gas exchange to water table depth in wetlands). Rearranging time-averaged half-hourly net ecosystem exchange (NEE) into a 48*N matrix has been used to visualize NEE as a "flux fingerprint" and suggests a different way of filling data gaps. In this paper, we introduce an image processing technique known as image inpainting to fill gaps in this two-dimensional representation of a one-dimensional data. This has the advantage that any short-term structure can be accommodated without expressly implying any particular functional response to driving environmental variables, and medium-term temporal structure (i.e. day-to-day covariance) can be incorporated into gaps in the flux signal. In this way, data gaps are filled solely using information contained in robust, primary data. This new method compares favorably with the marginal distribution sampling (MDS), when tested on twelve European-Flux datasets with four types of artificial gaps. Furthermore, we show that how random structures or noise embedded in the signal affect the gap-filling performance, which can simply be improved through a de-noising procedure by using a Fourier transform algorithm. The inpainting-based gap-filling approach is more effective than MDS on the de-noised data.

3.2 Introduction

The eddy covariance (EC) technique used for measuring the fluxes of greenhouse gases (GHG) and energy has flourished over the past 25 years (Baldocchi, 2014). It is considered as the only method that provides a direct sense of the gas/energy exchange at the biosphere–atmosphere interface at the canopy scale (Baldocchi et al., 1996; Baldocchi, 2003). Globally, more than 400 sites are equipped with gas sensors with high temporal resolution monitoring

[1] This chapter is based on: He, Y. and Rayment, M. (2016) A robust gap-filling method for Net Ecosystem Exchange based on CahnHilliard inpainting, Geosci. Model Dev. Discuss., doi:10.5194/gmd-2016-108, (In review)

gas exchange and dozens of groups have produced time-series spanning years and decades (Baldocchi, 2014). While the expansion in use of EC has greatly helped us in the understanding of land-atmosphere exchanges, the method does not yet provide perfectly reliable data on the magnitude and location of GHG sinks/sources as the result of several theoretical and practical limitations. Notably, the method is intrinsically limited to use in generally flat terrain with generally uniform vegetation and an adequate footprint area (Baldocchi, 2003; IPCC, 2000); such limitations are unassailable. Beyond this, however, data are lost by data rejection when theoretical requirements are not met, e.g. during low-turbulence periods, by other data-quality controls, or often by partial or complete equipment failure (Aubinet et al., 1999; Foken and Leclerc, 2004; Goulden et al., 1996; Papale et al., 2006). Such gaps can account for 20-60% of an annual dataset of the net ecosystem exchange (NEE) (Falge et al., 2001; Moffat et al., 2007). Thus, in spite of theoretical limitations, dataset incompleteness is a major hindrance to the impact of EC in the widespread quantification of GHG exchange.

Despite their incompleteness, fragmented data sets may contain sufficient information for short-term (i.e. half-hourly) interpolation and for limited evaluation of process-based models, however intactness is a fundamental requirement for estimating annual carbon budgets and for comparison with other biometric measurements. Traditional approaches to tackling gap filling in NEE measurements are mainly based on the idea of correlating the flux with other driving environmental variables (e.g., temperature, global radiation, water vapour, etc.) where fewer gaps and more predictable (or at least, more well understood) temporal variation occurs. This has led to a fruitful development of gap-filling techniques, broadly classifiable into four categories: process-based modelling, non-linear regression, moving window average and artificial neural network (ANN). The first two methods, based on a certain level of understanding in biophysical and/or biogeochemical processes, are either pure mechanistic or semi-mechanistic/empirical. The former has a highly complex form and is generally applicable in certain theoretical assumptions and/or land surface types (Verbeeck et al., 2011; Zhang et al., 2013). In contrast, the latter is based on building simple relationships between the flux and the environmental driving variables and is thus the most commonly used method for gap-filling NEE (Gomez-Casanovas et al., 2013; Kunwor et al., 2017; Sonnentag et al., 2010; Thomas et al., 2011). Unlike these two methods, the moving window average and ANN require minimal understanding of the system processes but construct variable relationships by learning data patterns. With the development of computational power, ANN

has become an active field of research in gap-filling the estimation of carbon flux (Dengel et al., 2013; Moffat et al., 2010; Papale and Valentini, 2003).

A recently comprehensive comparison (Moffat et al., 2007) of fifteen gap-filling methods based on 10 benchmark datasets showed that different techniques performed almost equally well, with ANN slightly (but not significantly) better because it is better able to replicate underlying patterns in the data. The reason why 15 independent methods resulted in similar performance however, remained unexplained. A plausible explanation is that the gap-filling efficiency was ultimately limited by the noise in the signal. Here "noise" represents stochastic, unstructured variation, unrelated to known environmental drivers (see details below). As noise becomes larger relative to the "real" signal, it becomes harder for any gap-filling algorithm to distinguish the real information that needs to be replicated. Thus, irrespective of gap-filling method, the estimation variance may be primarily a reflection of the variance in signal noise rather than the efficiency of the method itself.

Introducing auxiliary information from secondary environmental variables can assist in re-construction of the flux time-series but this is limited in two situations. Firstly, the flux response to driving variables may be poorly understood or unknown (e.g. the response of gas exchange to, for example, water table depth in wetlands), not least because of any non-linearity of the system (i.e. simple regression functions are not capable of capturing all variations in the system) (Lasslop et al., 2010). The form and parameters of regressions and look-up tables are site-specific, hindering progress in standardising the estimation of carbon exchange and reducing biases among sites (Reichstein et al., 2005). Secondly, any uncertainties or errors in environmental variables that are used in regressions or to train ANN propagate into the final NEE estimation. A further limitation in using ANN is that their intricately integrated structure makes it difficult to track the effect of, and noise introduced by, input variables, some of which may have limited predictive power and may even be redundant in terms of contributing to the real signal (Tu, 1996).

Rearranging a half-hourly time-series of NEE into a 48 * N matrix (where the rows represent the time of day (i.e. 48 half-hourly periods) and the N columns represent the day of year) provides us a way of visualising the time-series in two dimensions, commonly known as the flux fingerprint figure. In this paper, we present a gap-filling method of NEE based on a technique known as image inpainting (Bertalmio et al., 2000) which has become mature in fixing corrupted 2-dimensional images but not been used in tackling the gap-filling in time-series. This method has the advantage that any temporal structure (e.g. daily and half-hourly

covariance) is better incorporated into gaps in the flux signal without implying any particular functional response to driving environmental variables. Similar to the principle behind ANN-based machine learning, the image inpainting technique can sense any underlying structure in the time-series by iteratively and smoothly propagating information (see the methodology section for details). Moreover, compared with traditional methods such as the two standardized ones adopted by Carboeurope and FLUXNET (Papale et al., 2006) where many inputs (e.g. temperature, radiation, u*, VPD, etc.) and complex functions are needed, data gaps are filled solely using information contained in the flux data themselves, largely simplifying the gap-filling process and avoiding potential uncertainties introduced by auxiliary information (e.g. poor quality of auxiliary information and over-fitting).

3.3 Materials and methods

3.3.1 Data description

A total of twelve (12) years of data from 6 European sites were selected for conducting the comparisons of the gap-filling performance. The Level-3 NEE products (see code and data availability) were used for implementing the inpainting-based gap filling and the required driving environmental variables were added to run the Marginal Distribution Sampling (MDS) gap filling procedure. In this study, datasets from the process of quality control (QC) (e.g. u* criterion, spike detection, Steady state tests) (Foken et al., 2004) were used for simulation. The gap percentage varied among sites and years, from 29.5% up to 56.7% (see Table 3-1).

Table 3-1 Description of the datasets from the European fluxes database. The gap percentage was calculated by counting the half-hourly data missing of a whole year (i.e. 17520 of data records for 365 days).

Site-ID	Location	Vegetation Type	Lat/Long	Year	Gap(%)	Post-QC Gap(%)	PI
UKAMo	Scotland	Peatland	-3.23°, 55.79°	2010	9.9%	30.2%	Marc Sutton
UKEBu	Scotland	Grassland	-3.20°, 55.86°	2010	26.4%	44.8%	Marc Sutton
DEGeb	Germany	Cropland	10.91°, 51.10°	2010	43.1%	55.9%	Olaf Kolle, Mathias Herbst
DEGri	Germany	Grassland	13.51°, 50.95°	2010	9.9%	31.1%	Christian Bernhofer
				2011	17.9%	37.2%	
				2012	11.0%	29.5%	
ITRo3	Italy	Cropland	11.92°,	2011	23.6%	50.1%	Dario Papale

			42.38°	2012	22.0%	48.4%	
				2013	7.1%	42.7%	
ITRo4	Italy	Savannah	11.92°, 42.37°	2011	27.7%	56.7%	Dario Papale
				2012	19.1%	47.8%	
				2013	23.4%	52.2%	

3.3.2 Gap filling methods and artificial gap type

MDS – Marginal Distribution Sampling (MDS) is a moving window average method where both NEE and several driving environmental variables including heat flux, solar radiation, soil or air temperature, friction velocity and relative humidity are required as inputs for the algorithm (Reichstein et al., 2005). The R Package called REddyProc (Reichstein and Moffat, 2015) is used to implement MDS.

IIP – Image Inpainting (IIP), a fourth-order partial differential equation called the Cahn–Hilliard Equation is solved numerically to propagate information smoothly from outside the data-missing region into it (Burger et al., 2009; Schönlieb, 2015). The inpainted image can be considered as a highly smoothness estimator of the original image and the "smoothness" was solved gradually until a stable state is reached. A simple example is given below (Fig. 3.1), showing the reconstruction of corrupted images using IIP. Similarly, the fingerprint figure of NEE is converted to a grayscale image and the gaps are then filled by the inpainting algorithm based on the code from the MATLAB Central File Exchange (Schönlieb, 2011). Since IIP does not require any inputs from environmental drivers, rare events such as heat wave and extremely dry or wet conditions may not be captured by this method.

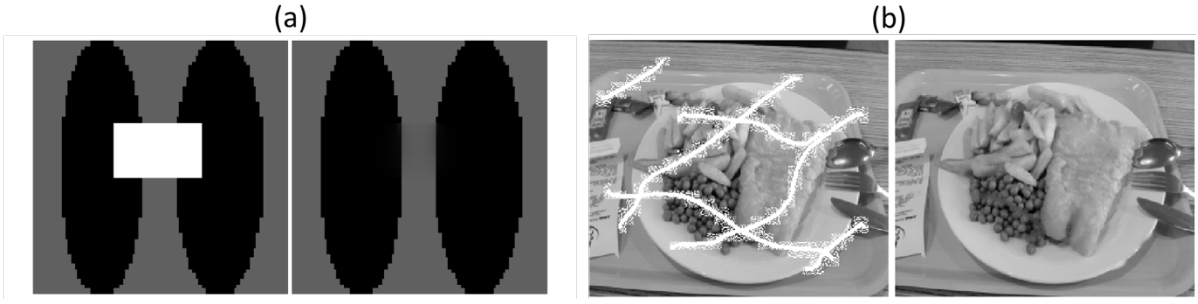

Figure 3.1 Examples of the Image Inpainting. (a) A simple structure with an artificial square gap represented by the white area (left) and its reconstruction (right); (b) A real photo corrupted with gaps (i.e. white stripes) (left) and its reconstruction (right).

In order to evaluate the performance of the gap-filling methods on the data points where real values exist, short and long artificial gaps amounting to about 10% of each dataset are considered in the simulations. Concretely, for the short type, half-hourly gaps are added uniformly randomly to the original NEE signal, while gaps with length of 3-day, 7-day and 14-day are added respectively (Fig. 3.2).

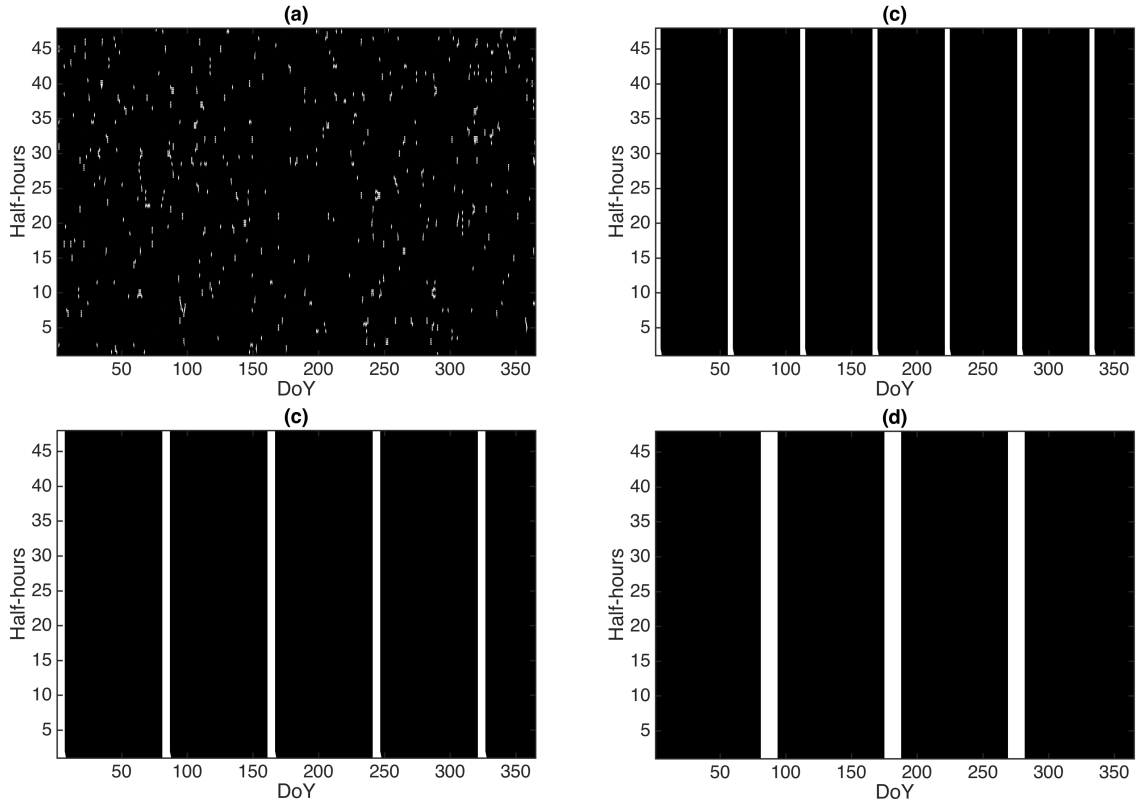

Figure 3.2 Four gap types generated are (a) random gaps; (b) 3-day; (c) 7-day; (d) 14-day. White strips represent the gap positions. Number of gaps for each gap type was about 10% of the whole year (i.e. ~1752 data points).

3.3.3 Noise reduction

To start with, we need to clarify what "noise" means in the context here. For a given signal, it can be partitioned into two parts: the trend part and the stochastic part. The trend part is called the de-noised signal and the stochastic part is referred as the noise. The noise characterized the randomness of a signal. As there is no general rule for reducing the noise from a NEE signal, the following assumptions are made for validating a de-noise method:

1. Noise has zero mean and symmetric/unbiased distribution;
2. Covariance between the noise and the de-noised signal is negligible (close to zero);

3. The difference between the before and after de-noising are small in the cumulative temperature and NEE.

Points 1 and 2 are used to show that the noise part was similar to a stochastic, unstructured and non-correlated signal. Since the underlying pattern of NEE is unknown, the cumulative and average temperature and NEE are used to show that the important information still remains after the de-noising process (see details in Results).

A simple method based on the Fourier transform of an entire time-series is used to reduce noise in the NEE and temperature signals. This process is illustrated by the block diagram:

$$x(n) \rightarrow \boxed{\mathcal{F}\big(x(n)\big)} \rightarrow \boxed{Threshold{:}\ \hat{x}(k) = g \cdot \mathcal{F}(x)} \rightarrow \boxed{\mathcal{F}^{-1}\big(\hat{x}(k)\big)} \rightarrow y(n)$$

where x(n) is the original "noisy" signal in the time domain (n), with any gaps initialized with the mean value of the rest of the signal. F and F $^{-1}$ are the fast Fourier transform and its inverse respectively. $\hat{x}(k)$ is the filtered signal at frequency (k) and y(n) stands for the de-noised signal. The threshold step was carried out using a simple binary function:

$$g(a) = \begin{cases} 0, & |a| \le T \\ 1, & |a| > T \end{cases} \qquad (3.1)$$

Two more sophisticated noise reduction techniques, the short-time Fourier transform and wavelets (each using various sized windows) were also tested in our study, but did not show distinct advantages over the simple Fourier transform, and the results are not presented here.

A dimensionless quantity is used to measure how much noise has been removed by the de-noising process. In image processing, the quality of a signal can be expressed quantitatively as the signal-to-noise ratio (SNR) (Schowengerdt, 2006), denoted as:

$$SNR = \frac{\sigma_{signal}}{\sigma_{noise}} \qquad (3.2)$$

where σ_{signal} and σ_{noise} are the standard deviation of post-filter signal and the standard deviation of the filter-out signal (noise) amplitude in the Fourier domain, respectively.

3.3.4 Measures of gap-filling uncertainty

To measure the gap-filling uncertainty in a more defensible way, three more quantities were included in addition to the commonly used root mean square error (RMSE). Following (Hanna, 1993) they are defined below:

$$FB = \big(\overline{X_0} - \overline{X_p}\big) / \Big(0.5\big(\overline{X_0} + \overline{X_p}\big)\Big) \qquad (3.3)$$

$$FAC2 = fraction\ of\ data\ for\ which\ 0.5 \le X_p/X_0 \le 2 \qquad (3.4)$$

$$VG = e^{\overline{(lnX_0 - lnX_p)^2}} \quad (3.5)$$

where *FB* is the fractional bias, *FAC2* is the fraction within a factor of two and *VG* is the geometric mean variance. X_0 is an observed quantity and X_p is the corresponding modelled quantity.

3.3.5 Analysis

The two gap-filling methods were applied to the original and the noise-reduced NEE data from 12 years of measurements at 6 European sites respectively. Following Moffat et al. (2007), we assumed that the differences between the traditional methods are negligible, and therefore comparisons were only conducted between IIP and MDS. Initially, we applied the two methods to the original NEE datasets and measure their performance on four types of artificial gaps, including short random gaps and long gaps up to 14 days. Further simulations were then conducted to show how noise or random structures in the signal may affect the gap-filling performance by partitioning the original signal using Fourier transform. Evaluating the gap filling performance on artificial gaps is more of a mathematical validation than a biophysical one, therefore we conducted comparisons of gap filled data against environmental driving variables (i.e. temperature and PPFD) to further demonstrate the validity of IIP based on biophysical meanings (i.e. temperature and light responses).

3.4 Results

3.4.1 Gap filling the NEE data with artificial gaps

Figure (3.3) shows an example of the comparison of the gap-filling performance between IIP and MDS on the post-QC NEE data with artificial gaps at site DEGri 2012. The general temporal patterns revealed by the two gap-filling methods are very similar across all four gap types. Clear diurnal and seasonal variations were well captured by both methods. In contrast to MDS, contour structures and boundaries generated by IIP are smoother or less “noisy”. This can be seen mostly clearly from a large gap (~ 2 weeks) in the middle of the year. Effects of gap type on the gap-filling performance were minimum and can hardly be noticed from the contour plots, which may suggest that IIP was able to reconstruct the signal even with the occurrence of the long-gap type up to 14 days.

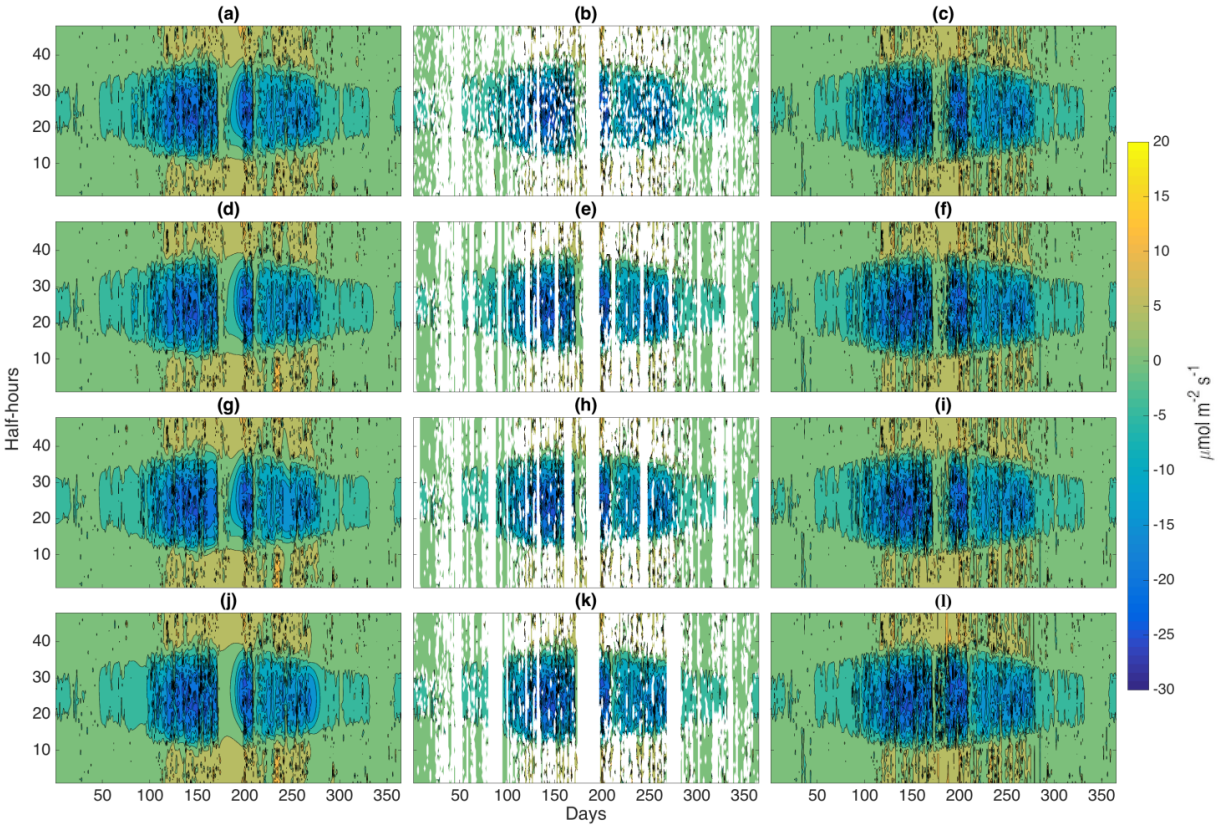

Figure 3.3 Image inpainting vs Marginal Distribution Sampling for the four gap types at site DEGri 2012. The middle column (i.e. (b), (e), (h) and (k)) are the original NEE data with random, 3-day, 7-day and 14-day artificial gaps respectively. The left (i.e. (a), (d), (g) and (j)) and right (i.e. (c), (f), (i) and (l)) column represent the gap-filling results from IIP and MDS accordingly.

The difference of gap-filling outcomes between the two methods shown on the finger-prints plots, however, are not sufficient to determine their performance quantitatively. The difference was further evaluated for all twelve datasets at the data points of artificial gaps where the true NEE values were available. The gap filling error was simply calculated by taking the difference of the estimated and real values at those data points. The error distributions represented by the error bar plot (Fig. 3.4) showed that there was little difference between methods, i.e. comparable means and variances in the gap-filling error, even though we see different levels of smoothness from the contour plots. Mean values close to zero suggests that both methods provided nearly unbiased estimations for the NEE signal. Combining all twelve datasets categorized by gap types and using a single metric for errors (i.e. *RMSE, FB, FAC2 and VG*), we again found that the two methods were hardly distinguishable from each other (Table 3-2). As might have been expected, gap-filling error tended to increase as gap length increased for both methods. One should notice, however, the increase amount was relatively small, with a difference of ~1.2 in *RMSE* between the random

and 14-day gap types (i.e. the two extremes). The facts above implied that, 1) Smoothly filling the gaps (by IIP) did not necessarily performed less well in terms of the estimation accuracy; 2) Large gaps did not significantly affect the gap-filling performance for either method. In fact, this result is consistent with a previous study (Falge et al., 2001) where the gap-filling residuals were not distinguishable by ANOVA. Both implications seem counter-intuitive, however, the simple way of understanding this is to recognise that both gap-filling methods "failed" to recover the missing signals. This happens if a signal contains a significant amount of noise/randomness which would be impossible for any method to recover.

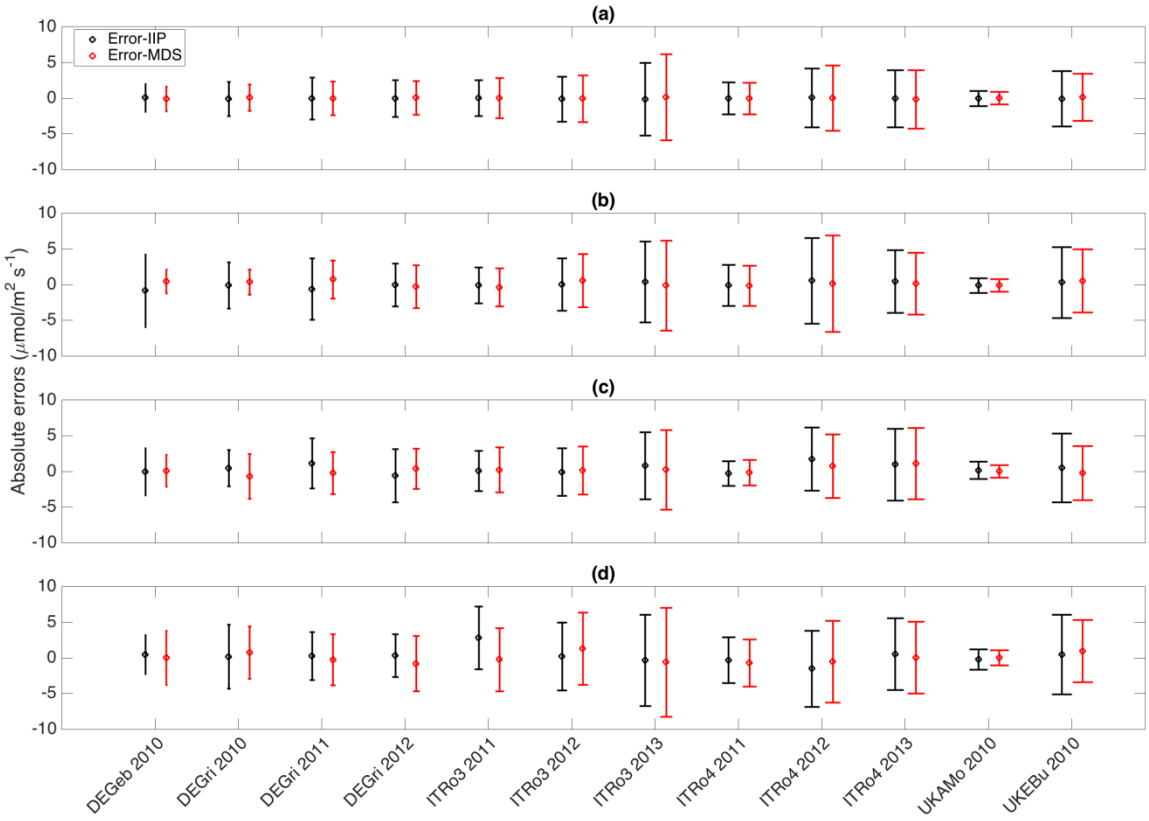

Figure 3.4 Comparisons of the gap-filling error between IIP and MDS for the four gap types, i.e. (a) Random gaps; (b)3-day gaps; (c) 7-day gaps; (d) 14-day gaps. Unit of the error values are in μmol m^{-2} s^{-1}. Error bar plot with mean ± one standard deviation of the absolute errors for each dataset.

Table 3-2 Overall statistics of the gap-filling error for all datasets for the four gap types.

Gap types	Random		3-Day		7-Day		14-Day	
Gap-filling methods	IIP	MDS	IIP	MDS	IIP	MDS	IIP	MDS
Sample size	11817	11817	11493	11493	10593	10593	13416	13416

RMSE	3.15	3.19	4.10	3.81	3.67	3.51	4.38	4.51
FB	-0.021	0.016	-0.0047	0.1231	0.24	0.10	0.11	0.03
FAC2	0.72	0.73	0.63	0.68	0.56	0.64	0.58	0.62
VG	1.75	1.68	2.46	1.88	2.47	2.12	2.37	2.25

In addition to the observation above, in Fig. (3.4), the gap-filling error showed the most variation at site ITRo3 2013, while it had the least variation at site UKAMo 2010 irrespective of gap types. This raises the question of where do the variations among datasets originate from? In other words, why were the estimations from some datasets always better than the others? The estimation confidence represented by one standard deviation (i.e. the span of the error bar) should be nearly zero for an ideally clean, noise-free image. As noise increases, the span becomes wider. We will address this problem in the next part by demonstrating that the variation of the gap-filling error originates from some random structures in the signal.

3.4.2 Random structures/noise affect the gap-filling performance

To start with, the temperature and the NEE signals were partitioned into two components respectively. To check that the de-noising procedure did not introduce bias, the average and cumulative temperature and NEE were compared before and after the signal de-noising process. An example of the de-noising is shown in Fig. (3.5&3.6) at site UKAMo in 2010. The mean and cumulative temperature signals are almost identical (Fig. 3.5a), suggesting that the system energetics remain the same even though some structures of randomness has been removed from the time series of temperature. The distribution of the removed part of temperature or the residual distribution shows a significantly good agreement with the normal distribution (not shown here), implying a Gaussian-structured/white noise embedded in the original temperature signal. Fig. (3.5b & 3.5d) show the fingerprint plots for the raw and de-noised temperature signals respectively. It is clear that the de-noising process smoothed out some variations from the raw signal, resulting in a much cleaner image.

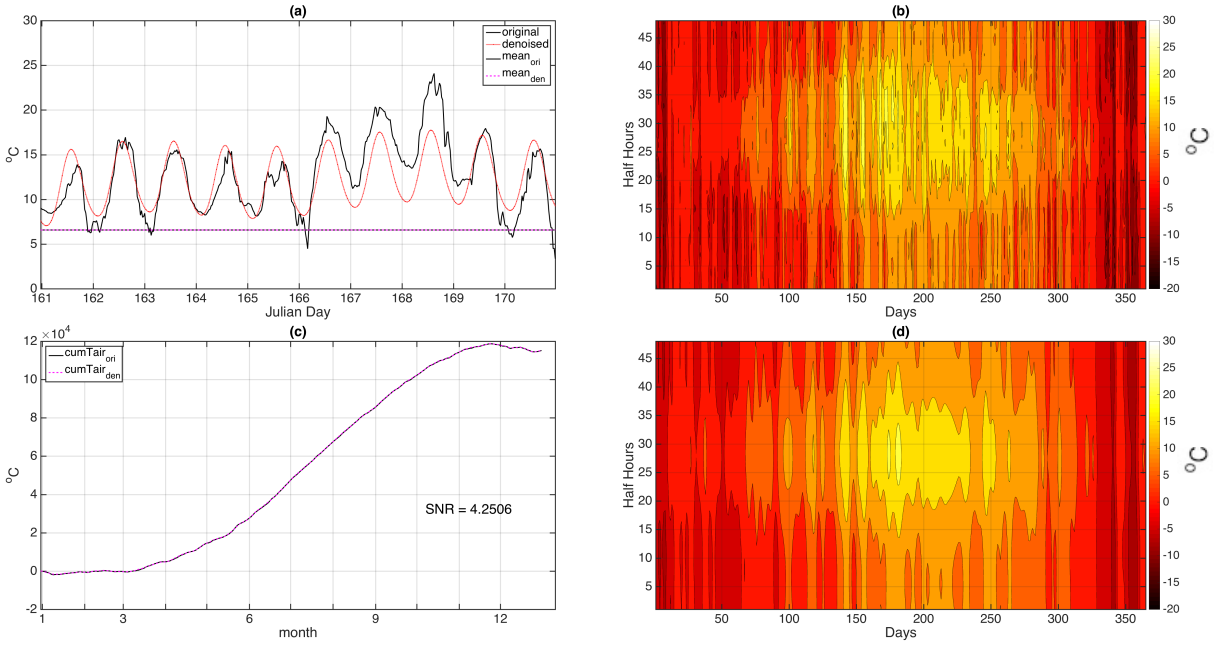

Figure 3.5 An example of a highly de-noised temperature data at site UKAMo for year 2010. Raw and de-noised half-hourly (a) and cumulative (c) temperature. 2-d visualizations (fingerprints) of raw and de-noised temperature in (b) and (d) respectively.

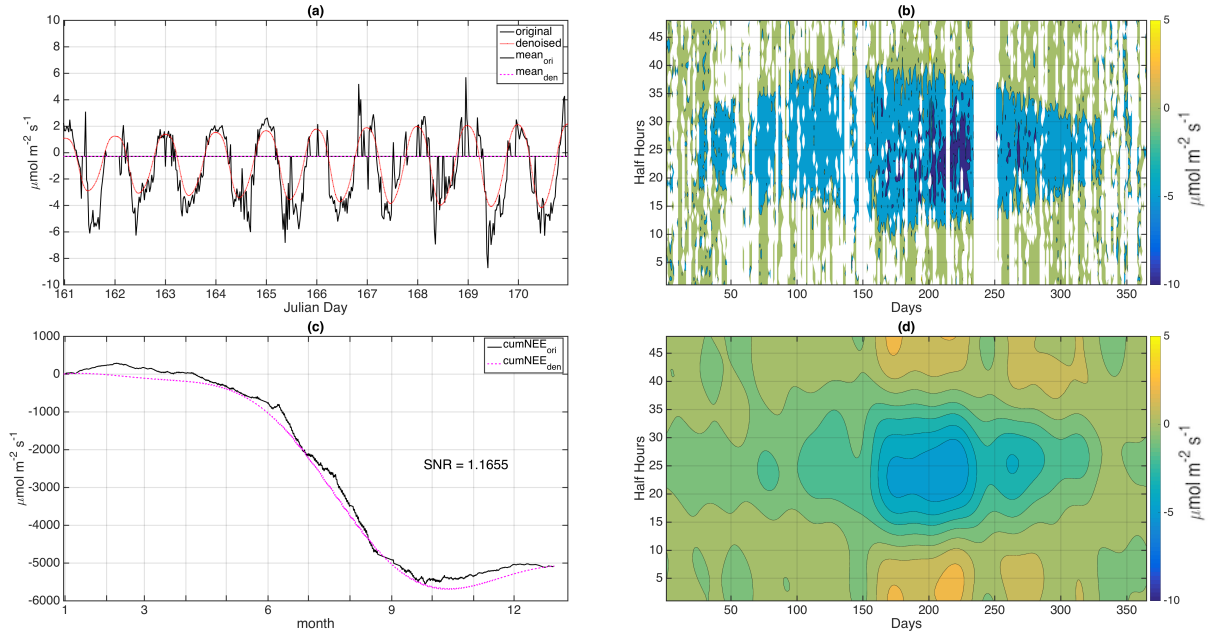

Figure 3.6 An example of a highly de-noised NEE data at site UKAMo for year 2010. Raw and de-noised half-hourly (a) and cumulative (c) NEE. 2-d visualizations (fingerprints) of raw and de-noised NEE in (b) and (d) respectively.

A similar result can be found in the de-noised NEE (Fig. 3.6) even though the SNR (~1.2) is much lower than that of temperature, suggesting that the NEE is initially noisier than the temperature. The value of SNR is determined by the thresholding step (Eq. 3.1) and for de-

noising the NEE signal, 1.2 of SNR was found to be approximately a lower limit of the noise removal in order to maintain a clear diurnal and seasonal variation (Fig. 3.6d). We show this largely smoothed NEE to demonstrate that the average and cumulative NEE after the de-noising are still good approximates to the original ones and for any less smoothed NEE with higher SNR values (see Fig 3.7) the cumulative NEE fits even better. Unrealistic fluctuations of the original NEE appear mostly at night-time and the de-noising method seems to fix this, as a traditional regression method would work, by replacing the night-time NEE with some simple variations (Fig. 3.6a), which might be the main cause for the discrepancy found in the accumulative de-noised NEE from the original (Fig. 3.6c). Intuitively this abnormality in the NEE signal at night-time supports our speculation about the existence of noise, which would affect the gap-filling performance by introducing the error variations. The distribution of the noise part of NEE, however, is not a good fit to the normal distribution but a rather steep, symmetry shape around 0, which is more like to be a t-distribution. This may suggest that the noise type embedded in the NEE, as shall be expected, is more complicated and different from the Gaussian-distributed noise found in the temperature. The covariance between the noise part and the de-noised part are very close to zero ($\sim 10^{-16}$) for both the temperature and NEE. A further investigation on the statistical feature of the noise is beyond the discussion of this study, however, this result has already provided an evidence that the noise parts removed from the original signals have some nice statistical feature that satisfies the criteria as proposed previously, i.e. it has zero means, symmetric distributions and negligible correlations/covariance with the real signal. Moreover, both the temperature and NEE remain almost unchanged in their average and cumulative quantities, enhancing the robustness and validity of this de-noise method.

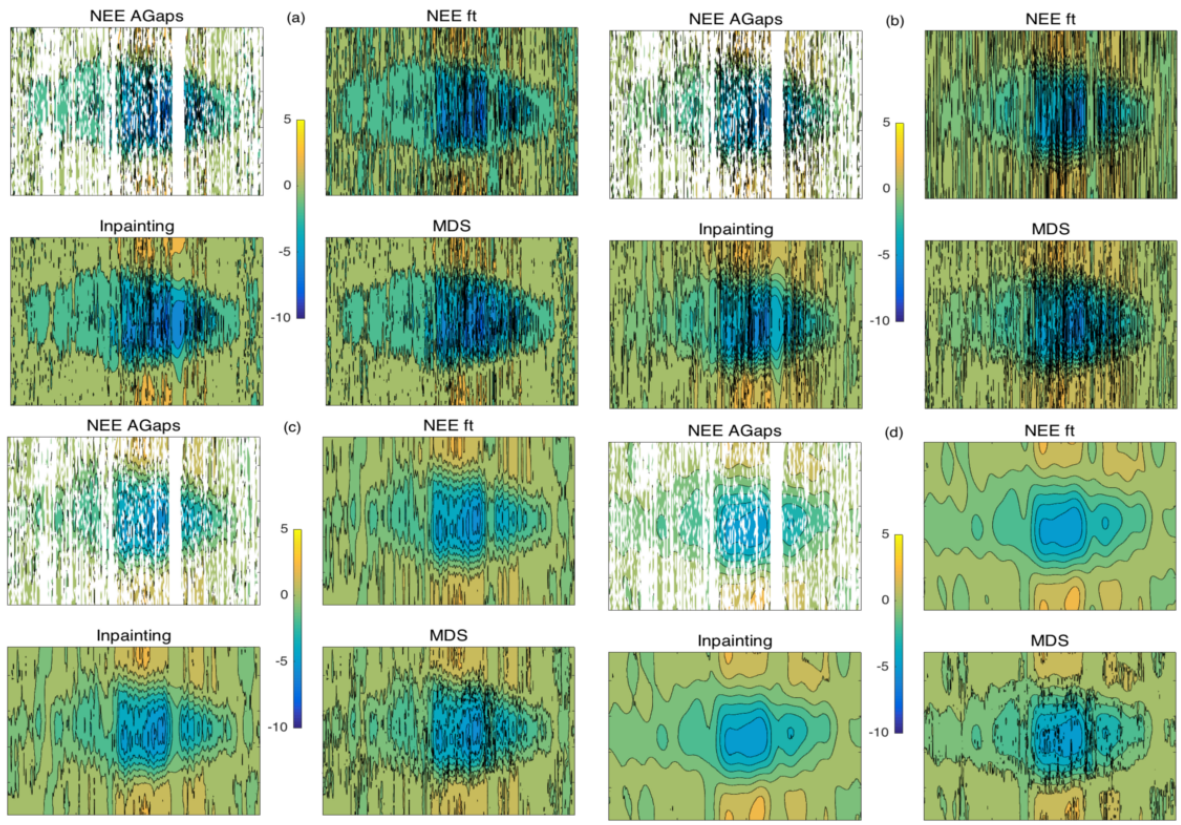

Figure 3.7 Data from UKAMo_2010. De-noising the NEE dataset and its gap filling. NEE ft is the de-noised NEE by Fourier transform. NEE AGaps stands for the post-denoise NEE with artificial gaps and real gaps. SNR levels are (a) 2.34, (b) 1.68, (c) 1.30, (d) 1.17. The unit for the colour bars is $\mu mol\ m^{-2}\ s^{-1}$.

Two sites, the UKAMo 2010 and ITRo3 2013 (see Table 3-1) were selected, as two extreme examples of the gap-filling error variation, for a further investigation on how the noise embedded in the signal affects the gap-filling performance as shown in Fig. (3.4) where the gap-filling error was found to be various among sites. We adjusted the threshold (Eq. 3.1) so that an increasing amount of noise can be gradually removed from the original signal until a highly smoothed one was reached (Fig. 3.6d). Only the cases with the random artificial gap type are presented here as it has been shown from the previous part that the gap type has little impact on the performance. Four of the de-noising states for the two sites are shown in Figs. 3.7 & 3.8 respectively. The NEE fingerprints become smoother as the SNR value decreases (i.e. more structures are removed from the original signal), with more visible periodic variations showing up. Because the inpainting method is a high-order PDE algorithm that pursues the smooth solutions, it produces a near-perfect reconstruction of the NEE images when the data are highly de-noised, clearly outweighing MDS (see Fig. 3.7d & 3.8d). Noticing that the starting value of SNR for ITRo3 2013 is significantly larger than that for

UKAMo 2010; it seems that more noise needs to be removed from ITRo3 2013 to reach a similar level of smoothness as UKAMo 2010. This further suggests that the larger variation of the gap-filling error found in ITRo3 2013 comes from an initially higher noise level embedded in the signal, which supports our speculation that the gap-filling performance is largely affected by the noise within a signal (Fig. 3.3). Because of the existence of these random structures, the gap-filling performance was found to be so similar between the two gap-filling methods (Fig. 3.4).

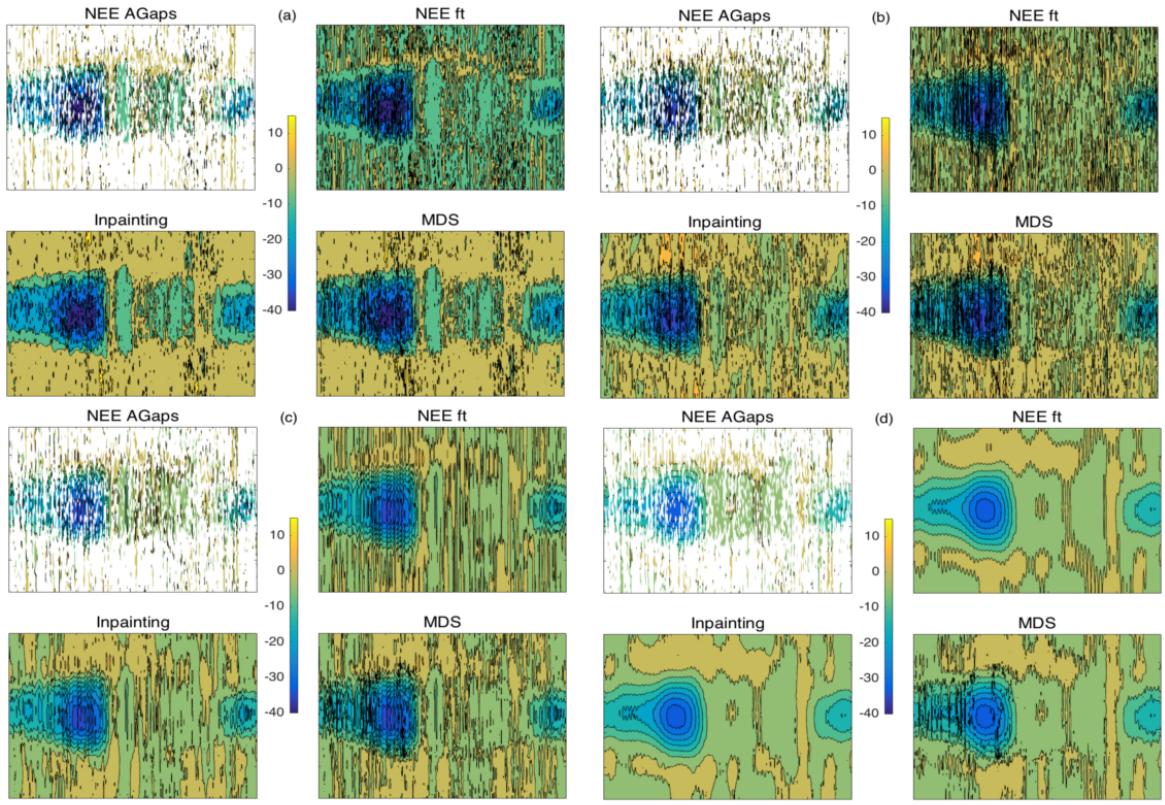

Figure 3.8 Site: ITRo3_2013. De-nosing the NEE dataset and its gap filling. NEE ft is the de-noised NEE by Fourier transform. NEE AGaps stands for the post-denoise NEE with artificial gaps and real gaps. SNR levels are (a) 24.87, (b) 1.90, (c) 1.50, (d) 1.35. The unit for the colour bars is μmol m^{-2} s^{-1}.

The response of the gap-filling error to the value of SNR can be seen most clearly in Fig. (3.9). Although the error decreases as expected for both methods as the SNR value decreases, the improvement gained from IIP is faster and better than that from MDS. Moreover, the uncertainty of estimation (i.e. error bar in Fig. 3.9) for IIP shows a trend to converge to zero as what an ideal performance should be for a noise-free image, compared with a converged constant significantly larger than zero for MDS. Although small in magnitude, this flux error could be accumulated and propagated into a large one in an annual flux estimate. To

summarize the two gap-filling methods, MDS, being based on a moving-window average algorithm, is a lower-order approximation to a time series, while IIP, being based on a higher-order non-linear equation, can sense and integrate more information in the process of gap-filling.

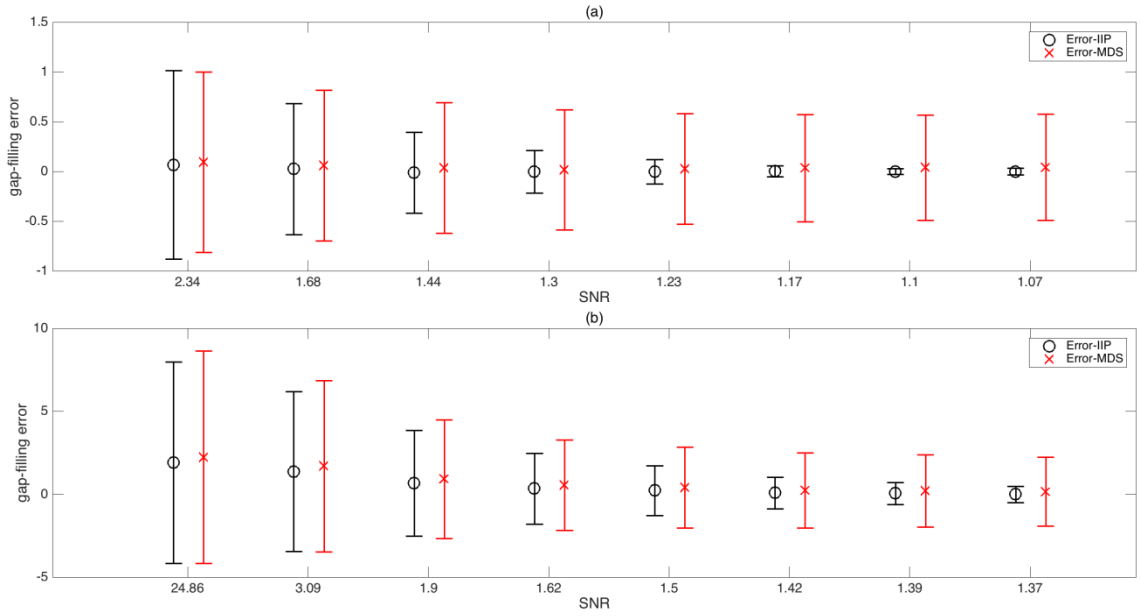

Figure 3.9 Gap-filling errors response to the ratio of energy remaining after de-noising (SNR). (a) Site: UKAMo_2010; (b) Site: ITRo3_2013. The gap-filling error simply refers to the difference between the gap-filling values and the real value at artificial gaps. Error bar plot stands for the mean ± one standard deviation of the errors.

3.4.3 Compare gap filled data against environmental drivers

Fig. 3.10 a&b show the raw and gap-filled NEE data against air temperature and light (i.e. PPFD) respectively at site UKAMo of year 2010. NEE data were separated into daytime and nighttime samples according to the solar radiation measurements, where nighttime NEE were plotted against air temperature to indicate the pattern of vegetation respiration. There is little difference on the gap-filled nighttime NEE between IIP and MDS, both of which captured the main variation of the raw NEE data. This suggests that the gap-filled NEE by IIP can effectively represent the pattern of the temperature response of respiration. Similarly, in Fig. 3.10b the daytime NEE were plotted against PPFD to examine the light response of the gap-filled NEE and little difference was found among the three types of NEE data. Both gap-filled NEE can be well fitted by using the commonly used hyperbolic function or light response function (Results omitted from here). It seems that there is a separation in the daytime NEE because of the seasonal variation in the vegetation physiology at this site.

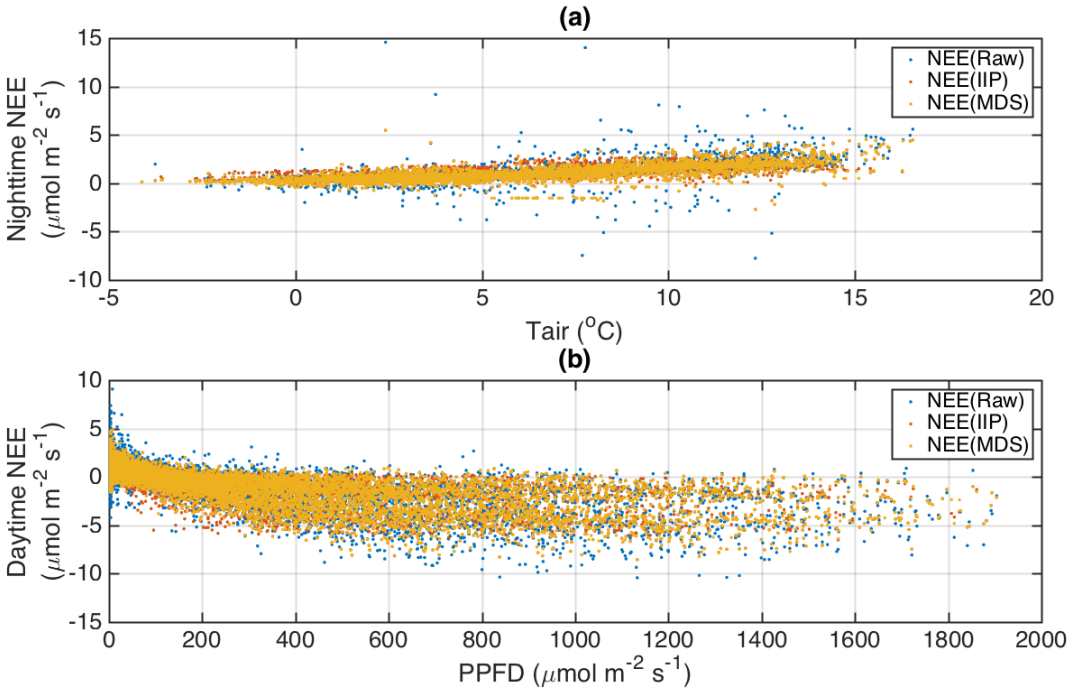

Figure 3.10 Relationships between NEE and environmental drivers. a) Raw, IIP and MDS gap-filled Nighttime NEE vs. air temperature at site UKAMo of year 2010. b) The three series of daytime NEE vs. PPFD.

3.5 Discussions and conclusions

We have seen that the inpainting-based gap-filling method (IIP) is highly comparable with the widely-used Marginal Distribution Sampling (MDS) in all simulation cases proposed in this study (Fig. 3.4 & Table 3-2). Evidence from the blurriness in the finger-print figures of NEE (e.g. Fig. 3.3), the unrealistic patterns at night-time (Fig. 3.6) and the gap-filling error variations (Fig. 3.4) pointed out the existence of noise in the signal, therefore we speculated that some random structures in the signal affect the gap-filling performance and contribute to the error variation. When the NEE data were de-noised by the simple Fourier transform, though both methods showed better accuracy of estimation, IIP was more effective in terms of capturing the smoothness (Fig. 3.9).

Nevertheless, a natural and fundamental question is, did we discard noise or real signal through the de-nosing process? To our knowledge, there is no definite answers to this question because the noise and signal are not distinguishable unless we know precisely and ahead of time what we are looking at. In contrast to de-noising an image or searching for objects from echo soundings, for instance, establishing criteria for identifying a noise-free

NEE signal is currently impossible because we do not, in fact, understand the underlying, process-based structure of NEE clearly. Our simplified de-noise algorithm based on the Fourier transform was capable of extracting the dominant variations in the signal while maintaining the average and cumulative quantities. Moreover, the removed parts from the original signals, or the so-called noise here, showed some good statistical features (Fig. 3.6), i.e. zero-mean, unstructured and non-correlated random structures. It is not, however, sufficient for providing a general rule for de-noising NEE (or other driving variables) because the performance of de-noising procedure depends on the amount of real signal underlying the time-series and the criteria used to distinguish real signal from noise. Taking the most conservative view (i.e. assuming that the NEE data are noise free after quality control), IIP, MDS and even other gap-filling methods are nearly equally good (Moffat et al., 2007). This suggests that these seemingly independent methods are simply alternative information processing machines, achieving the same level of approximation of a time series. In turn, this raises the prospect of unifying these gap-filling methods and adopting the most parsimonious.

In inpainting, only the target signal is needed to drive the gap-filling process. This simplicity is a distinct advantage of IIP because its internal coherence prevents potential biases being introduced from errors/incomplete auxiliary data and/or best-guess functions relating auxiliary data to NEE. Similarly robust methods are also found in other signal-processing techniques used to reconstruct noisy signals, i.e. singular spectrum analysis (Buttlar et al., 2014) and the discrete cosine transform (Garcia, 2010), however the utility of these methods for gap-filling NEE datasets remain untested.

While IIP shows some clear advantages over the traditional methods, some noteworthy limitations of this method need to be indicated. Firstly, IIP performed less well for long gaps where the information density is low (i.e. diameters of the gaps are big). This is especially true where extrapolation into long gaps at the beginning or the end of a time series is needed. In analogous situations where IIP is used to reconstruct missing areas in images, techniques based on finding and copying similar texture structure from other patches can be further explored (Bertalmio et al., 2003). Applying a similar approach to gap-filling NEE would require a hybrid of IIP for texture rendering and process-based understanding ecosystem dynamics (Knorr and Kattge, 2005) for texture mapping. Secondly, as IIP tends to find a smooth solution to a corrupted signal without incorporating information from environmental drivers, it would be difficult to detect rare/extreme events such as a pulse of gas exchange. Such pulses, however, may need careful examinations for any gap-filling techniques. An

environmental variable related regression model, for instance, would be better capturing a pulse if such anomaly also appeared in the driving variables. In some occasions, the anomaly may only be observed in the flux measurements (e.g. machinery faults of gas sensors). The type of pulse source is thus critical for determining the performance of a gap-filling technique. Besides, the uncertainties caused by pulses may become negligible in an estimation of the long-term flux budget. Thirdly, IIP is a purely numerical algorithm and cannot yet explain any system function. Notwithstanding this, however, the accuracy of IIP as an unsupervised process for filling artificial gaps, particularly when coupled with a de-noising algorithm, may contribute to bringing into focus underlying ecological and meteorological mechanisms not identifiable *a priori*.

In this paper, we show that the image inpainting (IIP) is a simple, compact and robust approach for gap-filling NEE, that it performs at least as well as a more complex gap-filling method, and we conclude that IIP should be added to the group of gap-filling methods for further research on gap-filling NEE. Evidence has been shown that the signal noise ultimately limits the gap-filling accuracy and de-noising the signal before the gap-filling procedure improves accuracy of estimation without introducing bias.

3.6 Code and data availability

The R Package called REddyProc for implementing MDS can be obtained either from R-Forge (https://r-forge.r-project.org/projects/reddyproc/) or the CRAN repository. The MATLAB code for implementing image inpainting is available from the MATLAB Central File Exchange (http://uk.mathworks.com/matlabcentral/fileexchange/34356-higher-order-total-variation-inpainting). In particular, the M-file called bvnegh_inpainting_convs.m was used for implementing the IIP-based gap filling.

All datasets used in this paper can be directly requested from the European Fluxes Database Cluster (http://www.europe- fluxdata.eu/). Please also refers to the details of data information from the request.

3.7 References

Aubinet, M., Grelle, A., Ibrom, A., Rannik, Ü., Moncrieff, J., Foken, T., Kowalski, A.S., Martin, P.H., Berbigier, P., Bernhofer, C., Clement, R., Elbers, J., Granier, A., Grünwald, T., Morgenstern, K., Pilegaard, K., Rebmann, C., Snijders, W., Valentini, R., Vesala, T., 1999. Estimates of the Annual Net Carbon and Water Exchange of Forests: The EUROFLUX Methodology. Adv. Ecol. Res. 30, 113–175. doi:10.1016/S0065-2504(08)60018-5

Baldocchi, D., 2014. Measuring fluxes of trace gases and energy between ecosystems and the atmosphere - the state and future of the eddy covariance method. Glob. Chang. Biol. 20, 3600–3609. doi:10.1111/gcb.12649

Baldocchi, D., Valentini, R., Running, S., Oechel, W., Dahlman, R., 1996. Strategies for measuring and modelling carbon dioxide and water vapour fluxes over terrestrial ecosystems. Glob. Chang. Biol. 2, 159–168. doi:10.1111/j.1365-2486.1996.tb00069.x

Baldocchi, D.D., 2003. Assessing the eddy covariance technique for evaluating carbon dioxide exchange rates of ecosystems: Past, present and future. Glob. Chang. Biol. 9, 479–492. doi:10.1046/j.1365-2486.2003.00629.x

Bertalmio, M., Sapiro, G., Caselles, V., Ballester, C., 2000. Image inpainting. Proc. 27th Annu. Conf. Comput. Graph. Interact. Tech. SIGGRAPH 00 2, 417–424. doi:10.1145/344779.344972

Bertalmio, M., Vese, L., Sapiro, G., Osher, S., 2003. Simultaneous Structure and Texture Image Inpainting. IEEE Trans. Image Process. 12, 882–889. doi:10.1109/TIP.2003.815261

Burger, M., He, L., Schönlieb, C.-B., 2009. Cahn–Hilliard Inpainting and a Generalization for Grayvalue Images. SIAM J. Imaging Sci. 2, 1129–1167. doi:10.1137/080728548

Buttlar, J. V., Zscheischler, J., Mahecha, M.D., 2014. An extended approach for spatiotemporal gapfilling: Dealing with large and systematic gaps in geoscientific datasets. Nonlinear Process. Geophys. 21, 203–215. doi:10.5194/npg-21-203-2014

Dengel, S., Zona, D., Sachs, T., Aurela, M., Jammet, M., Parmentier, F.J.W., Oechel, W., Vesala, T., 2013. Testing the applicability of neural networks as a gap-filling method using CH4 flux data from high latitude wetlands. Biogeosciences 10, 8185–8200. doi:10.5194/bg-10-8185-2013

Falge, E., Baldocchi, D., Olson, R., Anthoni, P., Aubinet, M., Bernhofer, C., Burba, G., Ceulemans, R., Clement, R., Dolman, H., Granier, A., Gross, P., Grünwald, T., Hollinger, D., Jensen, N.O., Katul, G., Keronen, P., Kowalski, A., Lai, C.T., Law, B.E., Meyers, T., Moncrieff, J., Moors, E., Munger, J.W., Pilegaard, K., Rannik, Ü., Rebmann, C., Suyker, A., Tenhunen, J., Tu, K., Verma, S., Vesala, T., Wilson, K., Wofsy, S., 2001. Gap filling strategies for defensible annual sums of net ecosystem exchange. Agric. For. Meteorol. 107, 43–69. doi:10.1016/S0168-1923(00)00225-2

Foken, T., Göockede, M., Mauder, M., Mahrt, L., Amiro, B., Munger, W., 2004. Post-Field Data Quality Control, in: Handbook of Micrometeorology. pp. 181–208. doi:10.1007/1-4020-2265-4_9

Foken, T., Leclerc, M.Y., 2004. Methods and limitations in validation of footprint models, in: Agricultural and Forest Meteorology. pp. 223–234. doi:10.1016/j.agrformet.2004.07.015

Garcia, D., 2010. Robust smoothing of gridded data in one and higher dimensions with missing values. Comput. Stat. Data Anal. 54, 1167–1178. doi:10.1016/j.csda.2009.09.020

Gomez-Casanovas, N., Anderson-Teixeira, K., Zeri, M., Bernacchi, C.J., Delucia, E.H., 2013. Gap filling strategies and error in estimating annual soil respiration. Glob. Chang. Biol. 19, 1941–1952. doi:10.1111/gcb.12127

Goulden, M.L., Munger, J.W., FAN, S.M., Daube, B.C., Wofsy, S.C., 1996. Measurements of carbon sequestration by long-term eddy covariance: Methods and a critical evaluation

of accuracy. Glob. Chang. Biol. 2, 169–182. doi:10.1111/j.1365-2486.1996.tb00070.x

Hanna, S.R., 1993. Uncertainities in air quality model predictions. Boundary-Layer Meteorol. 62, 3–20.

IPCC, 2000. Land Use, Land-Use Change, and Forestry, Forestry. doi:10.2277/0521800838

Knorr, W., Kattge, J., 2005. Inversion of terrestrial ecosystem model parameter values against eddy covariance measurements by Monte Carlo sampling. Glob. Chang. Biol. 11, 1333–1351. doi:10.1111/j.1365-2486.2005.00977.x

Kunwor, S., Starr, G., Loescher, H.W., Staudhammer, C.L., 2017. Preserving the variance in imputed eddy-covariance measurements: Alternative methods for defensible gap filling. Agric. For. Meteorol. 232, 635–649. doi:10.1016/j.agrformet.2016.10.018

Lasslop, G., Reichstein, M., Papale, D., Richardson, A., Arneth, A., Barr, A., Stoy, P., Wohlfahrt, G., 2010. Separation of net ecosystem exchange into assimilation and respiration using a light response curve approach: Critical issues and global evaluation. Glob. Chang. Biol. 16, 187–208. doi:10.1111/j.1365-2486.2009.02041.x

Moffat, A.M., Beckstein, C., Churkina, G., Mund, M., Heimann, M., 2010. Characterization of ecosystem responses to climatic controls using artificial neural networks. Glob. Chang. Biol. 16, 2737–2749.

Moffat, A.M., Papale, D., Reichstein, M., Hollinger, D.Y., Richardson, A.D., Barr, A.G., Beckstein, C., Braswell, B.H., Churkina, G., Desai, A.R., Falge, E., Gove, J.H., Heimann, M., Hui, D., Jarvis, A.J., Kattge, J., Noormets, A., Stauch, V.J., 2007. Comprehensive comparison of gap-filling techniques for eddy covariance net carbon fluxes. Agric. For. Meteorol. 147, 209–232. doi:10.1016/j.agrformet.2007.08.011

Papale, D., Reichstein, M., Aubinet, M., Canfora, E., Bernhofer, C., Kutsch, W., Longdoz, B., Rambal, S., Valentini, R., Vesala, T., Yakir, D., 2006. Towards a standardized processing of Net Ecosystem Exchange measured with eddy covariance technique: algorithms and uncertainty estimation. Biogeosciences 3, 571–583. doi:10.5194/bg-3-571-2006

Papale, D., Valentini, R., 2003. A new assessment of European forests carbon exchanges by eddy fluxes and artificial neural network spatialization. Glob. Chang. Biol. 9, 525–535. doi:10.1046/j.1365-2486.2003.00609.x

Reichstein, M., Falge, E., Baldocchi, D., Papale, D., Aubinet, M., Berbigier, P., Bernhofer, C., Buchmann, N., Gilmanov, T., Granier, A., Grünwald, T., Havránková, K., Ilvesniemi, H., Janous, D., Knohl, A., Laurila, T., Lohila, A., Loustau, D., Matteucci, G., Meyers, T., Miglietta, F., Ourcival, J.M., Pumpanen, J., Rambal, S., Rotenberg, E., Sanz, M., Tenhunen, J., Seufert, G., Vaccari, F., Vesala, T., Yakir, D., Valentini, R., 2005. On the separation of net ecosystem exchange into assimilation and ecosystem respiration: Review and improved algorithm. Glob. Chang. Biol. 11, 1424–1439. doi:10.1111/j.1365-2486.2005.001002.x

Reichstein, M., Moffat, A.M., 2015. REddyProc: Data processing and plotting utilities of (half-)hourly eddy-covariance measurements [WWW Document]. URL https://r-forge.r-project.org/projects/reddyproc/

Schönlieb, C.-B., 2015. Partial Differential Equation Methods for Image Inpainting. Cambridge University Press.

Schönlieb, C.-B., 2011. Higher-order total variation inpainting [WWW Document]. URL

http://www.mathworks.com/matlabcentral/fileexchange/34356-higher-order-total-variation-inpainting

Schowengerdt, R.A., 2006. Data Models, 3rd ed, Remote Sensing: Models and Methods for Image Processing. Academic Press. doi:10.1016/B978-012369407-2/50007-3

Sonnentag, O., Van der Kamp, G., Barr, A.G., Chen, J.M., 2010. On the relationship between water table depth and water vapor and carbon dioxide fluxes in a minerotrophic fen. Glob. Chang. Biol. 16, 1762–1776.

Thomas, M. V, Malhi, Y., Fenn, K.M., Fisher, J.B., Morecroft, M.D., Lloyd, C.R., Taylor, M.E., McNeil, D.D., 2011. Carbon dioxide fluxes over an ancient broadleaved deciduous woodland in southern England. Biogeosciences 8, 1595–1613.

Tu, J. V, 1996. Advantages and disadvantages of using artificial neural networks versus logistic regression for predicting medical outcomes. J. Clin. Epidemiol. 49, 1225–1231. doi:10.1016/S0895-4356(96)00002-9

Verbeeck, H., Peylin, P., Bacour, C., Bonal, D., Steppe, K., Ciais, P., 2011. Seasonal patterns of CO2 fluxes in Amazon forests: fusion of eddy covariance data and the ORCHIDEE model. J. Geophys. Res. Biogeosciences 116.

Zhang, X., Izaurralde, R.C., Arnold, J.G., Williams, J.R., Srinivasan, R., 2013. Modifying the Soil and Water Assessment Tool to simulate cropland carbon flux : Model development and initial evaluation. Sci. Total Environ. 463–464, 810–822. doi:10.1016/j.scitotenv.2013.06.056

Ch 4. Surface carbon fluxes to and from a heterogeneous UK fen: Understanding the difference between eddy covariance and chamber measurements[1]

4.1 Abstract

Wetlands are known to be significant sources and sinks of atmospheric carbon, both in the form of carbon dioxide (CO_2) and methane (CH_4). Quantifying the fluxes of these gases, and understanding the processes that control them, is therefore a priority task. This paper reports the simultaneous measurement of these fluxes at a heterogeneous fen on Anglesey, UK, using two independent methods, and describes the extent to which the flux estimates agree and differ. Static chamber and eddy covariance (EC) technique were used to estimate the net ecosystem exchange (NEE) and CH_4 flux during 2013 to 2015. Chamber samples for the two dominant vegetation types were interpolated and up-scaled using models to match the temporal and spatial scales represented by the EC-based measurements. Chamber measurements of NEE were interpolated using well-established functions driven by environmental variables, and were integrated to the plot scale using a two-dimensional flux footprint model. Regression analysis between the integrated and EC-based fluxes based on a 6-month observation period covering the growing season of 2014 showed a reasonable agreement for NEE (r^2=0.71, p<0.01), albeit with a significant bias - cumulative NEE during the whole season was -376.5 g/m^2 measured by chambers, 33% higher the EC-based estimates (-281.8 g/m^2). By contrast, using a similar approach generated poor agreement between the two CH_4 flux measurements, in part because the environmental variables driving the fluxes are poorly understood. We describe a novel method to interpolate chamber measurements using a parsimonious and unsupervised data fitting algorithm based on the Lasso regression. A significant improvement was made in reconciling the two estimates leaving a residual that resembled white noise (i.e. Gaussian distribution). The final cumulative CH_4 flux was 4.01 g/m^2 by chamber-based estimates, 43% more than that of EC-based estimates (2.81 g/m^2). This study contributes to an improved understanding of the two techniques of flux measurement in heterogeneous land surfaces.

[1] This chapter is based on: He, Y., Ridley, L., Brown, E., Callaghan, N., Rayment, M., (2016) Greenhouse gas exchange from a heterogeneous UK fen: Understanding the difference between eddy covariance and chamber measurements, JGR (In review)

4.2 Introduction

Measurements based on eddy covariance (EC) and static chambers are the two most common methods for quantifying carbon flux exchanges between the atmosphere and ecosystems. Because of the spatial complexity of most terrestrial ecosystems and the inherent limitations of the measurement techniques, estimates typically include significant uncertainties (Goulden et al., 1996; Hollinger and Richardson, 2005; Longdoz et al., 2000; Wohlfahrt et al., 2008). Without access to either the "true" flux values or to a fully understanding of the dynamics of the underlying biological and physical processes, it is difficult to evaluate precisely the data collected or validate the measurements without bias. In order to understand and improve the confidence of carbon estimation then, methods are needed to draw inferences about the "true" fluxes based on the error-containing data collected (i.e. experimental samples). A commonly used method is to subject data to some form of quality control using statistical techniques such as regression analysis, however a major drawback of using such analysis on data collected via a single sampling technique is that any systematic biases/errors are difficult or impossible to track (e.g. inherently faulty machinery). Where sufficient baseline data are available, it is possible to compare observed with expected values, but more rigorous science is possible where we have access to two independent methods of observing the same object (e.g. CO_2 and CH_4 flux), allowing a more robust approach to comparing observation with underlying (but ultimately inaccessible) reality. Comparison of independent methods assists not only in the evaluation of each method individually, but also identifies data "abnormalities" that might be discarded as artefacts when observed by a single method alone.

A number of studies have focused on the comparison of independent flux measurements from homogeneous source fields, where the spatial variation is negligible (Dore et al., 2003; Speckman et al., 2015; K. Wang et al., 2013) and any minimal discrepancy caused by spatial variation is within the uncertainty associated with individual data. The difficulty of making such a comparison in a heterogeneous source field, however, is that data sampled by the two techniques are seldom directly comparable because of the mismatch in their spatial distributions. Data collected by the EC-based system represent the field (sometimes termed ecosystem) scale, ranging from $10^2 – 10^4$ m^2, significantly larger than a plot scale ($10^{-2} – 10^0$ m^2) sampled by the chamber-based system (Fox et al., 2008). Therefore, in addition to the difference in temporal resolution between the two methods (which can normally be bridged by interpolation using regression models (e.g. Veenendaal *et al.*, 2007; Wille *et al.*, 2008)),

spatially-explicit downscaling of the EC data or upscaling of the chamber data is necessary before the actual comparison is feasible and justifiable.

In an EC-based system, micro-meteorological sensors are deployed to take measurements that reflect the turbulent exchange from a definable upwind area (at least in principle) of the underlying land surface. The effective fetch is the source field, commonly known as the flux footprint, which fluxes contributes to the sensors (Schmid, 2002). Importantly, the overall flux observed is not the simple average across the flux footprint area, but rather a probability density function describes how the fluxes emanating from each point upwind of the sensor is weighted in the integrated flux, depending on surface characteristics and the prevailing micrometeorological conditions which together determine the physical transfer of air from land surface to sensor. Thus, complex flux footprint modeling and a spatially explicit description of surface characteristics are needed to integrate across any heterogeneity within the observation area. Finally, in order to evaluate the EC and chamber observations they need to be articulated at the same spatial scale, so either a decomposition of the EC signals or an integration of the chamber signals is necessary. Four approaches for implementing footprint modelling have been widely used (Vesala et al., 2008): (1) analytical models, (2) Lagrangian stochastic particle dispersion models, (3) large-eddy simulations, and (4) closure models. Footprint models simulate particle (or flux) transportation where a key step is to determine the probability density function of flux contribution across the source area. For a heterogeneous field where the magnitude of the flux source varies spatially, the plot-scale chamber measurements can be mapped onto the field scale (as measured by EC) once they have been weighted by the footprint function. Several studies have used this concept to compare the EC and chamber measurements from landscapes including agricultural land (K. Wang et al., 2013), arctic tundra (Fox et al., 2008) and forestry (Dore et al., 2003). To our knowledge, no studies have been reported for semi-natural lowland peatlands where greenhouse gas emissions are highly heterogeneous both in space and time, and play a potentially important role in the current and future global carbon cycle (Blodau, 2002; Evans et al., 2016; Freeman et al., 1992).

In this paper, we compare EC and chamber measurements of surface carbon fluxes (i.e. NEE and CH_4 flux) from a heterogeneous UK fen during the 6-month growing season of 2014. Monthly chamber records spanning 30 months were modelled to generate half-hourly NEE estimates for two dominant vegetation types. The flux footprint for each half hour was then estimated using a two-dimensional footprint model, and the chamber-based NEE and CH_4

flux were up-scaled by integrating the half-hourly series weighted by the footprint functions. Chamber- and EC-based half-hourly fluxes were compared through regression analysis. A long-term carbon budget for this site was estimated and a comparison was made between the two independent methods.

4.3 Materials and Methods

4.3.1 Study site

The chamber- and EC-based measurements were made at the Cors Erddreiniog, a national nature reserve on the Isle of Anglesey, UK. This whole site is highly heterogeneous and comprises 85% of bogs, marshes, water fringed vegetation and fens, 13% of grassland and woodland and 2% of inland water bodies (JNCC, 2016). Our measurements in this study were conducted at a fen area as part of the reserve.

Based on the vegetation classification map provided by Natural Resources Wales (NRW), the whole fen area was classified into two groups according to the dominant vegetation species, denoted by PM (*Phragmites australis*) and CD (*Cladium mariscus*). Three replicated chambers were placed to measure each vegetation type at the locations (PM and CD) as shown on the map (Fig. 4.1), with a micro-meteorology tower placed at the eastern side (EC). An automatic weather station managed by NRW (not shown here) was situated at 30 m north to our EC tower, providing hourly records of wind speed, wind direction and radiation for the simulations in this study.

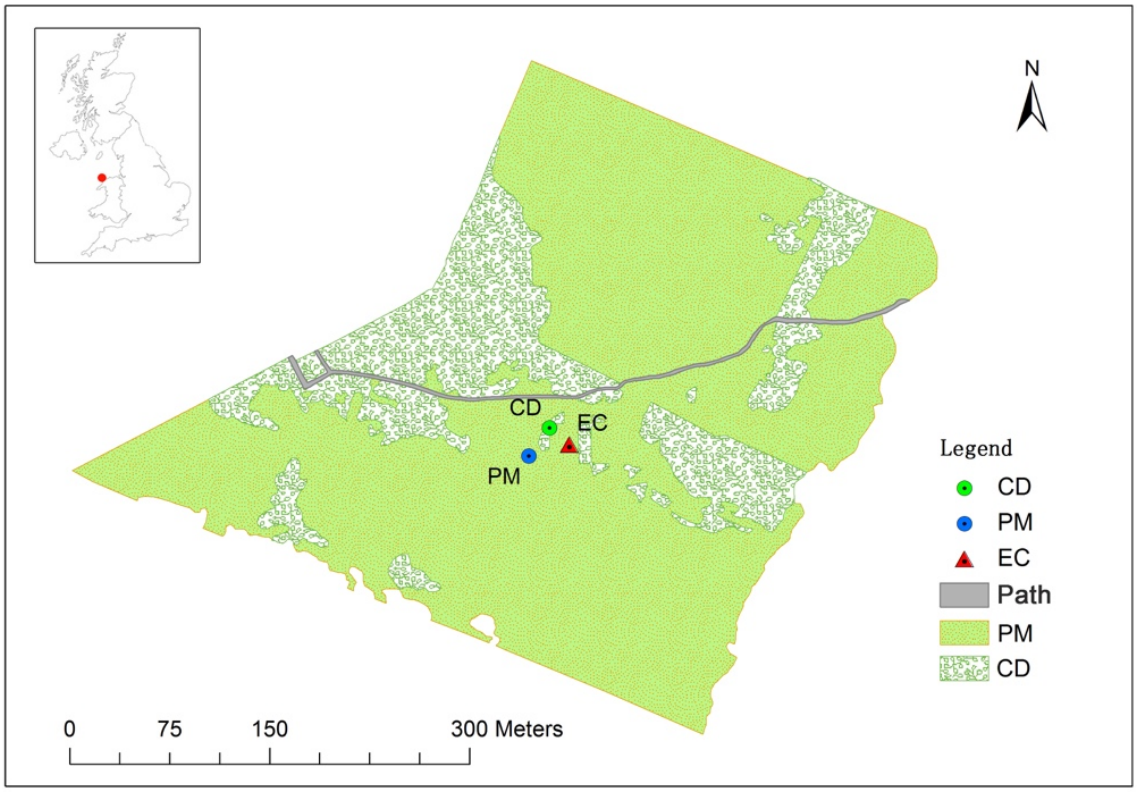

Figure 4.1Geo-information of the study site Cors Erddreiniog, a National Nature Reserve on the Isle of Anglesey, UK. Two classes of vegetation type measured by chambers are labelled with CD and PM. EC shows the location of the micro-meteorology tower. Image reproduced from the meta information of vegetation classification, courtesy of Natural Resources Wales.

4.3.2 Chamber-based measurements of NEE and CH_4 flux

4.3.2.1 NEE partition

Chamber data availability covered 30 months at the site, from March 2013 to October 2015. Data were collected between 9am to 4pm on the day once per month. Static flux chambers were custom built in a cubic shape with a bottom area of 60 cm x 60 cm (Evans et al., 2016). They were modular to accommodate different vegetation heights (with a volume of either 0.342 or 0.522 m^3) and included fans inside to keep air well-mixed. Gas samples were analysed *in situ* by the Los Gatos ultraportable greenhouse gas analyser (UGGA). Transparent and opaque chambers were used to measure CO_2 fluxes; net ecosystem exchange (NEE) and respiration (RE) respectively. CH_4 fluxes were measured concurrently.

To estimate half-hourly NEE from discrete chamber measurements, NEE was partitioned as:

$$NEE = -GPP + RE \qquad (4.1)$$

where *GPP* is the gross primary production and *RE* is the ecosystem respiration. Without considering the effects of water table, *RE* can be modelled using the classic exponential relation (Lloyd and Taylor, 1994). In this case, the sample area experienced significant seasonal variation in water table, therefore a two-degree polynomial was used to describe *RE* as follows (Howard and Howard, 1993),

$$\ln(RE) = \beta_0 + \beta_1 T_{soil} + \beta_2 WT + \beta_3 {T_{soil}}^2 + \beta_4 WT^2 \qquad (4.2)$$

where β_i are the coefficients fitted by linear regression. T_{soil} and *WT* are the soil temperature (°C) at 10 cm below the nominal soil surface and the depth of water table (cm) below to the nominal soil surface respectively, thus higher absolute value of *WT* reflects a lower water table and a drier environment.

GPP is mainly driven by photosynthetic photon flux density (*PPFD*) while temperature plays a role in determining the rate of photosynthetic enzyme activity. Therefore, we modified the Michaelis–Menten function (Falge et al., 2001) by including a temperature term:

$$GPP = \frac{a * e^{b*T} * Q_{PPFD} * c}{a * e^{b*T} * Q_{PPFD} + c} \qquad (4.3)$$

where *T* is the soil temperature (°C) at 10 cm below the nominal soil surface and Q_{PPFD} is the PPFD, here approximated by 1.8 times the solar irradiance (W/m^2). Coefficients *a*, *b* and *c* are fitted by nonlinear least square minimization.

4.3.2.2 Lasso regression for modelling CH_4 flux

Estimating half-hourly CH_4 flux is less convenient than NEE because widely applicable generic formulae such as Eqs. (4.1-4.3) have not yet been developed. As suggested in other studies (e.g. Olefeldt *et al.*, 2013; Turetsky *et al.*, 2014), we considered soil temperature and water table as the dominant variables driving CH_4 variation and therefore used multivariate regression analysis to create a function between CH_4 flux and environmental driving variables. By including in this model all other plausible potential driving variables (i.e. relative humidity, wind speed, friction velocity (*u**), net radiation and *PPFD*), we found that including *PPFD* improved the goodness of fit significantly by increasing r^2 by 18%. Statistical outliers were removed according to the Tukey boxplot (i.e. valid data lies within the 1.5*IQR (Interquartile range) of the upper and lower quartiles), which resulted in data availability of the two vegetation types of PM: N=40 (out of 48 measurements) and CD: N=29 (out of 32). The regression function included all combinations of the three driving variables, up to three degrees in total, giving 19 terms overall including a constant term. We

wanted to remove trivial terms and to prevent the regression from overfitting, and in these respects the traditional regression methods based on simple least square are of limited use (Tibshirani, 1996). Thus the Lasso regression was used to regularize the minimization of the least-square regression as follows (Hastie et al., 2009),

$$\min_{\beta_0,\beta}\left(\frac{1}{2N}\sum_{i=1}^{N}(y_i-\beta_0-{x_i}^T\beta)^2+\lambda\sum_{j=1}^{p}|\beta_j|\right) \qquad (4.4)$$

where N is the number of samples. y_i is the CH_4 flux. x_i is a combination of the normalized driven variables (a vector of p values at observation i). λ is a nonnegative regulation parameter. The parameters β_0 and β are regression coefficients which are determined by the minimization process. 5-fold cross validation was used to evaluate the model with different values of λ. The Lasso method tends to find a sparse solution by setting some coefficients to 0, and "select" an optimized model based on its performance on the cross validation datasets. We used the Lasso function in MATLAB to implement the regression, a similar package is also available in R called "Glmnet".

4.3.3 Micro-meteorology measurements and flux footprint modeling

The flux tower, deployed in Oct 2012, included an open path CO_2/H_2O analyzer (LI-COR LI-7500A), an open path CH_4 analyzer (LI-COR LI-7700), a 3-D sonic anemometer (Campbell CSAT3), a net radiation sensor (LI-190R) and a data logger (Campbell CR3000).

Other environmental sensors used were two self-calibrating soil heat flux plates (HFP01SC) and both manual and automated dip wells positioned to measure water tables both above and below the nominal soil surface (Evans *et al.*, 2016).

The raw data (at 20Hz) were processed using the software (LI-COR EddyPro) to generate half-hourly NEE and CH_4 flux data, which were then corrected for flux storage terms. Gaps of NEE were filled by the marginal distribution sampling method (Reichstein et al., 2005). We attempted to fill the gaps of CH_4 flux by following existed parametric formulae (Olefeldt et al., 2013; Wille et al., 2008), but the goodness of fit was incredibly poor ($r^2 \approx 0$) suggesting no significant relationship between CH_4 flux and potential environmental driving variables. Instead, the gaps were filled objectively by using Fourier transform and its inverse (He and Rayment, 2016).

The flux footprint was estimated for each half-hour by using a two-dimensional flux footprint prediction (FFP) model (Kljun et al., 2015). Compared to other footprint models, FFP is of high computational efficiency and has been validated for real-case applications of a wide

range of boundary layer conditions. Half-hourly wind speed and direction were used to determine the size and orientation of the footprint area and the relative contributions of areas within it. Aerodynamic roughness length (z_0) was used as an input parameter and only data that satisfied the relation $12.5*z_0>z_m$ were used in the final computation, where z_m (=2.33 m) is the sensor measurement height above the zero-plane displacement height.

4.3.4 Spatially upscaling chamber measurements

To contain computing capacity to manageable proportions, the half-hourly data from the period March 1st to September 16th 2014 (roughly the growing period) were used for comparing the EC and up-scaled chamber measurements. With the modelled half-hourly NEE/CH_4 flux for each vegetation type and the half-hourly footprint function ready, the chamber data were then up-scaled by spatially integrating the NEE/CH_4 flux according to:

$$NEE_{int} = \sum_{i=1}^{n} f_i * NEE_i \qquad (4.5)$$

where NEE_{int} is the spatially integrated NEE for the whole region, f_i is the flux footprint and NEE_i is the NEE value from chamber measurements at the i^{th} position. Since only two vegetation types were considered in this study, NEE_i took two values representing either PM or CD for each given half-hour. Simply replacing NEE with CH_4 in Eq. (4.5) gives us the upscaling function for CH_4 flux.

4.3.5 Analysis: orthogonal regression

With no *a priori* basis for supposing that either method is less error prone than the other, both the integrated and EC-based NEE/CH_4 estimates should be assumed to contain equal amounts of random errors. A normal regression based on ordinary least square (OLS) is thus not suitable for a regression analysis of the two NEE/CH_4 estimations because OLS considers only one direction of error (i.e. whatever is considered as the dependent variable). In this study, orthogonal regression (Leng et al., 2007) based on total least square (TLS) (i.e. considering the errors in both the x- and y-axis variables) was used to implement a regression analysis of the agreement between NEE and CH_4 flux estimations (Eq. 4.6). The regression coefficients are conveniently estimated by using the principle components (Eq. 4.7):

$$y = \beta_1 x + \beta_0 \qquad (4.6)$$

$$\beta_1 = \frac{v_y}{v_x}\ ,\ \beta_0 = \bar{y} - \beta_1 \bar{x} \qquad (4.7)$$

where (v_x, v_y) is the first eigenvector of the 2*2 covariance matrix constructed from (*x, y*), a two column matrix made up by the time series of NEE or CH_4 flux. $\bar{x}$ and $\bar{y}$ are the mean values of *x* and *y* respectively. Since the traditional way of calculating the coefficient of determination (r^2) is not appropriate for TLS, we simply adopted the squared Pearson's correlation coefficient to show the linearity between *x* and *y*.

4.4 Results

4.4.1 Modelling NEE and CH_4 flux from chamber measurements

Measured soil temperature and CO_2 fluxes from dark chambers were fitted to the two-degree polynomial (Eq. 4.2) for the two vegetation types, PM and CD independently. Both vegetation types showed good performance with r^2 over 0.72 (Fig. 4.2a&4.2b), compared with r^2 of 0.67 when using the Lloyd and Taylor's exponential equation only. In both cases, respiration rate initially increased exponentially with temperature and then decreased as the system becomes drier (i.e. larger absolute value of *WT*). The optimal depth of water table for respiration was slightly different between vegetation, -14 cm for CD and -16 cm for PM. The fitted surface for CD was flatter than that for PM, suggesting that CD was more adaptable to extreme conditions (i.e. it still retained a significant amount of respiration even in a very dry or wet condition).

GPP calculated from Eq. (4.1) were fitted to soil temperature and *PPFD* using Eq. (4.3). A very good performance (r^2=0.8, p<0.01) was found in the goodness of fit for PM, compared with a moderate one for CD (r^2=0.58, p<0.01). The fitted surfaces shown in Fig. (4.2c&4.2d) revealed a similar dependence of *GPP* on the environmental variables for both vegetation types, i.e. as *PPFD* increased, *GPP* increased asymptotically towards a saturation of level of photosynthetic uptake, the value of which increased as temperature increased. Similarly as for respiration, the fitted surface of *GPP* was flatter for CD in terms of temperature, which suggested that CD was again more adaptable to cold conditions but less effective in photosynthesis than PM under warm conditions. As evergreen vegetation, CD can photosynthesise year-round, which is also implied from the non-zero edge of the surface where the temperature was low (i.e. winter time).

Fig. (4.2e&4.2f) show the goodness of fit between the modelled and measured NEE against the 1:1 straight line. For both vegetation types, modelled NEE were a reasonably good fit to

the measured NEE, although r^2 was about 30% higher for PM than for CD, largely as a consequence of the fit for *GPP*.

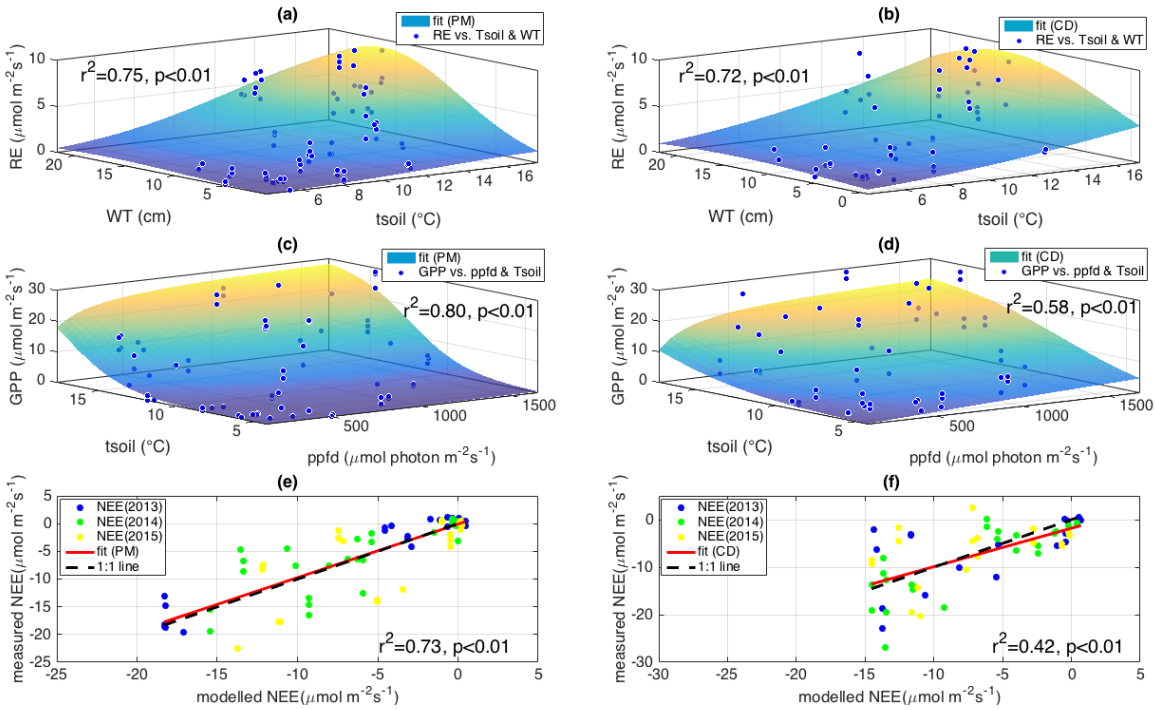

Figure 4.2 Modeling respiration (RE) (a&b), GPP (c&d) and NEE (e&f) for the two vegetation types, PM and CD.

For the Lasso regression, CH_4 flux was correlated with three variables (dimensions), namely soil temperature, water table and *PPFD*, a summary of which is thus not possible to be illustrated on a 2-D plane. The final performance of the multivariate regression is shown in Fig. (4.3). The modelled CH_4 flux showed good agreement with the measured flux for both vegetation types, with $r^2 \geq 0.5$ ($p<0.01$). Although the regression method is empirical, this level of r^2 suggested that the model is a good interpretation of the measured flux data. It should be noted that without including *PPFD* as a variable in the regression, the r^2 values were only 0.39 and 0.36 for PM and CD respectively, significantly smaller than the proposed model. Thus it is clear that *PPFD* contributes to the variation of CH_4 flux statistically, suggesting either a causative relationship, through some photochemical processes as proposed by previous researchers (Keppler et al., 2006; Vigano et al., 2008), or through autocorrelation between PPFD and another, unidentified driving variable, for example friction velocity (U^*). Table (4-1) shows the coefficients estimated by the Lasso regression for the two vegetation types. Some of the coefficients were precisely assigned to zero in the model, meaning that those terms were removed from the model, preventing the overfitting

that might occur through an unsupervised fitting process. In this way the model structure was largely simplified by retaining a small amount of significant terms only. Please find Appendix 1 for more details on how to choose an appropriate value of the regulation coefficient λ in Eq. (4.4). It should also be noticed that some combined factors such as soil temperature and water table showed high contributions to the modelled flux variation, suggesting a high autocorrelation between the two driving variables. In fact, the correlation coefficients between soil temperature and water table were significant for both vegetation types, i.e. 0.7 and 0.65 for PM and CD respectively.

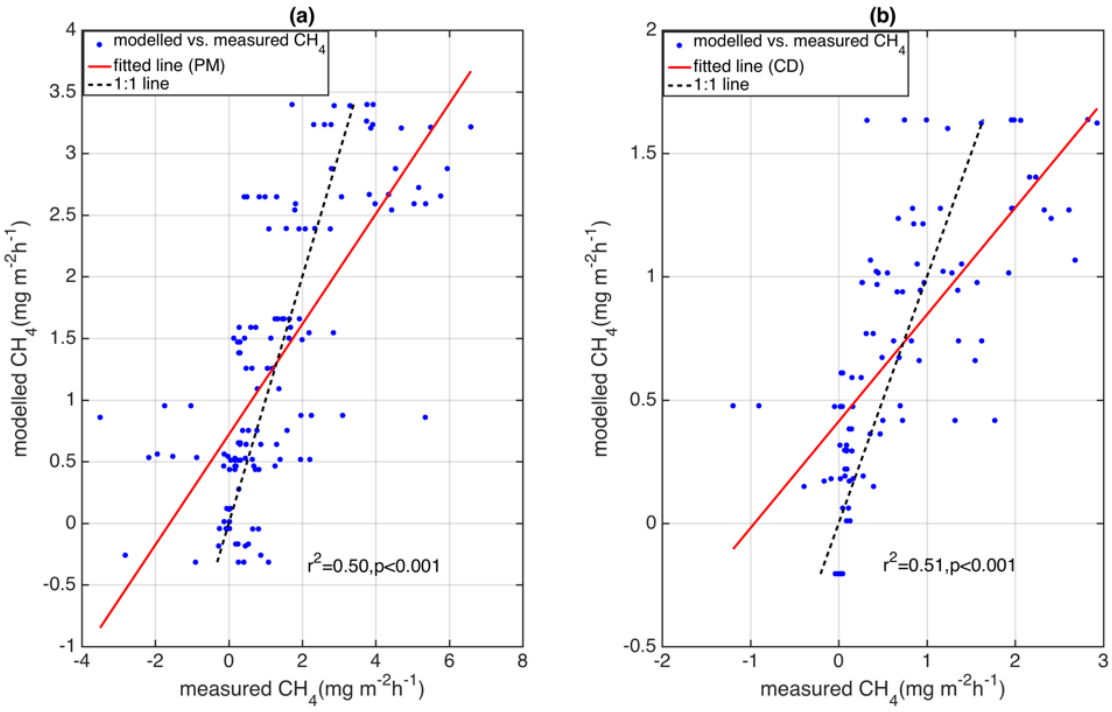

Figure 4.3 Modelled (by the Lasso) vs. measured CH_4 flux for vegetation PM (a) and CD (b).

Table 4-1 Lasso regression coefficients of modeling CH_4 flux for the two vegetation types. x_1, x_2 and x_3 are normalized soil temperature, PPFD and water table respectively.

Terms	β_i (PM)	β_i (CD)
Intercept	-2.43	-0.56
x_1	4.72	0.09
x_2	0	5.59
x_3	1.21	-0.83
x_1x_2	5.95	0
x_1x_3	0	0
x_2x_3	0	-0.93
x_1^2	0	3.68
x_2^2	-0.74	-7.57
x_3^2	0	0.22
$x_1x_2^2$	0	6.22
$x_1x_3^2$	0	0
$x_2x_3^2$	0	0
$x_2x_1^2$	0	-5.44
$x_3x_1^2$	-2.75	-0.79
$x_3x_2^2$	1.72	1.51
x_1^3	-0.64	0
x_2^3	-3.89	0
x_3^3	0	0

4.4.2 Flux footprint modelling

The prevailing wind at the study site came from southwest sector (Fig. 4.4a), and accounted for 46% of the total data during the study period, from March 1st to September 16th 2014. The average wind speed for this period was 3.1 ± 2.0 m/s (i.e. mean ± 1*std) with a maximum speed of 11.1 m/s. A significant second largest portion, about 30% of the wind, came from northeast sector and was characterized by low wind speeds. The average wind speed for the whole season was 2.5 ± 1.9 m/s.

53% of the total data satisfying the relation $12.5*z_0>z_m$ and a few other criteria required to ensure effective surface transport (Kljun et al., 2015) were used for the footprint calculation. For each half hour, a 2-D spatial footprint was estimated on a 300m*300m square centred at the position of the micrometeorology tower. A contour map of the average footprint for the whole season is shown in Fig. 4b. The overall footprint area was determined by the wind rose shown on the left, and extended approximately 100-150m around the tower, with a maximum upwind distance of contribution typically ca. 25 m (yellow hotspots in the figure). Over the whole period, the net probability of contribution from the area to the sensors was 0.70 ± 0.12 for PM and 0.10 ± 0.12 for CD, which suggested that PM made the major contribution to the

fluxes measured by the tower. The total contribution from the area was thus 0.80 ± 0.06, meaning that about 20% of the flux signal measured by the sensor was sourced from the area outside the square. The vegetation types outside this area were much more diverse and could not be properly classified by using PM and CD only.

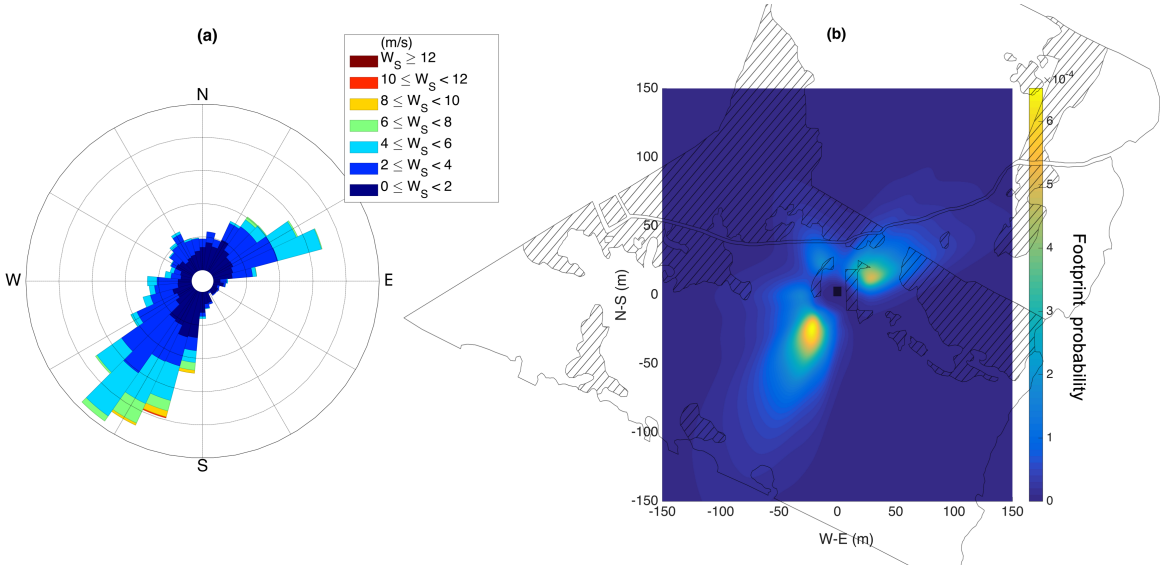

Figure 4.4 Wind rose (a) and flux footprint (b) at the study site, Cors Erddreiniog. The origin represented the location of the micro-meteorological tower. The shape of footprint in (b) was clearly determined by the wind distribution (a), with the dominant direction from south-west at the site. See Appendix 2 for an illustration on how to calculate the compass wind direction from CSAT3.

4.4.3 Comparing the Chamber-based and EC-based fluxes

Time series of the half-hourly NEE and CH_4 flux are shown in Fig. (4.5a&4.5b) respectively, zoomed in for a short period window in Fig. (4.5c&4.5d). NEE from chamber measurements integrated spatially over the area of interest using Eq. (4.5) showed a good agreement with the EC-based NEE in terms of temporal variation. As expected, there was a strong linear relation between the two estimates of NEE with a Pearson's correlation coefficient of 0.84 (p<0.01). An orthogonal regression of the two NEE estimates also showed a good linear relationship (r^2=0.71, p<0.01), but diverging slightly from the ideal 1:1 line (Fig. 4.5d) by a slope of 20%. This suggests that on average, for any given half hour, the estimation of NEE by chamber was about 20% higher than EC. By separating the daytime and nighttime NEE according to solar irradiance, similar to the whole NEE, the daytime NEE estimated by chamber was found to be similarly higher as shown by the green lines in Fig. (4.4d). Nighttime NEE estimates were less scattered than daytime NEE and the two estimates

showed a high degree of coherence ($r^2 \approx 0.6$, $p<0.01$). In contrast, the CH_4 flux estimated by the two methods showed little similarity except in the range of values observed. The time series of CH_4 flux shown in Fig. (4.5b&4.5d) suggests a poor relation between the integrated and EC-based CH_4 flux. This is further confirmed by the orthogonal regression in Fig. (4.5f), where the points were too scattered to suggest any coherent relation between the two estimates except randomness.

As indicated by the values of the regressed coefficients in Table (4-2), nighttime NEE (respiration) was higher as estimated by the integrated chamber measurements with a 23% larger slope than the whole day. Considering the significant larger interception (-0.78 $\mu mol\ m^{-2}s^{-1}$) and the small range of nighttime NEE values observed, however, the larger slope did not result in a significant difference between the two estimates of nighttime NEE; further evidenced in the cumulative nighttime NEE shown below. Nevertheless, since the night-time chamber measurements were implemented during daytime, environmental conditions such as temperature and turbulence would be higher. This may ultimately limit the model efficiency because we have not measured the night-time flux at night. The uncertainty in the estimation of night-time NEE could also occur in EC measurements when there was not enough turbulence for a well-mixed boundary layer, which, however, has been partly compensated by the flux storage correction.

Compared to the good fit ($r^2 = 0.71$) found in NEE, the value of r^2 was nearly zero for CH_4 flux; again suggesting a poor correlation between the two estimates of CH_4 flux. This profound mismatch between two ostensibly effective flux measurement methods may undermine our confidence in any attempt to measure CH_4 flux; the elliptical outline pattern of CH_4 flux (Fig. 4.5f) indicating large and random differences between the two methods.

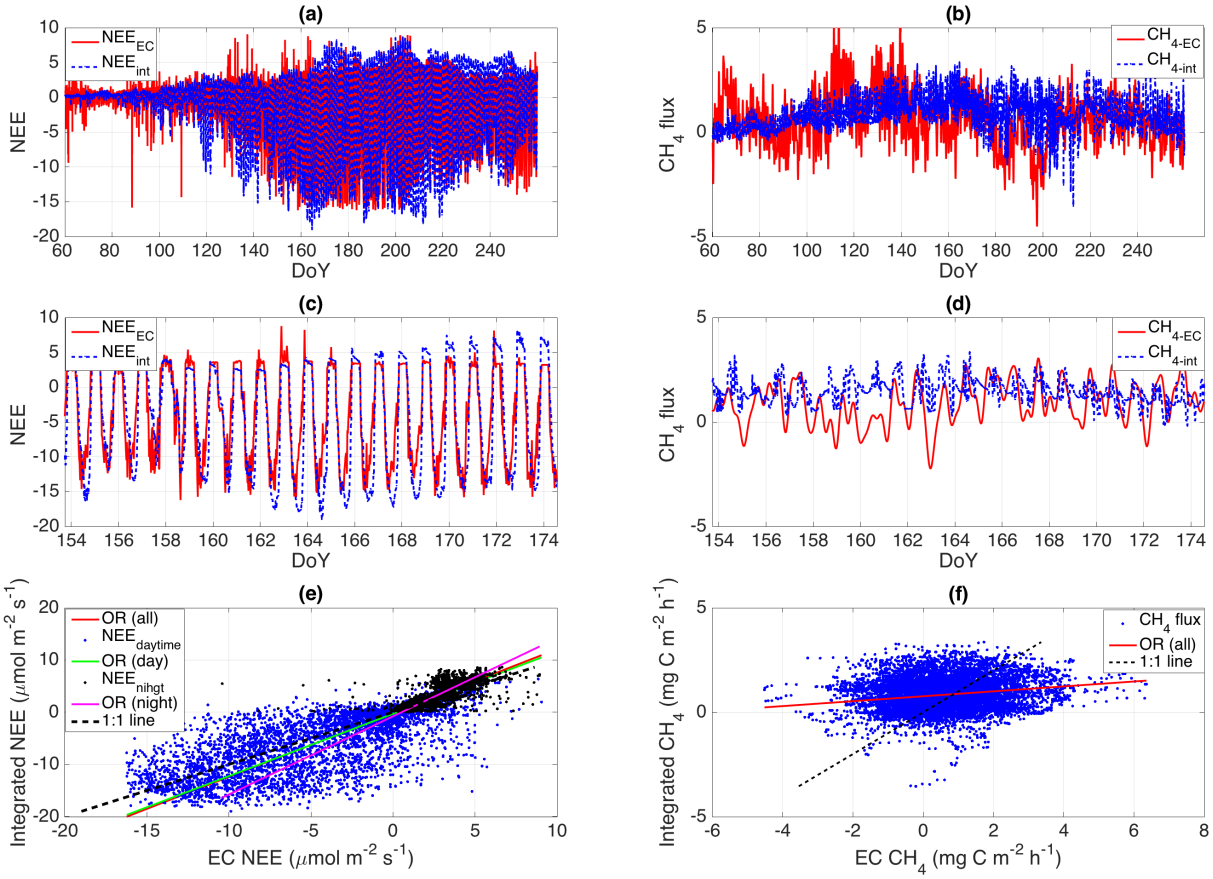

Figure 4.5 Comparison of NEE and CH4 flux between the EC- and chamber-based measurements. Times series of NEE (a) and CH_4 flux (b), zoomed in respectively in (c) and (d). Orthogonal regression analysis of NEE (e) and CH_4 flux (f), where NEE was further separated by day and night.

Table 4-2 Linear relation between the integrated and EC-based NEE and CH_4 flux as indicated by the orthogonal regression.

Orthogonal regression model	$Y_{int} = \beta_1 * Y_{EC} + \beta_0$			
GHG type	NEE			CH_4
Periods / Regression coefs	All	Daytime	Nighttime	All
β_1	1.22 (1.21, 1.24)	1.19 (1.17, 1.21)	1.50 (1.46, 1.53)	0.12 (0.11,0.13)
β_0	-0.15 (-0.17, -0.14)	-0.30 (-0.32, -0.28)	-0.78 (-0.82, -0.75)	0.77 (0.75,0.78)
r^2	0.71 (p<0.01)	0.58 (p<0.01)	0.60 (p<0.01)	0.02 (p<0.01)

Further analysis was conducted on the CH_4 flux to investigate the nature of the relationship between the two estimates. The raw and unfiltered CH_4 flux measure by EC is shown by the red line and dots in Fig. (4.6a). The range of values returned was extremely large, and greater than a plausible range of between -10 and 10 $mg\ m^{-2}\ h^{-1}$. The signal was de-noised by conducting a Fourier transform on the raw data series, and then conducting an inverse Fourier transform. These procedures filtered-out outliers and reconstructed/filled introduced data gaps respectively and resulted in a cleaned dataset where the highest and lowest values fell within a plausible range (the black line in Fig. 4.6a). This process of data cleaning preserved the mean value (Fig. 4.6b), as well as the cumulative trend (not shown here). The half-hourly interpolated chamber-based half-hourly CH_4 fluxes, derived from the output of the regression model, showed a narrower value range than that shown by the raw EC data, however the raw chamber measurements showed large variation, the average of which seemed to be larger than that of the EC signal. A t-test ($p<0.01$) showed that the mean value of the integrated chamber series ($0.84 \pm 0.76\ mg\ m^{-2}\ h^{-1}$) was indeed significantly larger than that of the EC-based series ($0.59 \pm 1.28\ mg\ m^{-2}\ h^{-1}$). The distribution of the residuals between the integrated and EC-based CH_4 flux was very close to the normal distribution (Fig. 4.6c) with a mean value slightly larger than zero (the green dashed line in Fig. 4.6c). Shifting the residuals by substracting the mean value resulted in a zero-mean normal distribution as confirmed by a t-test (p=1), meaning that apart from a constant systematic difference by a constant (i.e. the mean value difference), the two methods of measurement differed only by a Gaussian random structure (i.e. noise).

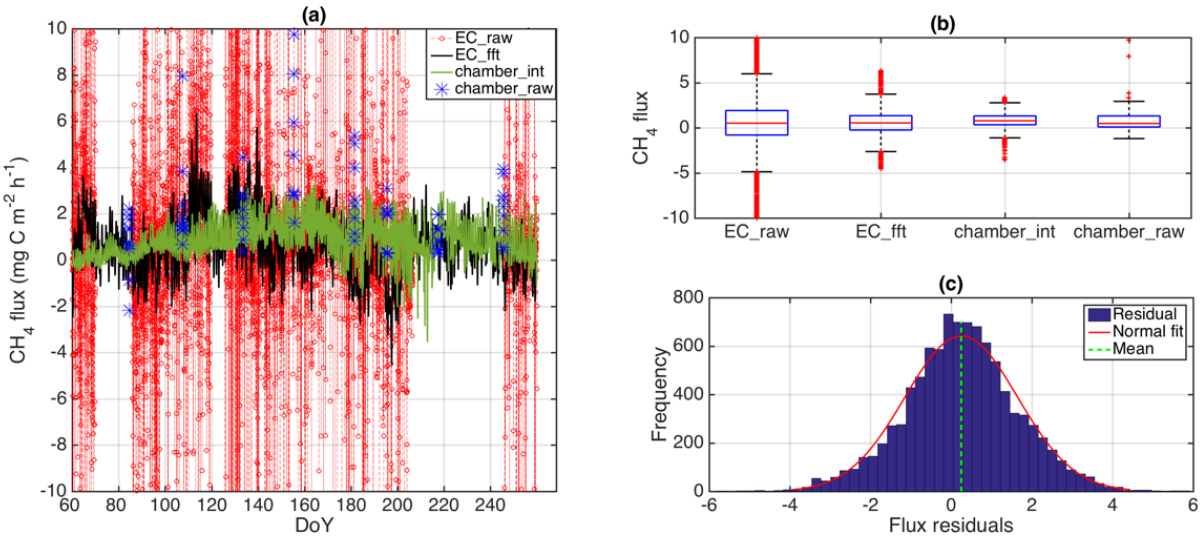

Figure 4.6 Raw and modeled/filtered EC- and chamber-based CH_4 flux (a). Boxplots of the four measured/modeled data series (b). Distribution of the residuals between the filtered EC and integrated chamber CH_4 flux (c).

Cumulative NEE and CH_4 flux over the 6-month period were shown in Fig. (4.7). The study fen was clearly a sink for CO_2 (i.e. NEE is negative) and a source for CH_4 flux, as indicated by both methods of measurement. From a reference perspective of EC-based measurements, chamber measurements overestimated both CO_2 and CH_4 flux. Cumulative NEE was -281.8 g/m^2 as estimated by the EC-based measurements, compared with -376.5 g/m^2 as estimated by the integrated chamber-based measurements. The average amount of overestimation by chamber was about 49.8 ± 45.3 g/m^2, namely 17.7% ± 16.1% of the EC estimates. Equally, this can also be interpreted as EC underestimating NEE by about 13% ± 12% compared to chamber estimates. We further noticed that this difference derives mainly from the cumulative daytime NEE (green lines in Fig. 4.7), while the cumulative nighttime NEE (orange lines in Fig. 4.7) agreed well between methods.

CH_4 flux was two orders of magnitude lower than NEE when measured in units of g C/m^2. The cumulative CH_4 flux estimated by EC was 2.81 g/m^2 and 4.01 g/m^2 (43% higher) when estimated by chamber. From the reference perspective of EC-based measurements, this overestimation was not consistent over the whole period. Compared to EC, chambers underestimated CH_4 flux in the first half of the year (between DoY 60-180), and overestimated afterwards. The average over/underestimation was 0.13 ± 0.60 g/m^2, about 4.8% ± 21.3% of EC estimates, a significantly smaller percentage than that seen in NEE. In comparison with the chamber-based estimations, there was a clear drop in the cumulative CH_4 flux during 180-200 DoY (blue solid line in Fig. 4.7), suggesting a CH_4 sink during that

period. Nevertheless, both methods identified the study site as a CH_4 source overall.

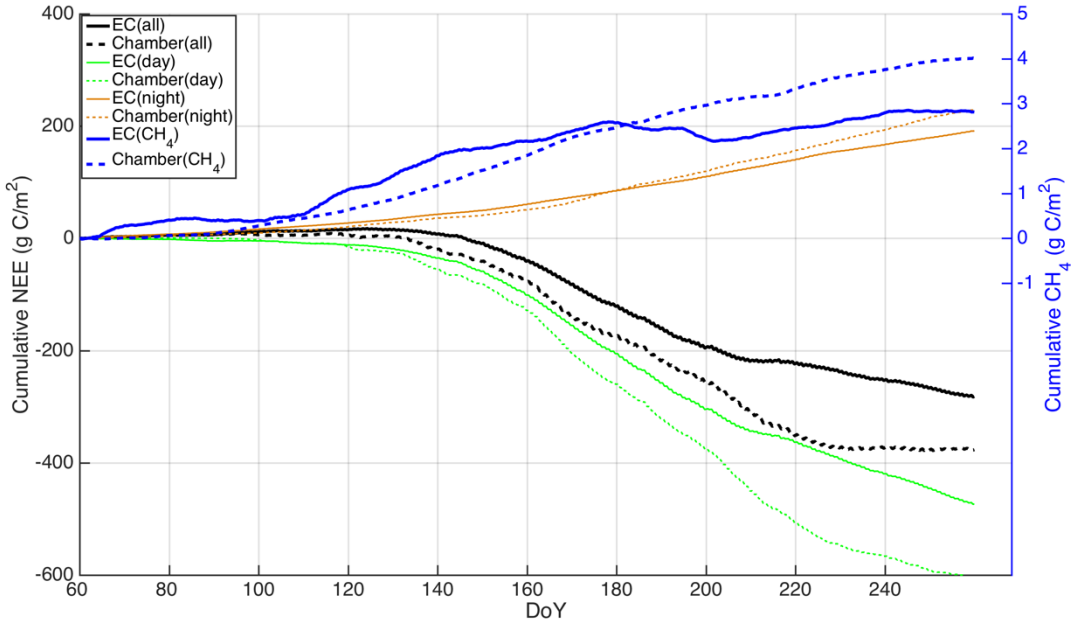

Figure 4.7 Cumulative NEE and CH_4 flux over the 6-month period. Daytime (green) and nighttime (orange) NEE were also shown in the figure.

4.5 Discussions and conclusions

4.5.1 Comparisons between EC and chamber measurements

The significance of comparing the EC- and chamber-based measurements is undoubted, considering that these two methods are used to estimate the same quantity (e.g. scalar flux) but we have no access to the "real" values that would allow a direct validation of the measurements. Making such comparisons, however, is not straightforward due to the fact that the two methods are very different in terms of their temporal and spatial representations. In this study, we chose the direction of converting monthly, plot-scale data from chambers into half-hourly, regional-scale estimates to compare with EC-based measurements (the opposite direction is less convenient to work with unless multiple EC towers are available). This requires two steps. First, a half-hourly time series of fluxes are estimated by modeling the chamber-measured fluxes against other environmental driving variables (e.g. regression models); Second, the chamber measurements are scaled up spatially by integrating the modeled half-hourly series for each vegetation type weighted by footprint functions (see Eq.

4.5). The second step is particularly important for heterogeneous landscapes where fluxes have a considerable spatial variation.

In this study, we made such comparison for two types of carbon flux, CO_2 flux (NEE) and CH_4 flux. Although the same techniques were used in the comparison, the results differed greatly between the two gases. For NEE, a strong linear relation was found between the integrated chamber- and EC-based estimations ($r^2 = 0.71$; $p < 0.01$), suggesting that the major variation of NEE was well captured by both methods. This level of agreement not only boosts our confidence in both measurement techniques, but also justified the proposed response of NEE to environmental variables, and the up-scaling scheme and flux footprint modelling. Applying the same method to CH_4 flux, however, did not generate a good agreement between the two estimations (see Fig. 4.5) as expected, nor have we found such agreement in any recent researches on methane emissions (Jackowicz-Korczynski et al., 2010; Schrier-Uijl et al., 2010; J. M. Wang et al., 2013). This disagreement implies that EC- and chamber-measured CH_4 flux were highly independent. The seemingly unstructured difference between the two methods, however, was found to be very close or identical to a Gaussian random structure as shown by the residual analysis (Fig. 4.6), suggesting that agreement between the flux estimates may be masked by random error and, importantly, the models have captured all the structured variation in CH_4 flux except for stochastic variation.

4.5.2 Chamber/EC over-/under- estimated fluxes

From the perspective of EC-based measurements, an overestimation by chamber measurements was found for both GHG fluxes. Based on the cumulative quantities (Fig. 4.7), the two estimates of cumulative NEE differed by an average of 49.8 ± 45.3 g/m^2 over the entire growing season, suggesting a systematic overestimation by chamber (i.e. true carbon sink was smaller than that measured) or equally speaking, an underestimation of NEE by EC (i.e. the true carbon sink was higher than that measured). Similarly, despite the fact that the ecosystem was found to be a source of CH_4 flux by both methods, chambers overestimated the cumulative CH_4 flux by about 4.8% ± 21.3%. At current stage of our research, no preference should be made in favour of either method since the “true” value is not, and cannot be, known.

The difference in the estimation of NEE between methods primarily originated from the daytime NEE (Table 4-1). This can be seen more clearly when the cumulative NEE was separated by day and night (Fig. 4.7), although it should be acknowledged that a small

systematic error will accumulate into a large one when we consider a long-term carbon budget. This result is comparable to some previous studies. EC measurements were reported to underestimate CO_2 fluxes by 10 – 30% over a grassland (Twine et al., 2000). Marushchak *et al.* (2013) found that the up-scaled chamber measurements overestimated the cumulative NEE by 2-30% during the growing season over a subarctic tundra. Dore *et al.* (2003) also found that the integrated chamber measurements were 10% higher (i.e. overestimated) than EC for half-hourly NEE, the same order of magnitude to the number found here (13% ± 12%) even though the types of underlying ecosystems are very different. Schrier-Uijl *et al.* (2010) reported a difference between methods from 16.5% to 31.0% for CO_2 flux and from 13.0% to 55.1% for CH_4 flux at a heterogeneous grassland on peat. Similarly, Fox *et al.* (2008) reported an overestimation of CO_2 uptake (i.e., more negative NEE) from up-scaled chamber measurements and further speculated that this might be a general issue for any type of ecosystem.

4.5.3 Potential causes for the difference between techniques

Although we have captured the major variations in both CO_2 and CH_4 flux through the techniques proposed in this paper, the cause for the systematic difference between the two methods of measurement is still unclear. Potential causes could be: (1) Errors introduced in interpolating NEE and CH_4 flux from chamber measurements; (2) Incongruence between the flux footprint model and the chamber integrated source area; (3) Known intrinsic uncertainties attached to each measurement technique; (4) Unknown error sources. (1) The regression models used for NEE and CH_4 worked well (see Fig. 4.2&4.3) but not perfectly. In particular, a less good fitting performance (r^2=0.42) was found in the model describing chamber measurement of GPP for vegetation CD, uncertainties of which were likely to be propagated into the major discrepancy found in the daytime NEE. This may imply that the use of the rectangular hyperbola function (Eq. 4.3) was not sufficient to capture all the variation of GPP for this vegetation type, possibly because some variation is driven by factors other than temperature and light. The flux contribution from this vegetation type, however, accounted for only 10% ± 12% of the total flux, which in this case will mitigate the effects on the overall NEE estimation. A comprehensive investigation on the reliability of the regression models for NEE and CH_4 flux is needed in further research. 2) The flux footprint model used in this study has been validated against other models and wind tunnel experiments, however in practical, biases can still be considerable and multiple towers are thus recommended (Schmid and Lloyd, 1999) as a more rigorous treatment. It should also be noted that the total

flux contribution was about 80% of the actual total, implying that 20% of the footprint incorporated other unspecified sources which would be embedded in EC data, but ignored from the integration process of chamber signals (Eq. 4.5). This part of contribution to the fluxes would be significant if the un-sampled (by chambers) areas produce a significant amount of NEE and/or CH_4 flux.

3) Intrinsic uncertainties from measurement techniques. Although both the chamber and EC techniques are fairly mature with many years of methodological refinement (Oren et al., 2006; Parkin et al., 2012; Rayment and Jarvis, 1997), recognising the strict technical requirements for applying them in practice does not always translate into artefact-free measurements. 4) Unknown error sources. Even if we assume that all uncertainties above are small enough to be ignored, the possibility remains that there are yet other sources of error that are currently unidentified. The curve fitting performance for the NEE of vegetation PM, for instance, whilst good (r^2 = 0.73) leaves more than 20% of variance unexplained. This residual is normally considered as unsystematic random errors, but is it? Is there a technical limit to our capability of estimating NEE and CH_4 flux? Are the simple functions of GPP and RE response to light and temperature over-simplified in a complex system? Use of simple functions seems very likely to over-simplified a complex system. The cloudy scatter points found for CH_4 flux (Fig. 4.5f) and the disagreement between methods also suggested the existence of knowledge gaps in our understanding of the flux mechanism itself, potentially highlighting the role of stochastic processes such as ebullition or pumping by fluctuating atmospheric pressure.

4.5.4 Implications from the Lasso regression of CH_4 flux

As shown in Table (4-1), some of the coefficients were automatically assigned to zero by the regression process. This result suggested the following: 1) Some terms were neglected from the model for one vegetation, but not necessarily for the other, highlighting the distinction between vegetation type; 2) Only six terms were non-zero for both species, namely the intercept, T_{soil}, WT, $PPFD^2$, $WT*T_{soil}^2$ and $WT*PPFD^2$. This could help shed light on the mechanism of underlying processes of CH_4 production and emission, and serves as a guide to constructing a generic model of CH_4 flux that suits different types of vegetation. Therefore, an investigation into the biophysical meaning of these terms would be a sensible follow-up study. Traditional regression analysis without regularization (e.g. stepwise regression) is limited in its fundamentals, particularly unreliable for multivariate analysis (Flom and Cassell,

2007). We thus highly recommend further investigations on the use of the Lasso and its equivalents in data mining of complex systems such as CH_4 flux.

4.5.5 Summary

A good linear correlation was found for NEE estimations based on the two completely independent measurement techniques, while a reasonable agreement was found for the estimations of CH_4 flux once random noise was considered. This result increases our confidence in quantifying surface carbon flux using either of these two methods in the sense that they were generally linearly correlated, even though the integrated chamber-based estimation was consistently higher than EC for both GHG fluxes. The cause of the systematic difference between methods remains unclear. The study fen was a NEE sink and a CH_4 source as indicated by both methods. Both methods indicated that the study fen was a CO_2 sink and a small CH_4 source, and was, overall, a small carbon sink.

4.6 References

Blodau, C., 2002. Carbon cycling in peatlands: A review of processes and controls. Environ. Rev. 10, 111–134. doi:10.1139/a02-004

Dore, S., Hymus, G.J., Johnson, D.P., Hinkle, C.R., Valentini, R., Drake, B.G., 2003. Cross validation of open-top chamber and eddy covariance measurements of ecosystem CO2 exchange in a Florida scrub-oak ecosystem. Glob. Chang. Biol. 9, 84–95. doi:10.1046/j.1365-2486.2003.00561.x

Evans, C., Morrison, R., Burden, A., Williamson, J., Baird, A., Brown, E., Callaghan, N., Chapman, P., Cumming, A., Dean, H., Dixon, S., Dooling, G., Evans, J., Gauci, V., Grayson, R., Haddaway, N., He, Y., Heppell, K., Holden, J., Hughes, S., Kaduk, J., Jones, D., Matthews, R., Menichino, N., Misselbrook, T., Page, S., Pan, G., Peacock, M., Rayment, M., Ridley, L., Robinson, I., Scowen, M., Stanley, K., Worrall, F., 2016. Lowland peatland systems in England and Wales – evaluating greenhouse gas fluxes and carbon balances. Final report to Defra on Project SP1210, Centre for Ecology and Hydrology, Bangor.

Falge, E., Baldocchi, D., Olson, R., Anthoni, P., Aubinet, M., Bernhofer, C., Burba, G., Ceulemans, R., Clement, R., Dolman, H., Granier, A., Gross, P., Grünwald, T., Hollinger, D., Jensen, N.O., Katul, G., Keronen, P., Kowalski, A., Lai, C.T., Law, B.E., Meyers, T., Moncrieff, J., Moors, E., Munger, J.W., Pilegaard, K., Rannik, Ü., Rebmann, C., Suyker, A., Tenhunen, J., Tu, K., Verma, S., Vesala, T., Wilson, K., Wofsy, S., 2001. Gap filling strategies for defensible annual sums of net ecosystem exchange. Agric. For. Meteorol. 107, 43–69. doi:10.1016/S0168-1923(00)00225-2

Flom, P.L., Cassell, D.L., 2007. Stopping stepwise: Why stepwise and similar selection methods are bad, and what you should use, in: NorthEast SAS Users Group Inc 20th Annual Conference: 11-14th November 2007; Baltimore, Maryland.

Fox, A.M., Huntley, B., Lloyd, C.R., Williams, M., Baxter, R., 2008. Net ecosystem

exchange over heterogeneous Arctic tundra: Scaling between chamber and eddy covariance measurements. Global Biogeochem. Cycles 22, 1–15. doi:10.1029/2007GB003027

Freeman, C., Lock, M.A., Reynolds, B., 1992. Fluxes of CO2, CH4 and N2O from a Welsh peatland following simulation of water table draw-down: Potential feedback to climatic change. Biogeochemistry 19, 51–60. doi:10.1007/BF00000574

Goulden, M.L., Munger, J.W., FAN, S.M., Daube, B.C., Wofsy, S.C., 1996. Measurements of carbon sequestration by long-term eddy covariance: Methods and a critical evaluation of accuracy. Glob. Chang. Biol. 2, 169–182. doi:10.1111/j.1365-2486.1996.tb00070.x

Hastie, T., Tibshirani, R., Friedman, J., 2009. The Elements of Statistical Learning. Data Mining, Inference, and Prediction, Springer Series in Statistics. doi:10.1007/b94608

He, Y., Rayment, M., 2016. A robust gap-filling method for Net Ecosystem Exchange based on Cahn–Hilliard inpainting. Geosci. Model Dev. Discuss. doi:10.5194/gmd-2016-108

Hollinger, D.Y., Richardson, A.D., 2005. Uncertainty in eddy covariance measurements and its application to physiological models. Tree Physiol. 25, 873–885. doi:10.1093/treephys/25.7.873

Howard, D.M., Howard, P.J.A., 1993. Relationships between CO2 evolution, moisture content and temperature for a range of soil types. Soil Biol. Biochem. 25, 1537–1546. doi:10.1016/0038-0717(93)90008-Y

Jackowicz-Korczynski, M., Christensen, T.R., Backstrand, K., Crill, P., Friborg, T., Mastepanov, M., Strom, L., 2010. Annual cycle of methane emission from a subarctic peatland. J. Geophys. Res. G Biogeosciences 115. doi:10.1029/2008JG000913

JNCC, 2016. Corsydd Môn/ Anglesey Fens (web page) [WWW Document]. URL http://jncc.defra.gov.uk/ProtectedSites/SACselection/sac.asp?EUCode=UK0012884 (accessed 6.3.16).

Keppler, F., Hamilton, J.T.G., Brass, M., Röckmann, T., 2006. Methane emissions from terrestrial plants under aerobic conditions. Nature 439, 187–191. doi:10.1038/nature04420

Kljun, N., Calanca, P., Rotach, M.W., Schmid, H.P., 2015. A simple two-dimensional parameterisation for Flux Footprint Prediction (FFP). Geosci. Model Dev. 8, 3695–3713. doi:10.5194/gmd-8-3695-2015

Leng, L., Zhang, T., Kleinman, L., Zhu, W., 2007. Ordinary least square regression, orthogonal regression, geometric mean regression and their applications in aerosol science. J. Phys. Conf. Ser. 78, 12084. doi:10.1088/1742-6596/78/1/012084

Lloyd, J., Taylor, J., 1994. On the temperature dependence of soil respiration. Funct. Ecol. 8, 315–323. doi:10.2307/2389824

Longdoz, B., Yernaux, M., Aubinet, M., 2000. Soil CO_2 efflux measurements in mixed forest: impact of chamber disturbance, spatial variability and seasonal evolution. Glob. Chang. Biol. 6, 907–917. doi:10.1046/j.1365-2486.2000.00369.x

Marushchak, M.E., Kiepe, I., Biasi, C., Elsakov, V., Friborg, T., Johansson, T., Soegaard, H., Virtanen, T., Martikainen, P.J., 2013. Carbon dioxide balance of subarctic tundra from plot to regional scales. Biogeosciences 10, 437–452. doi:10.5194/bg-10-437-2013

Olefeldt, D., Turetsky, M.R., Crill, P.M., Mcguire, A.D., 2013. Environmental and physical controls on northern terrestrial methane emissions across permafrost zones. Glob. Chang. Biol. 19, 589–603. doi:10.1111/gcb.12071

Oren, R.A.M., HSIEH, C.I., Stoy, P., Albertson, J., Mccarthy, H.R., Harrell, P., Katul, G.G., 2006. Estimating the uncertainty in annual net ecosystem carbon exchange: Spatial variation in turbulent fluxes and sampling errors in eddy-covariance measurements. Glob. Chang. Biol. 12, 883–896. doi:10.1111/j.1365-2486.2006.01131.x

Parkin, T.B., Venterea, R.T., Hargreaves, S.K., 2012. Calculating the detection limits of chamber-based soil greenhouse gas flux measurements. J. Environ. Qual. 41, 705–15. doi:10.2134/jeq2011.0394

Rayment, M.B., Jarvis, P.G., 1997. An improved open chamber system for measuring soil CO_2 effluxes in the field. J. Geophys. Res. Atmos. 102, 28779–28784. doi:10.1029/97JD01103

Reichstein, M., Falge, E., Baldocchi, D., Papale, D., Aubinet, M., Berbigier, P., Bernhofer, C., Buchmann, N., Gilmanov, T., Granier, A., Grünwald, T., Havránková, K., Ilvesniemi, H., Janous, D., Knohl, A., Laurila, T., Lohila, A., Loustau, D., Matteucci, G., Meyers, T., Miglietta, F., Ourcival, J.M., Pumpanen, J., Rambal, S., Rotenberg, E., Sanz, M., Tenhunen, J., Seufert, G., Vaccari, F., Vesala, T., Yakir, D., Valentini, R., 2005. On the separation of net ecosystem exchange into assimilation and ecosystem respiration: Review and improved algorithm. Glob. Chang. Biol. 11, 1424–1439. doi:10.1111/j.1365-2486.2005.001002.x

Schmid, H.P., 2002. Footprint modeling for vegetation atmosphere exchange studies: a review and perspective. Agric. For. Meteorol. 113, 159–183. doi:10.1016/S0168-1923(02)00107-7

Schmid, H.P., Lloyd, C.R., 1999. Spatial representativeness and the location bias of flux footprints over inhomogeneous areas. Agric. For. Meteorol. 93, 195–209. doi:10.1016/S0168-1923(98)00119-1

Schrier-Uijl, a. P., Kroon, P.S., Hensen, a., Leffelaar, P. a., Berendse, F., Veenendaal, E.M., 2010. Comparison of chamber and eddy covariance-based CO2 and CH4 emission estimates in a heterogeneous grass ecosystem on peat. Agric. For. Meteorol. 150, 825–831. doi:10.1016/j.agrformet.2009.11.007

Speckman, H.N., Frank, J.M., Bradford, J.B., Miles, B.L., Massman, W.J., Parton, W.J., Ryan, M.G., 2015. Forest ecosystem respiration estimated from eddy covariance and chamber measurements under high turbulence and substantial tree mortality from bark beetles. Glob. Chang. Biol. 21, 708–721. doi:10.1111/gcb.12731

Tibshirani, R., 1996. Regression Selection and Shrinkage via the Lasso. J. R. Stat. Soc. B. doi:10.2307/2346178

Turetsky, M.R., Kotowska, A., Bubier, J., Dise, N.B., Crill, P., Hornibrook, E.R.C., Minkkinen, K., Moore, T.R., Myers-Smith, I.H., Nyk??nen, H., Olefeldt, D., Rinne, J., Saarnio, S., Shurpali, N., Tuittila, E.S., Waddington, J.M., White, J.R., Wickland, K.P., Wilmking, M., 2014. A synthesis of methane emissions from 71 northern, temperate, and subtropical wetlands. Glob. Chang. Biol. 20, 2183–2197. doi:10.1111/gcb.12580

Twine, T.E., Kustas, W.P., Norman, J.M., Cook, D.R., Houser, Pr., Meyers, T.P., Prueger, J.H., Starks, P.J., Wesely, M.L., 2000. Correcting eddy-covariance flux underestimates

over a grassland. Agric. For. Meteorol. 103, 279–300. doi:10.1016/S0168-1923(00)00123-4

Veenendaal, E.M., Kolle, O., Leffelaar, P.A., Schrier-Uijl, A.P., Van Huissteden, J., Van Walsem, J., Möller, F., Berendse, F., 2007. CO_2 exchange and Carbon balance in two grassland sites on eutrophic drained peat soils. Biogeosciences Discuss. doi:10.5194/bgd-4-1633-2007

Vesala, T., Kljun, N., Rannik, U., Rinne, J., Sogachev, a, Markkanen, T., Sabelfeld, K., Foken, T., Leclerc, M.Y., 2008. Flux and concentration footprint modelling: state of the art. Environ. Pollut. 152, 653–66. doi:10.1016/j.envpol.2007.06.070

Vigano, I., Van Weelden, H., Holzinger, R., Keppler, F., Mcleod, A., Röckmann, T., 2008. Effect of UV radiation and temperature on the emission of methane from plant biomass and structural components. Biogeosciences 5, 937–947. doi:10.5194/bgd-5-243-2008

Wang, J.M., Murphy, J.G., Geddes, J. a., Winsborough, C.L., Basiliko, N., Thomas, S.C., 2013. Methane fluxes measured by eddy covariance and static chamber techniques at a temperate forest in central Ontario, Canada. Biogeosciences 10, 4371–4382. doi:10.5194/bg-10-4371-2013

Wang, K., Liu, C., Zheng, X., Pihlatie, M., Li, B., Haapanala, S., Vesala, T., Liu, H., Wang, Y., Liu, G., Hu, F., 2013. Comparison between eddy covariance and automatic chamber techniques for measuring net ecosystem exchange of carbon dioxide in cotton and wheat fields. Biogeosciences 10, 6865–6877. doi:10.5194/bg-10-6865-2013

Wille, C., Kutzbach, L., Sachs, T., Wagner, D., Pfeiffer, E.-M.M., 2008. Methane emission from Siberian arctic polygonal tundra: eddy covariance measurements and modeling. Glob. Chang. Biol. 14, 1395–1408. doi:10.1111/j.1365-2486.2008.01586.x

Wohlfahrt, G., Fenstermaker, L.F., Arnone Iii, J.A., 2008. Large annual net ecosystem CO2 uptake of a Mojave Desert ecosystem. Glob. Chang. Biol. 14, 1475–1487. doi:10.1111/j.1365-2486.2008.01593.x

Ch 5. A Simple parameterisation of windbreak effects on wind speed, thermal microclimate and sheep welfare[1]

5.1 Abstract

It is well known that windbreaks can provide favourable conditions for livestock and may increase agricultural productivity, however, establishing a windbreak incurs both a direct cost (of materials and time), and an indirect cost in terms of competition for resources between the windbreak and the pasture. Determining the cost vs. benefit of any given windbreak system first requires that the impact of the windbreak on the wind microclimate is characterized, but in practice, modelling wind flow around obstacles is complex and computationally intensive. We report a simple parameterized model to estimate the wind speed reduction around a windbreak. Analytically, model parameters showed close links to the real-world attributes that characterize windbreaks. The model was validated with field measurements on farmland in the UK; a Monte Carlo simulation was used to measure model parameter uncertainties. Results showed that the model produced an excellent fit to the relative wind speed (i.e. normalized by ambient wind speed) with RMSE value of 4%±0.5%. The model was further applied to literature data to characterise the dependence of the relative wind speed on windbreak porosity. A field-scale simulation of a sheep grazing system, including an explicit description of wind-chill effects, was conducted to estimate the net gain associated with including a windbreak in sheep productivity. The maximum productivity gain (27%) was found at a porosity of 0.5 and a wind speed of 12 m/s. Wind-chill effects were further simulated for lowland and upland environments, and related to ovine-specific thermal tolerance limits. Results showed a distinct response to reduced wind speeds between sites, indicating different levels of thermal risk to livestock and different, microclimate-specific, windbreak benefits for each location. The simplified models proposed in this study provides a generic framework for an efficient and precise quantification of windbreak effects and optimising the design of windbreak systems.

5.2 Introduction

Windbreaks or shelter belts have been used in the agricultural landscape for centuries, and are considered to have a generally positive effect on livestock productivity (Gregory, 1995). In

[1] This chapter is based on: He, Y., Jones, P., Rayment, M. (2016). A simple parameterization of windbreak effects on wind speed, thermal microclimate, crop productivity and livestock welfare. *Agricultural and Forest Meteorology* (In review).

livestock production systems, animals benefit not only from the direct physical protection from a stressful environment (Cleugh, 1998) (e.g. rain, wind and sun), but also because their immediate microclimatic conditions determine their energy balance. Energy generated by metabolism over and above requirement for vital processes, is, in agricultural systems ideally apportioned to weight gain (i.e. production), but in cold conditions is utilized in meeting the increased demands thermoregulation. When exposed to a cold and windy environment, the insulating boundary layer formed by fur, hair or fleece is diminished and heat conduction between the body and surrounding air is thus increased. This is commonly known as the wind-chill effect, meaning that the apparent temperature experienced by the animal under windy conditions is lower than the ambient temperature. Low-wind microclimates provided by windbreaks reduce heat loss and increase overall productivity (Ames and Insley, 1975; McArthur and Monteith, 1980) as well as lowering lamb mortality (Pollard, 2006).

In the literature there have been many attempts to grapple with numerical simulations of the equations that govern windbreak aerodynamics (e.g. Bitog et al., 2012; Bourdin and Wilson, 2008; Speckart and Pardyjak, 2014; Torita and Satou, 2007; Wang and Takle, 1995; Yusaiyin and Tanaka, 2009). In addition to the technical problems of solving these partial differential equations (e.g. how to choose a discretized scheme and a proper grid size), a fundamental obstacle to using these models is that they are typically derived from wind tunnel experiments are necessarily simplified and unrealistic given the complexity of a real windbreak (i.e. one made up of flexible and irregular shaped trees and leaves). It is also for this reason that previous studies using fences as field measurements to validate numerical simulations (Wilson, 1987; Wilson and Flesch, 2003; Wilson and Yee, 2003), despite their significance in theoretical understanding, may also be unsuitable for a windbreak consisting of green infrastructures. Moreover, the procedure of implementing such simulations is computational intensive and is cumbersome to apply to any real-world scenario. In short, there is a need for a simple parameterized model, based on real-world observations, that would provide not only a computationally-efficient estimation of the wind speed reduction around a real windbreak, but also the follow-up quantification of the effects of that windbreak on livestock productivity. Several previous researchers have tried to build and/or apply a parameterized model to estimating the wind speed reduction around a windbreak. Vigiak et al. (2003) used a function with five parameters (analogous to the sum of two normal distributions) and Stredova et al. (2012) suggested a 2-degree polynomial with six parameters, to describe the wind speed reduction against distance and optical porosity. In both of these cases, however,

crucial information is missing in terms of how or whether these parameters have any physical meaning or any relation to attributes of windbreaks that might be measured in the field.

Critically, only three parameters are required to characterize wind speed reduction around a windbreak (Heisler and Dewalle, 1988; Wang and Takle, 1997; Yusaiyin and Tanaka, 2009); These are illustrated in Fig. (5.1): L_{20}, x_{min} and y_{min}, where L_{20} is the distance between which the wind speed reduction is 20% (i.e. wind speed is 80% of ambient wind speed), x_{min} is the distance downwind of the windbreak at which wind speed is at its lowest, and y_{min} is the minimum wind speed (i.e. the wind speed at x_{min}). Consequently, a simple parameterisation of the wind speed around a windbreak is achievable in principle because 1) just three parameters should be sufficient to uniquely determine the trend of wind speed; 2) further downwind of the windbreak, the wind speed asymptotically approaches the ambient wind speed (i.e. zero reduction).

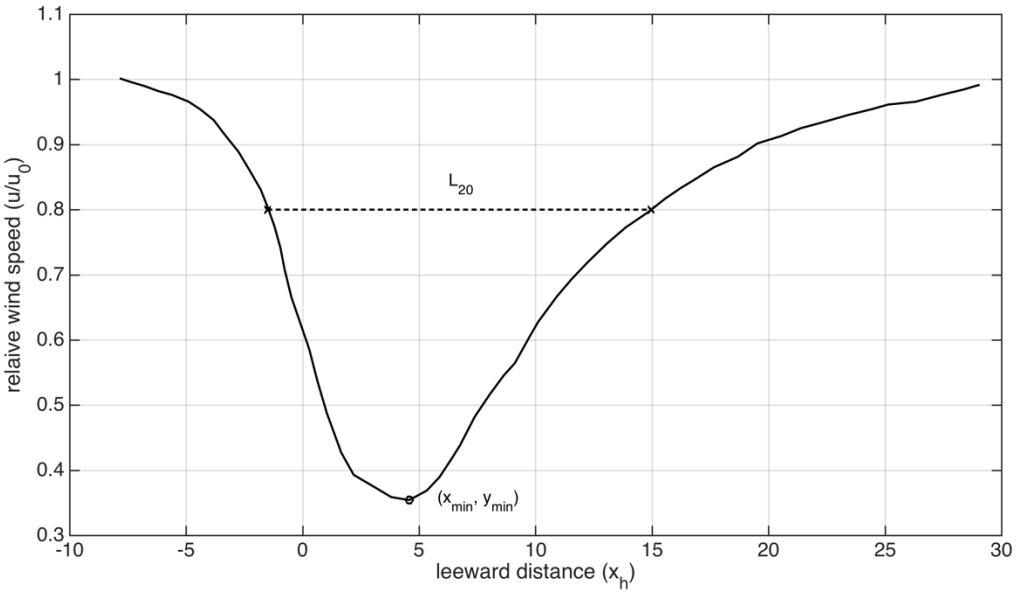

Figure 5.1 Characteristic trend of wind speed reduction around a windbreak and parameters required to define this.

In this study we use a simple parameterized model in the form of the probability density function of a single logarithmic normal distribution with three parameters, the physical meanings of which can be explicitly expressed in terms of L_{20}, x_{min} and y_{min}. The estimation error and the parameter uncertainty are analysed thoroughly with field measurements and we further extended this model to literature datasets so that the dependence on porosity can be estimated and analysed. The wind-chill temperature (WCT) is modelled by using a sigmoid

function fitted to a published dataset relating to adult sheep (3-6cm fleece depth). The wind attenuation and WCT models are then combined to evaluate the impacts of wind shelter on sheep productivity. Last but by no means least, we simulate the response of the thermal benefits to the wind speed reduction by using historical climate datasets measured at a lowland and an upland.

5.3 Data and Methods

5.3.1 Site description and measurements of wind speed

Field measurements were made at the Bangor University Research farm at Henfaes in Llanfairfechan, Wales, UK. Five sonic anemometers (four Gill WindSonic-2D and one Campbell CSAT3-3D) were positioned along a transect running perpendicular to a linear tree barrier forming a windbreak. The windbreak was of mixed species composition, including sycamore, alder, hazel and oak. Physically, the windbreak had an average height (H) of 10m and ran in a southeast – northwest orientation, such that the prevailing wind (from the southwest) meant that the anemometers were situated in the downwind region for most of time. Fig. (5.2) shows the distance (in H) of each anemometer downwind of the windbreak, namely 1H, 2.5H, 5H, 7.5H and 15H.

Figure 5.2 Site map at Henfaes and downwind locations (in barrier height H) of the five sonic anemometers. Photo taken by Y. He on 2 Aug. 2016, reproduced by Y. Xuan. Map credit: Google Earth.

In total, fourteen days of 10-min averages were collected between 8-22 August 2016. Only data when wind direction was from the southwest sector (180°-270°) were included in the simulation. Because southwest is the dominant wind direction for this region, 1353 samples out of 2031 (67%) were included.

We assumed that the wind speed measured by the furthest anemometer at 15H was ambient wind speed and the relative wind speed at each position downwind was calculated as a proportion of the wind speed at 15H. Calculating the proportion at each data point exacerbated noise resulting from stochastic events, because the fraction can be significantly impacted by a small change in the numerator and/or denominator, especially when their values are small. For example, an error of 0.1 in the numerator contributes much more to a fraction of 0.5/1 (i.e. 50% attenuation) than 5/10 (again 50% attenuation).

Therefore, to minimize such errors/uncertainties, the proportion was estimated by taking the slope of the linear regression between wind speed measured by paired anemometers.

5.3.2 Model development and error estimation

Previous attempts to approximate the wind speed reduction around a windbreak have used a single, or the sum of two, normal distributions (Hipsey, 2003; Schwartz et al., 1995; Vigiak et al., 2003). In this study, we modified the density function of a single normal distribution by taking the logarithm of the downwind distance. The relative wind speed (u/u_0) at any distance from a windbreak (i.e. from $-10H$ windward and up to $40H$ leeward) can thus be calculated as:

$$y = \frac{u}{u_0} = 1 - a * e^{-b*(\ln(x_H+10)-c)^2} \qquad (5.1)$$

where x_H is the distance from the barrier normalized by the barrier's height H. u is the wind speed at x_H and u_0 is the incoming ambient wind speed. Fig. (5.1) shows a typical picture of the relative wind speed around a windbreak. The general characteristics of this curve can be expressed by the following, 1) It is asymptotic towards 1 at both ends; 2) It has a single minimum point; 3) The shelter distance (L_{20}) is defined as the distance between which the wind speed reduction is at least 20%. Coefficients a, b, c in Eq. (1) are closely related to the minimum point and L_{20},

$$x_{min} = e^c - 10 \qquad (5.2)$$

$$y_{min} = 1 - a \qquad (5.3)$$

$$L_{20} = e^c * (e^{\sqrt{\frac{\ln\left(\frac{a}{0.2}\right)}{b}}} - e^{-\sqrt{\frac{\ln\left(\frac{a}{0.2}\right)}{b}}}) = 2 * e^c * \sinh\left(\sqrt{\frac{\ln\left(\frac{a}{0.2}\right)}{b}}\right) \qquad (5.4)$$

where x_{min} represents the downwind location where the minimum wind speed (y_{min}) is reached. This formulation clearly points out the potential physical meanings of the coefficients in Eq. (1). a is related to the maximum wind speed reduction, b is related to the initial deceleration and acceleration of airflow and c is related to the downwind position of x_{min}. In the discussion below, we speculate on how these parameters are related to the physical characteristics of the windbreak.

5.3.3 Model error estimation

In order to determine the robustness of the model, we quantified parameter errors by splitting our dataset randomly into two parts; a training set (70%) and a validation set (30%). The training set was used to estimate the parameters in Eq. (5.1) and the validation set was used to calculate model error that was evaluated by the root mean square error (RMSE). This process was repeated 500 times using a Monte Carlo method to generate independent training and validation sets so that all variation (uncertainty) in the estimations of the coefficients was captured. Note that here we do not require a cross-validation set and test set as used to test an artificial neural network (ANN) procedure. ANNs optimise parameters by iteration and require evaluations on independent cross-validation sets to update coefficient estimates in real time. Our goal, however, is simply to measure the model prediction error through Monte Carlo sampling. In fact, statistically the confidence interval (CI) estimated by this method is more reliable than that associated with an ANN because even poor parameter estimations will be included in the CI estimates.

5.3.4 Literature data and windbreak porosity

Neglecting atmospheric stability, the three parameters (i.e. x_{min}, y_{min} *and* L_{20}) uniquely define airflow modified by any given windbreak. Despite the fact that a windbreak has a plethora of characteristics (e.g. tree species, leaf shape, density and distribution), optical porosity alone has often been used to describe windbreak aerodynamics and distinguish between windbreak type (e.g. Stredova et al., 2012; Vigiak et al., 2003; Wang and Takle, 1997). In order to build a function of porosity against the parameters in Eq. (5.1), we applied the model to two published data sets as shown in Fig. (5.3). For the sake of simplicity, we call the dataset extracted from Heisler and Dewalle (1988) dataset 1 and that extracted from Wang and Takle (1997) dataset 2. Dataset 1 was obtained from field observations of five types of windbreak (Fig. 5.3a) and dataset 2 was the result from numerical simulations of a boundary-layer turbulence model (Fig. 5.3b). By fitting Eq. (5.1) to each data set, we estimated the parameters which could then be correlated to reported values of porosity. It should be noted, however, that dataset 1 did not represent porosity numerically, so for the sake of this simulation we assigned values of 0.2, 0.4, 0.5, 0.6 and 0.7 to the data reported for very dense, dense, medium, loose and very loose respectively. Despite this setting was purely empirical and we have simulated different combinations of values, it appeared to be the most reliable

one when we interpolated the wind speed reduction at other porosities by regression for this dataset.

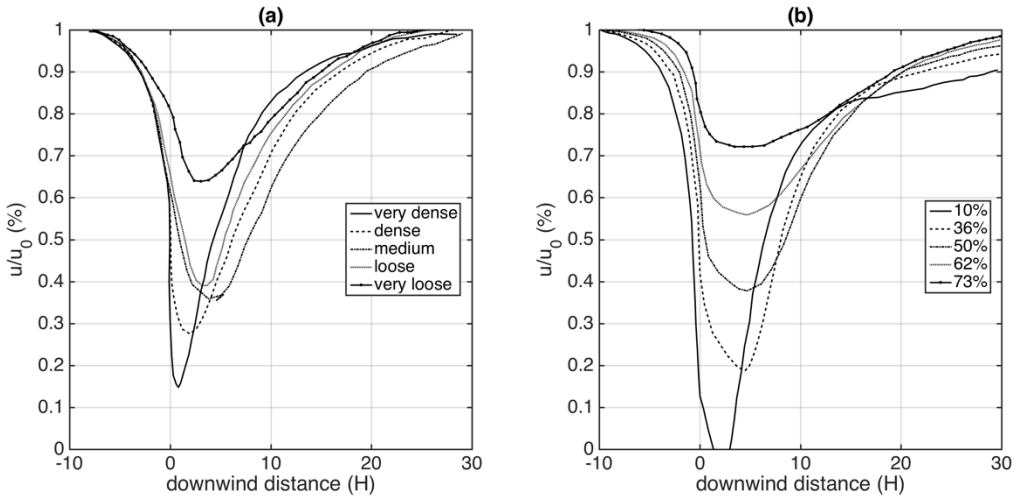

Figure 5.3 Digitized data extracted from (a) Fig. 2a in (Heisler and Dewalle, 1988)*; (b) Fig. 2 in* (Wang and Takle, 1997).

5.3.5 Wind-chill effects and heat loss from sheep

Barnes (1974) measured the wind-chill temperature (*WCT*) for sheep with three types of fleece: shorn, medium (3-6 cm) and full (>6 cm). In the experimental setting, wind speed varied from 0 m/s up to 18 m/s, and temperature varied from -15 °C to 20 °C. Whilst initially considered, the equation developed by (Osczevski and Bluestein, 2005) for wind chill effect in humans, $WCT = 35.74 + 0.6215 * T - 35.75 * V^{0.16} + 0.4275 * TV^{0.16}$, is unsuitable for the purposes of this study physiologically: the insulative properties and proportions of ovines somewhat different to those of a human. Instead, we used a sigmoid function to fit the data of medium fleece sheep as follows,

$$WCT = -39 + T + \frac{39}{1+e^{0.28*(V-12.12)}} \qquad (5.5)$$

where *WCT* is the wind-chill temperature. *T* and *V* signify ambient temperature and ambient wind speed respectively. The goodness of fit was great with $R^2 = 0.98$ ($p < 0.01$) and RMSE=2.44. The value 39 represents sheep core body temperature and the other two values were obtained by curve fitting: 0.28 shows the heat conductance rate and 12.12 is the wind speed above which the wind-chill effect starts to slow down asymptotically. Heat loss (in W/m^2) was determined from the WCT (see below).

As endothermic homeotherms, ovines defend internal homeostasis, with a mean core thermal set-point of 39°C (with a typical range of 37.9-39.8°C (Bligh et al., 1965)). Within a narrow range of environmental temperature (thermo-comfort zone: TCZ, A-A' in Fig. 5.4), metabolic heat production is sufficient to balance energetic flux between animal and microclimate without requiring the initiation of additional thermoregulatory strategies, however with an increasing thermal gradient between core body temperature and the environment, behavioural then physiological responses must be initiated, necessitating an increasing energetic cost. Animals experiencing temperatures outside the TCZ, but within thermo-neutral zone (TNZ; Fig. 5.4) cease feeding and seek shelter or shade; beyond the limits of TNZ, physiological changes to the animal's insulative properties and intensification of metabolic heat production, catabolism of tissue and shivering thermogenesis (cold temperature) or increase in evaporative heat loss occur to meet the energetic cost of thermal stress. Once outside lower or upper critical temperature limits (LCT, UCT), probability of death to hypo or hyperthermia is a direct product of time and temperature. Thermal limits for an adult sheep are detailed in Fig. (5.4).

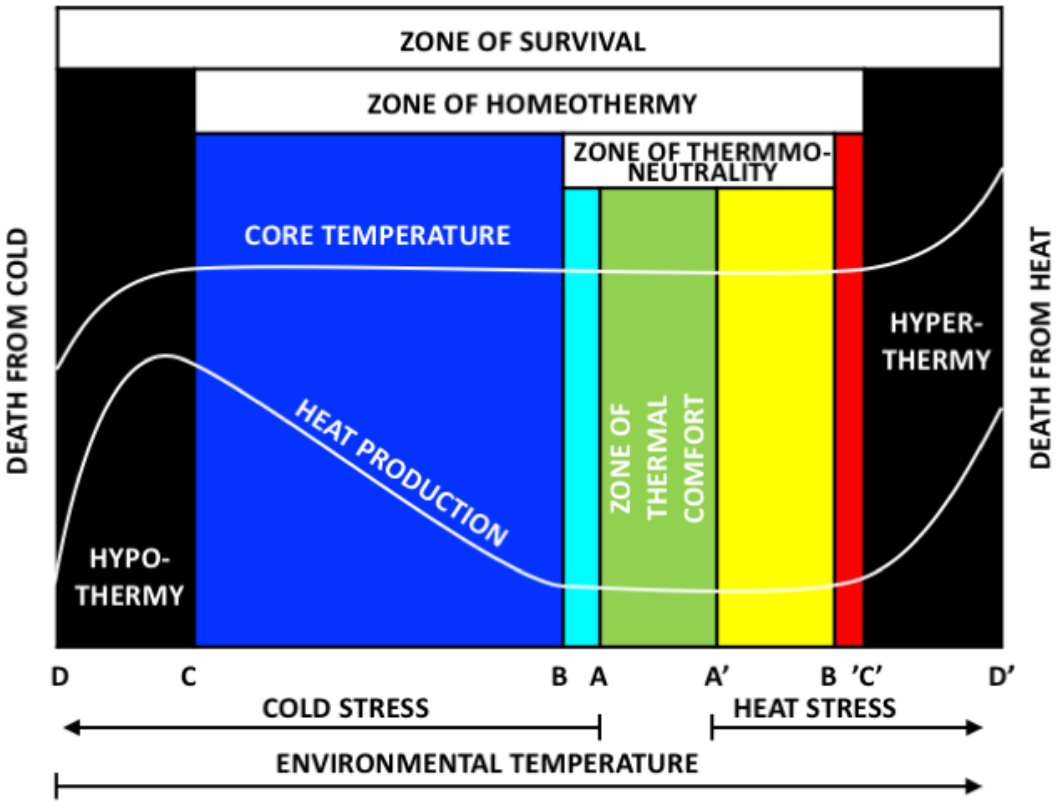

Index	Physiological Definition		Temperature (°C)
A	Zone of thermal	Lower limit	8
A'	comfort (TCZ)	Upper limit	18
B	Zone of thermal	Lower limit	-3
B'	neutrality (TNZ)	Upper limit	24
C	Lower critical temperature (LCT)		-10
C'	Upper critical temperature (UCT)		32
D	Death through hyperthermy		ND
D'	Death through hypothermy		ND

Figure 5.4 Zones of thermal comfort (TCZ), neutrality (TNZ) and critical thermal limits illustrated graphically with equivalent temperatures for a temperate acclimatised adult ewe on maintenance diet with 50mm of fleece shown below. Graph adapted from: (Bianca, 1968); Temperature source: (Bianca, 1971, 1968; Blaxter, 1962; CAgM report, 1989).

When ambient temperature is below the lower limits of TNZ, metabolic heat production increases linearly with decreasing ambient temperature (Alexander, 1974) (until outside critical limits and suffering hypothermia), i.e. $\Delta Q = k * \Delta T$. For a new-born lamb in still air, $k \approx \frac{15}{7}\ W\ m^{-2}\ °C^{-1}$. This value will be lower for a medium fleeced adult sheep because of better insulation and lower surface area: volume ratio.

The reduction of heat loss (P_Q) due to reduced wind-chill effects was calculated as,

$$P_Q = 1 - \frac{k*(T-WCT)}{k*(T-WCT_0)} = 1 - \frac{T-WCT}{T-WCT_0} \qquad (5.6)$$

where T is ambient temperature. WCT and WCT_0 are the wind-chill temperature with and without windbreak effects. P_Q is always positive as $WCT \leq T$.

The thermal limits described above have been defined in conditions of negligible wind-chill. Thus, Alexander (1974) observed the effect of wind upon critical temperature limits, noting that limits appeared to increase as wind speed increased. This effect is a product of the chilling effect of the wind lowering the effective temperature felt by the animal. Whilst the animal's thermal tolerance does not alter (so long as insulation and physical properties remain constant), change in heat loss is proportional to both ambient temperature and wind speed (i.e. wind chill).

5.3.6 Historical climate data

In order to simulate real-world environments, we used historical datasets from two meteorological stations in North Wales, namely the Llanberis station (53.1180° N, 4.1275° W) and the Clogwyn station (53.0642° N, 4.0864° W). The former site is located in a lowland area with an elevation of about 130m and the latter in an upland area with an elevation of about 700m. Therefore, the climatic condition at Clogwyn is generally more extreme (i.e. higher wind speed and wider temperature range) than Llanberis. Hourly wind speed and temperature datasets were directly retrieved from the data archives: (http://www.fhc.co.uk/weather/archive/main.asp). data availability from both sites covered more than 10 years, i.e. from July 1998 to April 2011 for Clogwyn and from July 1999 to September 2015 for Llanberis.

Hourly data were plotted on a graph of wind speed and ambient temperature and a boundary, shown by a polygon, was then drawn to include all data points (excluding obvious data errors). This represents the environmental envelope experienced by livestock at these sites. Please see results, Fig. (5.9) for graphical details.

5.3.7 The metric for the total benefit

Because our goal is to measure the impact of windbreaks on the heat loss from sheep (P_Q), a single metric representing the total benefit spatially is helpful. We propose the following equation to estimate the total benefit (B), which is simply the average of the integration of P_Q over the leeward distance,

$$B = \frac{1}{x_1 - x_0} \int_{x_0}^{x_1} P_Q \, dx \qquad (5.7)$$

x_1 and x_0 are the start and end points for the integration.

5.4 Results

5.4.1 Model uncertainty of wind speed reduction

The time series of our measurements showed clear and consistent separations among, but good correlation between, the five anemometers (Fig. 5.5a). As expected, wind speed increased further away from the windbreak. Fig. (5.5b) shows the model fit against the observations located at five downwind positions (i.e. 1H, 2.5H, 5H, 7.5H and 15H). It is clear that the log-normal function (Eq. 5.1) captured the trend of wind speed at downwind locations, with only small discrepancies (RMSE = 0.06). The model uncertainty including parameter variation and validation error was further estimated by the 500-repetition Monte Carlo simulation (Fig. 5.6). The variations in the three parameters of Eq. (5.1) were almost negligible with standard deviations less than 1% of the respective mean values for all three parameters (Fig. 5.6a, 5.6b&5.6c). Similarly, the validation error (RMSE) was between 3.5% and 4.5%, that is to say, the estimation by the model of the relative wind speed (u/u_0) had an average error of 4%. In summary, despite its simple form, the proposed model was capable of capturing most variation in wind speed downwind of the windbreak.

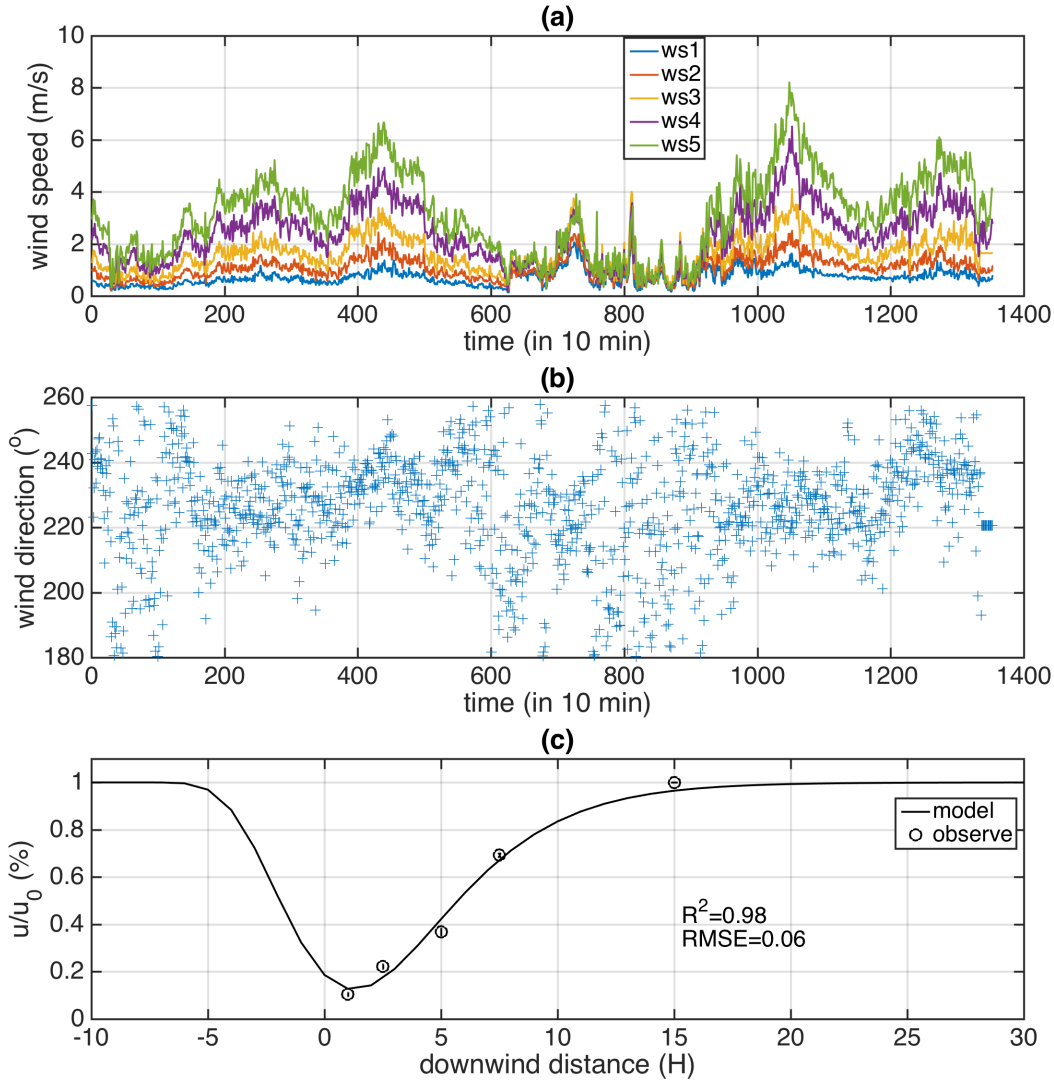

Figure 5.5 (a) Time series of wind speed observed by five anemometers downwind, (b) Time series of wind direction between 180 and 270 degree and (c) modelled wind speed reduction against the observations.

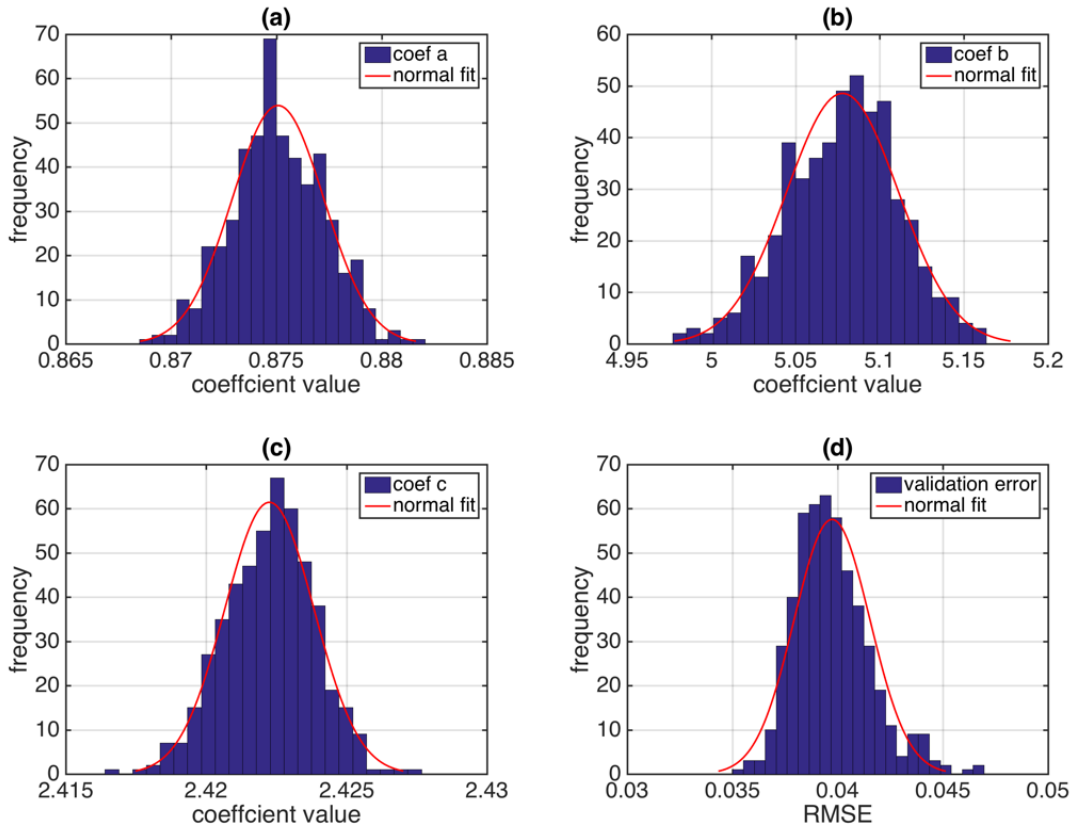

Figure 5.6 Distributions of the estimation of the coefficients and the model error (RMSE) estimated on the 500 validation datasets generated by the Monte Carlo method.

5.4.2 Modelling literature data and porosity dependence

By applying a similar method to the two literature datasets, a sensitivity analysis was conducted to determine how windbreak porosity affected model parameters and RMSE (Table 5-1). Model performance was consistently good with R^2 values over 0.92 for all cases, once again illustrating the robustness of this simple model. RMSE values ranged from 0.01 to 0.08, meaning that the average estimation error of u/u_0 was between 1% and 8%. There was a simple dependence of RMSE on porosity: as porosity increased, RMSE decreased, suggesting that the model resulted in smaller uncertainties for looser windbreaks. This result can also be observed in the dependence of the estimation of coefficients *a* and *b* on porosity where the error bars tended to decrease in size as porosity increased. Uncertainties of the coefficient *c*, however, were constantly small for all cases, with the standard deviation of 0.02.

The relationships between porosity and the coefficients themselves was built empirically by fitting the quadratic function ($y = mx^2 + nx + l$) as shown in Fig. (5.7). The fit performance was generally good with R^2 over 0.85 for all cases (Fig. 5.7a & 5.7b). Relative wind speed was estimated for windbreaks of different porosity as shown in Fig. (5.7c & 5.7d). As porosity increased, the wind attenuation effects of the windbreak diminished and the point of minimum wind speed tended to move downwind. Although the wind speed curves agreed well between the two literature datasets at a medium porosity of 0.5, the two estimations of wind speed differed significantly for other porosities, especially so for the lowest porosity. The windbreak used in our field experiments was clearly very dense (see photos in Fig. 5.1). Fig. (5.7e) showed that the wind speed curve estimated from our measurements was close to the 0.1 and 0.2 porosity curves from dataset 2, suggesting that the porosity of the experimental windbreak observed was between 0.1 and 0.2 as defined in dataset 2.

Table 5-1 Fitting the model to the two literature datasets. The codes for dataset 1, XD, D, M, L and XL, represent very dense, dense, medium, loose and very loose respectively. The last column with porosity 1 represents an open area without windbreak, simply used as a boundary condition for parameter a (i.e. a=0 when porosity=1). The values for the rest parameters, however, were undefined (ND).

	Porosity	XD (0.2)	D (0.4)	M (0.5)	L (0.6)	XL (0.7)	O (1)
Dataset 1	RMSE	0.080	0.047	0.018	0.025	0.014	ND
	a	0.76±0.05	0.69±0.05	0.63±0.01	0.57±0.02	0.35±0.01	0
	b	8.19±1.53	4.85±0.56	3.89±0.16	5.00±0.38	3.95±0.26	ND
	c	2.48±0.02	2.57±0.02	2.65±0.01	2.59±0.01	2.64±0.01	ND
	R^2	0.92	0.96	0.99	0.99	0.99	ND
Dataset 2	Porosity	0.10	0.36	0.5	0.62	0.73	1
	RMSE	0.084	0.046	0.030	0.022	0.018	ND
	a	1.00±0.05	0.82±0.04	0.63±0.03	0.45±0.01	0.29±0.01	0
	b	6.81±1.04	5.07±0.54	3.84±0.35	3.27±0.28	2.92±0.28	ND
	c	2.50±0.02	2.62±0.02	2.67±0.02	2.71±0.02	2.75±0.02	ND
	R^2	0.94	0.97	0.98	0.98	0.97	ND

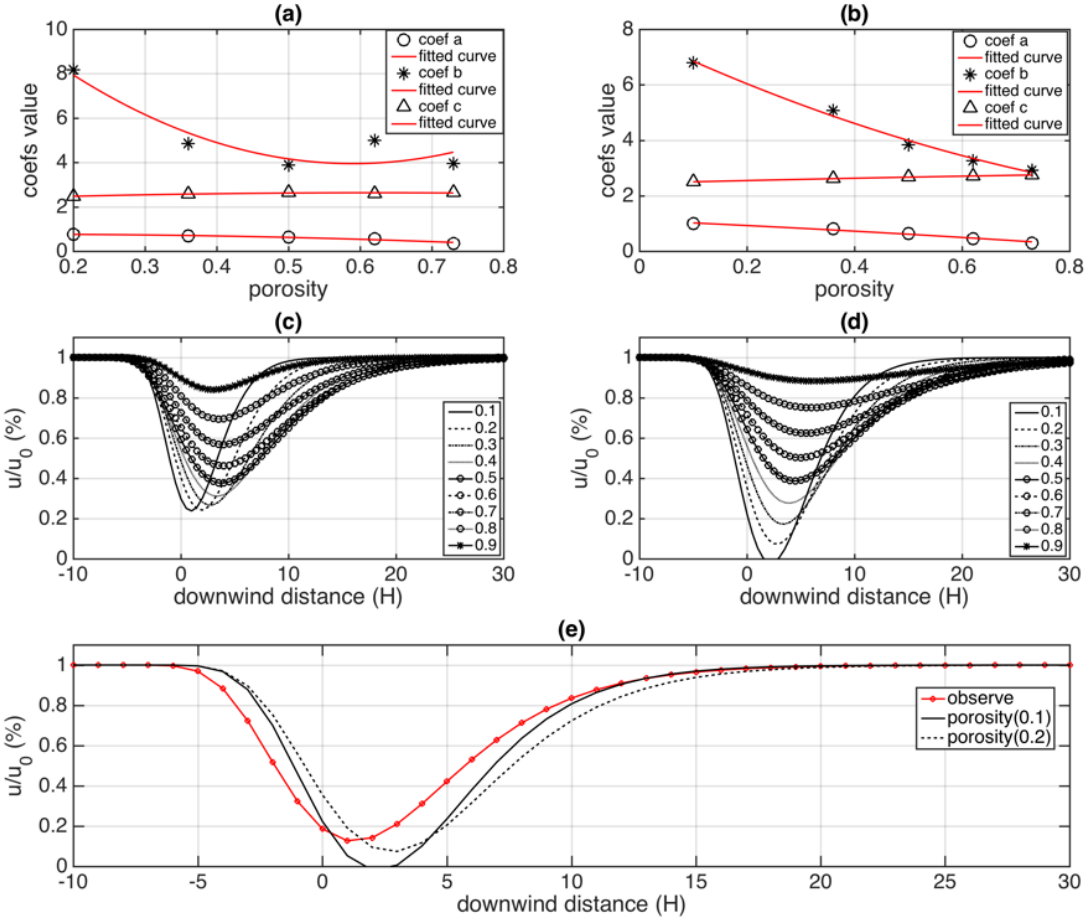

Figure 5.7 Fitted model parameters and porosity and the curve of relative wind speed for porosity values ranging from 0.1-0.9. (a, c) From dataset 1; (b, d) Dataset 2. (e) Field measurements compared with curves for porosity of 0.1 and 0.2 from dataset 2.

5.4.3 Estimated benefits in the heat loss of sheep

Building upon the above results and combining equations (5.5-5.7), it was possible to apply the wind speed model to estimate potential climatic benefits due to reduced heat loss from sheep. Fig. (5.8a & 5.8b) shows heat loss reduction under a fixed ambient wind speed of 10 m/s, an ambient temperature of 5 °C and a windbreak porosity of 0.2. The reductions in heat loss increased significantly at the locations near the windbreak because of decreased wind speed and wind-chill effect. In fact, for a given ambient temperature (e.g. 5 °C here), the heat loss reduction is highly correlated with the wind speed reduction through Eq. (5.6).

Combining the benefits in crop growth and heat loss reduction using Eq. (5.7), we implemented a sensitivity analysis of the total gain against a range of porosity from 0.1-0.9 and ambient wind speed from 1-30 m/s. This relationship is shown as a 2-D contour plot in Fig. (5.8c). When the air is nearly still (i.e. wind speed close to zero), the total gain is nearly null because of the absence of wind chill. As wind becomes stronger, reduced heat loss gradually increases, adding to the total productivity benefit, suggesting that greater advantages are conferred in windier conditions. The total benefit increased as the ambient wind speed increased for all porosities, but dependence on porosity was not monotonic. The total benefit starts to increase as porosity increases above zero, reaches a peak benefit of +27% at a porosity of 0.5 and a wind speed of 12 m/s, and then starts to fall as porosity approaches 1. As wind speed increases above 12 m/s, the total benefit to productivity conferred by the windbreak asymptotically approached a constant because of diminishing wind-chill effects determined by Eq. (5.5). In physical terms, this can be understood as the gradual erosion of the surface boundary layer as the fleece is penetrated by high winds, leading ultimately to a point where conduction of heat through the endodermis, rather than through the surface boundary layer, limits heat loss.

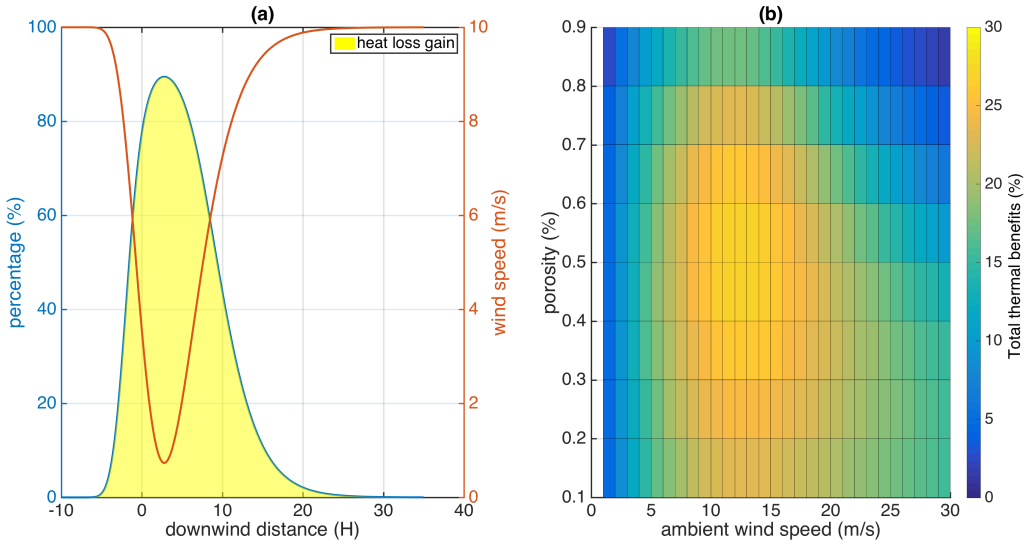

Figure 5.8 (a)Effects of windbreak on wind speed reduction and heat loss gain. (b) The spatial total benefit against a range of porosity (0.1-0.9) and ambient wind speed (1-30 m/s).

5.4.4 Wind-chill effects on a habitable thermal condition

Based on historical climate data for two sites representative of upland and lowland environments inhabited by sheep, we related simulated wind-chill to sheep-specific limits of thermal comfort, neutrality and critical tolerance to determine the impact of a chilling wind on the physiology of livestock, and importantly, the influence of reducing wind speed to the physiological response to shown by livestock to the warmer temperature effectively experienced.

Eq. (5.5) summarises the wind-chill temperature (WCT) as a function of ambient temperature and wind speed. Subtracting WCT from ambient temperature allows us to modify the six physiologically significant temperature points for sheep (-10°C, -3°C, 8°C, 18°C, 24°C, 32°C) in terms of temperature experienced, rather than ambient temperature (see details in Fig. 5.4). Each sector was assigned to a colour and the relation between critical temperature limits and ambient temperature and wind speed are illustrated by filled contour plots (Fig. 5.9a&5.9b), hereafter simply denoted by the term wind-chill thermal tolerance (WTT) plot. The ambient temperature scale from -40°C to 50°C and wind speed from 0 to 50 m/s represents a generic environment inclusive of most natural microclimates. Any individual location will experience only a sub-area of the WTT plot, corresponding to the environmental conditions experienced over any given time period.

The areas enclosed by the dotted white lines in Fig. (5.9a&5.9b) represented the environmental conditions in Llanberis and Clogwyn station respectively.

As expected, the WTT plot suggested a more physiologically-stressful thermal environment at the upland in Clogwyn, with a large black area indicating the range of WCT temperatures in which a sheep's environmental temperature falls below LCT and the sheep would eventually suffer fatal hypothermia.

Without wind, the boundaries of each monochromatic area on the WTT plot would be mutually parallel (i.e. no dependence on wind speed), but because of the presence of wind-chill effects, these boundaries bend towards higher temperature, creating a larger cold zone and a smaller warm zone. Consequently, the areas representing optimum conditions for livestock health and productivity denoted by the green 'thermo-comfort' zone (8-18°C, green area on Fig. 5.9a&5.9b) and the wider, sub-optimal but 'thermo-neutral' zones (indicated by light blue and yellow areas) become a smaller part of the total micro-climatic environment represented on the graph. As the boundary layer becomes eroded, further increases in wind lead to smaller and smaller increases in wind chill, until a point is reached at a wind speed of about 20m/s where the boundaries become parallel and vertical.

The introduction of a windbreak, and the reduction in winds speed and chilling can be visualized on the WTT plot. Here, the probability of experiencing a given thermal environment can be estimated by the proportion of the area it represents (e.g. the proportion of green area shows the probability of having a thermo-comfortable temperature). Therefore, reducing ambient wind speed by a certain amount (e.g. moving the dashed horizontal lines in Fig. 5.9a&5.9b downwards), reduces the relative area of hypo/hyperthermy (black) and increases the relative areas of thermocomfort and thermoneutrality (green, yellow, light blue).

We used the historical climate data to constrain our simulation to a real-world scenario (i.e. only the area within the polygon representing the actual climatic envelope was considered in the computation). Four coloured lines represented the changed probability of experiencing thermocomfort (green), thermoneutral (light blue) and thermostress (red) conditions when wind speeds were reduced by 5 to 95% for the Llanberis and Clogwyn sites respectively. As expected, the impact of reduced wind speeds differed significantly between sites. At Llanberis (Fig. 5.9c), the relative proportion of different thermal conditions remained nearly constant, suggesting that there is little benefit obtained by reducing wind speed. This is unsurprising because conditions at Llanberis are naturally above critical limits (i.e. little black

area was initially included). At Clogwyn (Fig. 5.9d), however, the probabilities of experiencing thermo-comfortable (green line) or thermo-neutral (blue line) conditions both increased significantly as the wind speed decreased. The probability of a thermally stressful condition (i.e. conditions requiring increased thermogenic compensation for heat loss) (red line) also increased but with a slighter gradient. Consequently, the probability of experiencing fatal (black line) conditions decreased greatly as wind speed decreased. Given a wind speed reduction of 60%, for instance, we can reduce the chance of experiencing fatal thermal conditions by 27%, whilst increasing the probability by 8% and 14% respectively of experiencing a thermo-comfortable (optimum for production) or thermo-neutral condition.

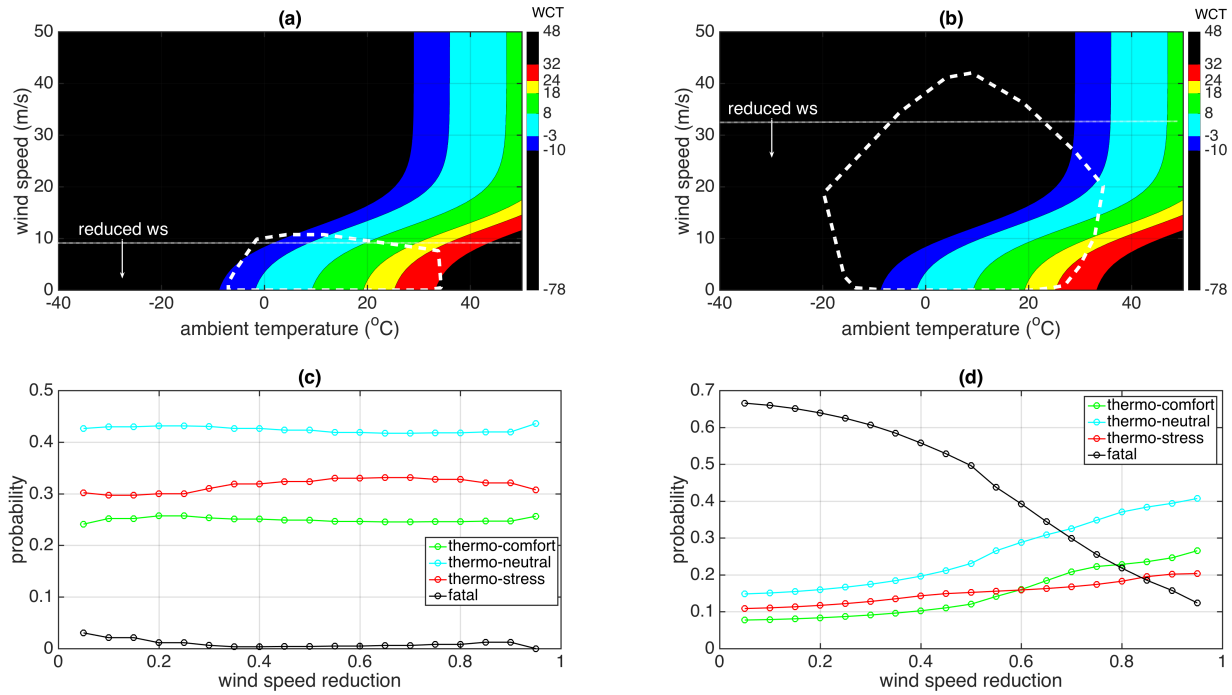

Figure 5.9 (a, b) Contour plots of wind-chill thermal tolerance (WTT plot) for sheep. Wind-chill temperature (WCT) was grouped according to the thermal categories shown in Fig. (5.4). (c, d) The probability of experiencing a certain thermal condition against reduced wind speed. Line colour meaning: Green: thermo-comfort; Blue: thermal-neutral; Red: thermo-stress; Black: fatal.

5.5 Discussions and conclusions

Although Eq. (5.1) was found to provide a good approximation to literature reports of wind speed reduction around windbreaks, real data was required to determine model parameters for a given windbreak. We have tried to correlate the parameters with a single driving variable (i.e. porosity), but the differences depicted by the two literature datasets suggest that porosity alone is not able to unify the two datasets. The concept of windbreak porosity has been

frequently used in the literature (Heisler and Dewalle, 1988; Torita and Satou, 2007; Wang and Takle, 1995), presumably because it is the most intuitive structural feature to characterise a windbreak.

As an index to describe how much wind resistance different windbreaks introduce, porosity has not, to our knowledge, been properly defined mathematically and is thus not a very useful term to apply computationally. Optical porosity is well defined and can be calculated conveniently, however it may only be justifiable for 2-D windbreaks and may not work for 3-D situations (Torita and Satou, 2007). Physically, porosity may represent a combination of several characteristics that reflect the complexity of a windbreak, such as tree and branch flexibility, leaf size, tortuosity, etc. In aerodynamics, drag force is often used to describe a windbreak (Guan et al., 2003; Wang and Takle, 1997), but similarly to porosity, this quantity is neither conveniently calculated or measured.

The model parameters in Eq. (5.1) have explicit relations with the real-world parameters x_{min}, y_{min} and L_{20} as given by Eqs. (5.2-5.4) respectively. It is clear that coefficient *c* determines the downwind location where the minimum wind speed is reached. Similarly, coefficient *a* describes the percentage of wind speed at that location. Although coefficient *b* was found be connected with L_{20} through Eq. (5.4), the form of this equation was not clear enough to suggest an obvious physical meaning of *b.* In fact, the right-hand side of the formula also incorporates coefficients *a* and *c*, making the interpretation of this parameter even more difficult. The hyperbolic function shown in Eq. (5.4), however, may suggest some deep relationship between the coefficient *b* or L_{20} with some fundamental aerodynamic process (e.g. an analytical solution of the Navier-Stokes equation under certain conditions). It is well known that the solutions to some equations that describe ocean waves can be represented by hyperbolic functions (Majda, 2003). Further analytical exploration of Eq. (5.4) and its links to fluid dynamics may be a fertile area to follow-up.

Similarly, the wind-chill effect estimated in this study represented the heat loss from sheep through convection only, and a fuller description of the energetics of the sheep body requires that consideration is also given to solar gain. Here incoming and outgoing radiation should be considered in the model given the fact that windbreaks can normally provide shade from sunlight. This shading effect may be positive during hot conditions or negative when solar gain may exceed wind-chill in still, cold conditions. Therefore, in addition to the spatial integration shown in this study, a temporal integration of heat loss benefit, over the full range of conditions experienced, should be made to obtain the total benefit over time. A companion

paper focusing on the measurement and modelling of tree shading effects on animal heat loss is expected soon.

These approaches and models developed in this study, despite their simplicity, have shown great robustness. However, the model for the wind speed reduction was only validated by using our measurement at the farmland. The model for the sheep wind-chill was also derived based on a single measurement. More data that represent different types of windbreak and climate zones are needed to validate and apply these approaches to a broader range of conditions.

The WTT plot (Fig. 5.9) is very helpful for an intuitive analysis of the wind-chill effects on the thermal stress or comfort experienced by a given organism in a given micro-climate. Generally, the climate conditions actually experienced by a particular location are a sub area of the WTT plot. In this study, we simulated two scenarios representing lowland (Llanberis) and upland (Clogwyn) thermal conditions. Results showed that there was little benefit to be gained by reducing wind speed at Llanberis, where the thermal condition was naturally within the thermo-neutral zone (or in rare cases just outside thermal critical limits) of sheep for the majority of time (Fig. 5.9a&5.9c). In contrast, significant benefits could be obtained at Clogwyn where the temperature range was much more extreme and often below the critical boundaries of cold tolerance for sheep (Fig. 5.9b&5.9d). The information to be extracted from this result is inspired: despite the benefits of windbreak practise in general, its effectiveness is dependent on regional micro-climate. A region with conditions which invoke a greater thermal stress as a result of being frequently beyond thermo-neutral and critical physiological limits (e.g. uplands) gains more benefit from using windbreak. In our simplified analysis, conditions inside the environmental envelope are considered equally probable. A more accurate quantification of the actual benefits of establishing a windbreak at a given location would require that each pair of wind speed and ambient temperature conditions is weighted by its frequency of occurrence. Nevertheless, the thermal/wind envelope of a particular location, superimposed on the WTT plot for a given organism, provides a useful and convenient tool of illustrating the response of livestock to wind-chill and to the effects introducing a windbreak. A follow-up study will focus on a spatial and temporal integration of the thermal benefits by combining the WTT plot and the windbreak model at a farm and landscape scale.

In summary, a simple parameterised model was capable of capturing most of the variation in relative wind speed around a real-world windbreak. The model error was low, about 4%±0.5%

as estimated by a Monte Carlo simulation. Total microclimatic benefits of windbreaks were highest at a porosity of around 0.4 and an ambient wind speed of 15 m/s (Fig. 5.7). An organism-specific WTT plot (Fig. 5.9) has the potential to be applied to a wide range of real-world situations and forms the framework for an efficient and precise quantification of windbreak effects on animal productivity.

5.6 References

Alexander, G., 1974. Heat loss from sheep, in: Monteith, J.L., Mount, L.E. (Eds.), Heat Loss from Animals and Man: Assessment and Control. Butterworths, London, pp. 173–203.

Ames, D.R., Insley, L.W., 1975. Wind-Chill effect for cattle and sheep. J. Anim. Sci. 40, 161–165. doi:10.2134/jas1975.401161x

Barnes, T.A., 1974. Wind-chill index for sheep. Kansas State University.

Bianca, W., 1971. Die Anpassung des Haustieres an seine klimatische Umgebung. Schweiz. Landw. Forsch. 10, 155–205.

Bianca, W., 1968. Neuzeitliche Ergebnisse und Aufgaben der Bioklimatologie bei Haustieren. Der Tierzüchter 20, 438–442.

Bitog, J.P., Lee, I.B., Hwang, H.S., Shin, M.H., Hong, S.W., Seo, I.H., Kwon, K.S., Mostafa, E., Pang, Z., 2012. Numerical simulation study of a tree windbreak. Biosyst. Eng. 111, 40–48. doi:10.1016/j.biosystemseng.2011.10.006

Blaxter, K.L., 1962. The energy metabolism of ruminants. energy Metab. ruminants.

Bligh, J., Ingram, D.L., Keynes, R.D., Robinson, S.G., 1965. The deep body temperature of an unrestrained Welsh Mountain sheep recorded by a radiotelemetric technique during a 12-month period. J. Physiol. 176, 136.

Bourdin, P., Wilson, J.D., 2008. Windbreak aerodynamics: Is computational fluid dynamics reliable? Boundary-Layer Meteorol. 126, 181–208. doi:10.1007/s10546-007-9229-y

Cleugh, H.A., 1998. Effect of windbreaks on air-flow, microclimate and productivity. Agroforesty Syst. 55–84.

Gregory, N.G., 1995. The role of shelterbelts in protecting livestock: a review. New Zeal. J. Agric. Res. 38, 423–450.

Guan, D., Zhang, Y., Zhu, T., 2003. A wind-tunnel study of windbreak drag. Agric. For. Meteorol. 118, 75–84. doi:10.1016/S0168-1923(03)00069-8

Health, Ca.W.G. on W. and A.D.& Ca.W.G. on W. and A., 1989. Animal health and production at extremes of weather : reports of the CAgM Working Groups on Weather and Animal Disease and Weather and Animal Health. Secretariat of the World Meteorological Organization, Geneva, Switzerland.

Heisler, G.M., Dewalle, D.R., 1988. 2. Effects of windbreak structure on wind flow. Agric. Ecosyst. Environ. 22–23, 41–69. doi:10.1016/0167-8809(88)90007-2

Hipsey, M.R., 2003. Parameterizing the effect of a wind shelter on evaporation from small

water bodies. Water Resour. Res. 39, 1–9. doi:10.1029/2002WR001784

Majda, A., 2003. Introduction to PDEs and Waves for the Atmosphere and Ocean. American Mathematical Soc.

McArthur, A.J., Monteith, J.L., 1980. Air movement and heat loss from sheep. II. Thermal insulation of fleece in wind. Proc. R. Soc. London. Ser. B, Biol. Sci. 209, 209–17.

Osczevski, R., Bluestein, M., 2005. The new wind chill equivalent temperature chart. Bull. Am. Meteorol. Soc. 86, 1453–1458. doi:10.1175/BAMS-86-10-1453

Pollard, J.C., 2006. Shelter for lambing sheep in New Zealand: a review. New Zeal. J. Agric. Res. 49, 395–404. doi:10.1080/00288233.2006.9513730

Schwartz, R.C., Fryrear, D.W., Harris, B.L., Bilbro, J.D., Juo, A.S.R., 1995. Mean flow and shear stress distributions as influenced by vegetative windbreak structure. Agric. For. Meteorol. 75, 1–22. doi:10.1016/0168-1923(94)02206-Y

Speckart, S.O., Pardyjak, E.R., 2014. Journal of Wind Engineering A method for rapidly computing windbreak fl ow fi eld variables 132, 101–108.

Stredova, H., Podhrazska, J., Litschmann, T., Streda, T., Roznovsky, J., 2012. Aerodynamic parameters of windbreak based on its optical porosity. Contrib. to Geophys. Geod. 3, 213–226. doi:10.2478/v10126-012-0008-5

Torita, H., Satou, H., 2007. Relationship between shelterbelt structure and mean wind reduction. Agric. For. Meteorol. 145, 186–194. doi:10.1016/j.agrformet.2007.04.018

Vigiak, O., Sterk, G., Warren, A., Hagen, L.J., 2003. Spatial modeling of wind speed around windbreaks. Catena 52, 273–288. doi:10.1016/S0341-8162(03)00018-3

Wang, H., Takle, E.S., 1997. Momentum budget and shelter mechanism of boundary-layer flow near a shelterbelt. Bound. Layer Meteorol. 82, 417–435. doi:10.1023/A:1000262020253

Wang, H., Takle, E.S., 1995. Boundary-layer flow and turbulence near porous obstacles. Boundary-Layer Meteorol. 74, 73–88. doi:10.1007/BF00715711

Wilson, J.D., 1987. On the choice of a windbreak porosity profile. Boundary-Layer Meteorol. 38, 37–49. doi:10.1007/BF00121553

Wilson, J.D., Flesch, T.K., 2003. Wind measurements in a square plot enclosed by a shelter fence. Boundary-Layer Meteorol. 109, 191–224. doi:10.1023/A:1025414805676

Wilson, J.D., Yee, E., 2003. Calculation of winds disturbed by an array of fences. Agric. For. Meteorol. 115, 31–50. doi:10.1016/S0168-1923(02)00169-7

Yusaiyin, M., Tanaka, N., 2009. Effects of windbreak width in wind direction on wind velocity reduction. J. For. Res. 20, 199–204. doi:10.1007/s11676-009-0039-6

Ch 6. General discussion and conclusion

Defensible and accurate estimations of land-atmosphere exchanges are significant not only because of practical concerns (e.g. GHG estimation, climate change and agricultural applications), but also because answering existing uncertainties introduces scientific challenges that require new ideas and methods to solve them. This can be seen most clearly in real-world scenarios featuring heterogeneous land surfaces, where traditional experimental and theoretical methods are not directly applicable.

Real world phenomena are typically imperfect compared to scientific expectation, but seeking precision (or, ultimately, perfection) is essential in order to identify and overcome limitations in understanding, and to make any substantial scientific progress. Even with today's advanced techniques (e.g. high speed sensors and fast computers) most of the experimental and theoretical methods we have for measuring land-atmosphere exchanges are still restricted to homogeneous conditions. As shown in this thesis, any difficulty in quantifying exchange is amplified in the heterogeneous land surfaces that, in fact, represent the real-world situation.

This thesis has sought to make a significant scientific contribution by developing/finding real-world solutions to improve our understanding of fluxes from heterogeneous land surfaces.

Starting from the basics, this thesis considers some of the fundamentals of the two mostly used methods of observing land-atmospheric GHG fluxes, namely chamber- and EC-based measurements. The former often suffers from poor spatial representation of heterogeneous land surfaces because of sample size deficiency; The latter often contains a large amount of missing data points in what should be a continuous time series because of machinery failure and/or data quality control[1]. What is in common between these two problems is that they both require an inference/prediction of unknowns based on a limited amount of information. Even though it might be impossible to completely overcome these limitations (i.e. we must accept that resources will always limit sample size and technical failures will inevitably lead to missing data), improving estimation accuracy is not impossible if better strategies can be developed.

[1] This issue exists, in fact, irrespective of the heterogeneity of the underlying surface.

In chapter 2, a two-stage sampling strategy (2SS) was introduced to improve chamber-based measurements of GHG fluxes. The main idea is quite straightforward. When we have complete ignorance of the actual population (e.g. unknown population distribution, mean and variance), increasing sample size is the only way to improve sample-based estimations based on a randomization-based sampling strategy. In practice, however, we are always constrained by a limited number of chambers which are insufficient to obtain a complete sample across heterogeneous land surfaces. Combining these two points suggests a two stage sampling strategy: stage one: take an initial sample with a relatively large sample size to maximise spatial representation; stage two: select from this large sample a much smaller, but spatially representative, sub-sample for ongoing monitoring. Despite its limited sample size, the stage two sample inherits all the information from its more reliable predecessor and the estimation accuracy per unit sampling resource is thus improved. A Monte Carlo simulation showed that 2SS can improve the estimation on population mean and variance by 30% ± 30%, the actual amount being dependent on the heterogeneity of the underlying land surface and the sample size settings for the two stages.

Chapter 3 deals with missing-data imputation for EC-based measurements (or indeed any structured time series or signal), commonly known as gap-filling. Similar to the sampling problem above, dealing with the gap-filling problem also requires that we make an inference about something unknown (the behaviour of the system) based on an imperfect and incomplete data sample. The difference, however, is that the inference here is made about missing samples, instead of the population as a whole (e.g. we are not concerned with identifying the population mean or variance). An essential issue that limits the precision of any gap-filling methods is the existence of a stochastic component that can be found, almost without exception, in a natural signal. Mathematically, this means that a natural signal is a combination of a periodic/trend component and a noise component, the former deterministic and the latter stochastic. Therefore, any attempt to gap-fill a natural signal raises two immediate questions: 1) Without knowing the "true" values, can we still distinguish the deterministic and stochastic components of a signal? 2) Since it is neither possible (nor worthwhile) to recover a stochastic series[2], are seemingly independent gap-filling methods just estimators of the best-guess non-stochastic component? In answer to question 2, we speculate that the existing gap-filling methods are not distinguishable in their performance

[2] What we observe/sample from a stochastic time series is only a realization of many possible paths over time, hence it is of little sense to try to recover a single realization.

(i.e. their performance is largely determined by the variation of noise), as found by comprehensive comparisons among methods (e.g. see CH3-Refs-Moffat et al., 2007). The inpainting-based gap-filling method proposed in this study, in addition to its simplicity and intuitive basis, it is as effective in gap filling signals with noise and is superior when applied to noise-reduced signals. Follow-up studies could focus on a signal and noise analysis of the EC-based measurements, aiming to answer question 1.

Even if the above issues could be resolved to the extent that the individual flux estimate (chambers or EC) is considered robust in itself, how can one decide whether the measurement tells the "truth" without actually having the "real" values to compare it to? Clearly, when both measurements are in agreement we may be confident that both approximate the truth, but because the two have different spatial coverage, a direct comparison is not possible. This becomes particularly important for heterogeneous land surfaces (e.g. the two should give identical results for a perfectly homogeneous land surface; but not otherwise, except in the case where reported error bars are unhelpfully large). In order to improve the confidence in our estimations using both methods, an indirect comparison is possible if appropriate steps are taken to include spatial structure explicitly. Chapter 4 describes such a comparison between EC- and chamber-based measurements of CO_2 and CH_4 flux. Making this comparison is meaningful not only in the interests of enhancing the robustness of the final GHG and carbon balance estimates, but also because it prescribes a logical connection between a series of techniques (e.g. Lasso and orthogonal regression, the footprint model) to bridge the spatial and temporal discrepancies between methods. The comparison results were certainly encouraging: CO_2 flux was highly linearly correlated between methods, whilst CH_4 flux differences followed a Gaussian distribution, suggesting that these differences were nothing more than noise and that, once again, it is of little sense to over analyse this data What's more satisfying and important, is that the models, methods and techniques use to bridge these methods have the potential to be used across a wide range of topics because of their generality in mathematical forms.

Between homogeneity and natural heterogeneity, there is an intermediate type of land-surface heterogeneity that might be called structured or quasi-heterogeneity. This can commonly be found in an agricultural land use system where artificial structures are often introduced, either increasing or reducing heterogeneity to benefit productivity. Chapter 5 focussed on a special type of land surface structured heterogeneity that has potential benefits for pasture and livestock, namely a windbreak system. By introducing structured heterogeneity into the

momentum flux field, a windbreak alters the local micro-climate, which may have a direct impact on productivity, especially in cold areas. Our simulations showed that the total benefits of crop and livestock productivity can reach up to 34%. Again, the methods and models (i.e. the sigmoid function, the log-normal function and the WTT plot) offer great potential to be further studied and applied to general cases. Perhaps most importantly, the simple parameterisation suggested here is easily realised computationally, and when combined with a spatially explicit map of current, or potential future windbreaks, could provide an effective tool for planning landscape features that enhance farm profitability.

In short, the basic scientific idea of this thesis is that, even given existing constraints (e.g. sample size limitation, homogeneity assumption for EC, inevitable observation errors, etc.), mathematical modelling can help reduce/minimize uncertainties in environmental monitoring in the real world. Moreover, mathematical methods, combined with the computation power of modern computer, can be an effective tool for quantitatively understanding how the landscape works currently and enhancing landscape function in the future.

List of potential (and feasible) follow-up studies:

- Extend the two-stage sampling strategy to incorporate temporal variation of GHG flux.
- Expand the second-stage sample selection to maintain spatial heterogeneity characteristics by selecting a data sub-sample that retains the variogram parameters of the initial sample.
- Develop signal-specified de-noise techniques and estimate the upper-limit of gap-filling EC-based signals.
- Find out the source of the systematic difference between EC- and chamber-based measurements.
- Analytically and numerically demonstrate the superiority and validity of the Lasso regression over traditional regressions (e.g. stepwise regression) by exemplifying in Environmental Science.
- Develop process-based models to describe the crop productivity around windbreaks. Potentials processes include water-nutrient-light completion near windbreak, leaf absorbed radiation and convection.
- Systematize the definition of the wind-chill thermal tolerance (WTT), including term definition, physical/thermal significance and applicability.

- Apply the analysis of WTT to different livestock production systems, integrating the windbreak benefits over time and space to account for impacts at the farm and landscape scales.

Appendix 1

On the choice of λ for Lasso regression

An important step in Lasso regression (Eq. 4.4) is to choose an appropriate value of λ such that: 1) The estimation error (MSE) on the cross-validation set is small; 2) while 1) is considered, λ should be as large as possible to have enough restrictions on the coefficients (i.e. preventing overfitting). In order to achieve this, we plot the MSE against a range of λ values as:

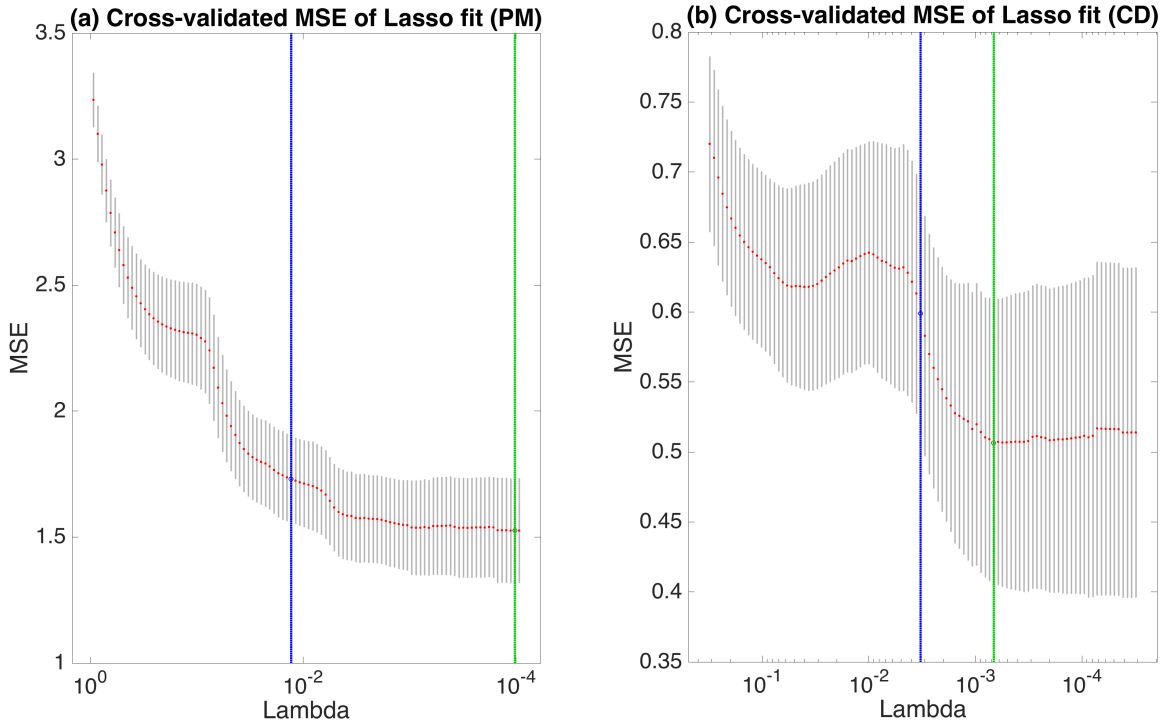

The green line shows the λ value with the minimum MSE and the blue line shows the largest λ value such that MSE is within one standard error of the minimum. We chose the λ values indicated by the blue lines (i.e. 1*SE) for the regression analysis of CH_4 flux for the two vegetation types, namely $\lambda = 0.0129$ for PM and $\lambda = 0.0033$ for CD.

Appendix 2

Formula for determining the compass wind direction (i.e. 2-d wind direction) from CSAT3 measurements

As shown in the figure below, the direction that the transducers point at is –x direction under a standard right-handed coordinate system.

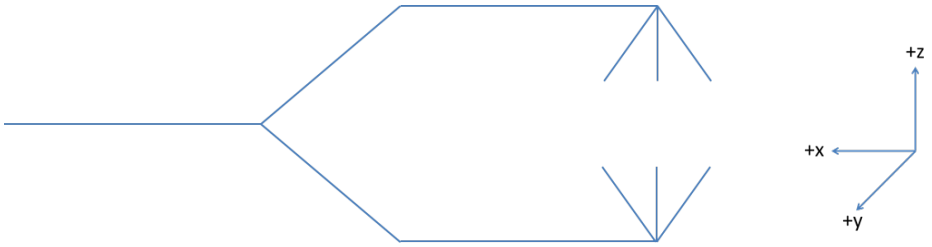

Given a compass direction of the direction (θ) that the transducers point at (i.e. this should be measured on site) and the wind speeds at x and y directions (denoted as *Ux* and *Uy* respectively), the actual compass wind direction can be calculated as:

$$\alpha = \theta - \arctan\left(\frac{Uy}{Ux}\right) * \frac{180}{\pi} \; mod \; 360$$